Proceedings of the 5th Meeting of Japan CF Research Society

Edited by Hiroshi YAMADA

December 15-16, 2003

Kobe University, Japan

Preface

This book is Proceedings of the 5th Meeting of Japan CF-Research Society, JCF5 which was held at Fukae Campus of Kobe University, Kobe, Japan, on December 15-16 , 2003.

Japan CF-Research Society (JCF) was established in March 1999. The main aim of the society is to investigate the nuclear reactions that occur in the solid-state or condensed matter, especially in low energy regions. CF stands for Condensed-matter Fusion, Coherently-induced Fusion, Cleaner Fission, Clean Fusion, Cold Fusion and other nuclear reactions in condensed matter. And the main goal is expected to develop science and technologies to extract useable energy from CF phenomena. CF researches cross traditional academic domains and require an interdisciplinary approach in collaboration efforts of nuclear physics, fusion science, radiation physics, condensed-matter physics, surface and catalysis science, metallurgy, hydrogen science, electrochemistry, calorimetry, accelerator and beam science, laser science, nuclear and quantum-science and engineering, molecular dynamics, acoustics, thermodynamics, physical chemistry, and so on. Another significant goal of the society is to enhance Japan's role as a focal point of research in this area and to act as a clearing house for international cooperation and information exchange. This commonly reasons why we employ English as conference language and publish books of ABSTRACTS and PROCEEDINGS in English. For the past three meetings, JCF1, JCF2, and JCF3 , we published books of ABSTRACTS only on our web-site (http://wwwcf.elc.iwate-u.ac.jp/jcf/). The society has decided to issue books of PROCEEDINGS for further meetings from the JCF4 meeting, as both of printed versions and electronic versions in our web-site(same address as above one).

Submitted papers to JCF5 were peer-reviewed by the editorial board (Chairman: Prof. Hiroshi Yamada, Iwate University). One or two reviewers were selected by the board to review papers, comment problems and errors, and return to authors for correction. Most papers were accepted to publish via one-through reviewing processes with minor corrections.

In JCF5 Meeting, there came about 50 participants and 22 papers were presented (see JCF5 ABSTRACTS). This book of JCF5 PROCEEDINGS contains 19 full papers through submission and reviewing processes. For non-JCF members, inquiry to obtain a copy of book should be sent to Prof. Hiroshi Yamada (Faculty of Engineering, Iwate University, Morioka Japan; yamada@dragon.elc.iwate-u.ac.jp).

We thank all participants of JCF5 for their efforts to make this PROCEEDINGS and hope the information of this proceedings useful to further progress of CF studies.

Akito Takahashi (Prof., Osaka University), Director-in-Chief of JCF

Hiroshi Yamada (Prof., Iwate University), Chairman of JCF Editorial Board

April, 2004

CONTENTS

GAS PERMEATION

THEORY

EXPERIMENTS TO CONFIRM ^{7}Li(d,nα)^{4}He REACTION RATE ENHANCEMENT IN LIQUID LITHIUM

T. Minari, S. Awano, R. Nishio, T. Hirao, Y. Awa, A. Taniike, Y. Furuyama, and A. Kitamura*
Faculty of Maritime Sciences, Kobe University
5-1-1 Fukaeminami-machi, Higashinada-ku, Kobe 658-0022, Japan
*kitamura@maritime.kobe-u.ac.jp

Abstract: Recently, ^{7}Li(d,nα)^{4}He reaction rate enhancement by a factor of 10^{10} - 10^{15} has been claimed to take place under deuteron implantation of liquid Li. We investigate the reproducibility of this phenomenon to determine the reaction rate quantitatively.

Keywords: liquid Li, ^{7}Li(d,nα)^{4}He, reaction rate enhancement, Arrhenius equation

1. INTRODUCTION

Deuterium-induced reactions in condensed matter in keV energy range have been studied extensively and a variety of findings has been published; *e.g.* increase in the nuclear reaction rate and observation of nuclear transmutation. The former includes the research made by H. Ikegami *et al.*, where enormous enhancement of ^{7}Li(d,nα)^{4}He reaction rate in liquid phase has been observed [1].

The experiments were carried out for metallic Li targets in both solid and liquid phase. In the solid phase, no event was observed with the α-particle and neutron detectors, which was consistent with the reaction rate estimation based on the published nuclear cross-section data. On the other hand, in the liquid phase, a large number of MeV α-particles were observed on the silicon surface barrier detector (SSBD), indicating a rate enhancement by a factor of 10^{10}-10^{15}.

They explain the phenomenon as follows. Deuterons with keV energy ("buffer energy"), where the nuclear collision dominates over the electronic one in the stopping process, penetrate deep into the s-electron cloud of Li atoms to form "united atoms" at the classical turning point. This means formation of the atomic fusion which makes adiabatic transition to the nuclear fusion reaction with some probabilities determined by the well-known Gamow factor. Regarding the energetic deuterons as solutes, this process can be treated within the framework of thermodynamics of chemical reactions in dilute solutions. As a consequence the Arrhenius equation for spontaneous chemical reactions is naturally applicable. The Gibbs free energy change ΔG in the exponent of the Arrhenius factor is negative in the present case of endothermic reaction d+^{7}Li$\rightarrow$[DLi]. Thus an enhancement exp(-$\Delta G/kT$) by many orders of magnitude of nuclear fusion reactions in the metallic Li liquids could be realized.

We have started on experiments to confirm reproducibility of the phenomenon; reaction rate enhancement for the ^{7}Li(d,nα)^{4}He reaction with a Q-value of 15.1 MeV. In the present paper we

describe the experimental apparatus consisting of an ion source, a target chamber and a liquid-Li-loop, and preliminary results of the first experiment. We observe α-particles as products of the $^{7}Li(d,n\alpha)^{4}He$ reaction using an SSBD and some sheets of solid-state track detectors (CR-39), and neutrons using a rem counter.

2. EXPERIMENTAL PROCEDURE

2.1. EXPERIMENTAL SETUP

A schematic of the apparatus is shown in Fig. 1 and Fig. 2. Beams of 20 keV deuterons are extracted from a duoplasmatron ion source and mass-analyzed with a 60-deg. sector magnet. Deuterons are injected into the liquid Li target through an aperture of 10 mm in diameter.

A total amount of 400 g of Li is reserved in the upper reservoir. Liquid Li heated in the upper reservoir is dripped into a manifold through a 1/4 inch pipe to form spherical liquid droplets which are bombarded with deuterons at the center of the beam line.

The temperature of Li is controllable to 570 K at the maximum so that the pipe will not be got clogged. It took about 90 minutes to finish dropping the total amount of Li as 5500 or more droplets (one run). After one run Li is pumped from the bottom reservoir up to the upper reservoir by pressurizing the former.

During the run the D.C. beam current measured with a Faraday cup placed at the downstream end of the manifold is monitored with an oscilloscope. A current dip due to a droplet crossing the beam is a measure of the current flowing into the droplet.

To detect α-particles produced in the surface region of Li droplets, an SSBD is

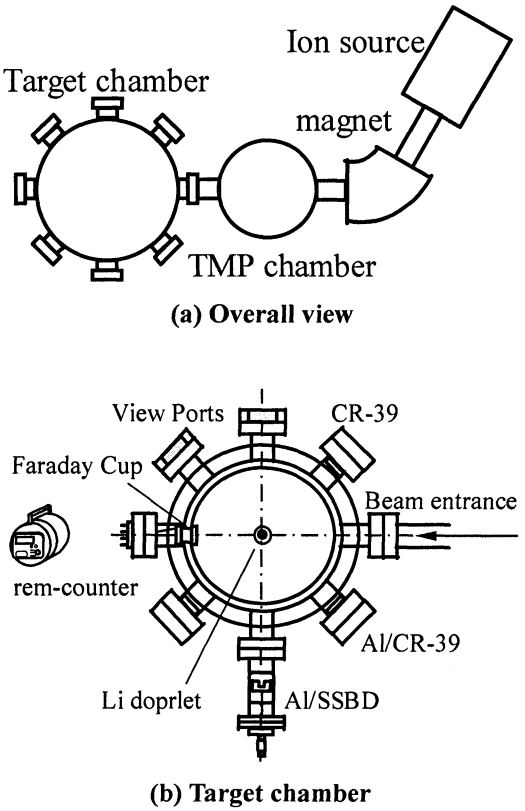

(a) Overall view

(b) Target chamber

Fig.1. Plane view of the experimental system.

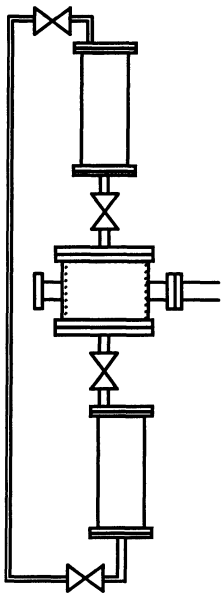

Fig.2. Vertical view of the target chamber and the Liquid Li loop.

prepared at 270°, and three sheets of CR-39 are at 45° and 315°, with respect to the direction of the incident ion beam. The solid angles are defined to 1.17×10^{-3} sr by the active area of the detector with a 5.64 mm diameter. The SSBD has been calibrated for energy using an ^{241}Am alpha source. A 12.5-μm-thick aluminum film is mounted on each detector to shield it from the Li vapor.

2.2. DATA ANALYSIS

The ^{7}Li(d,nα)^{4}He reaction rate R_m per an incident deuteron is calculated from the measured α-particle yield Y_α as;

$$R_m = \frac{Y_\alpha/2}{(N_d/2)\times N_{Li}} \times \frac{4\pi}{\Delta\Omega}, \quad (1)$$

where N_d is the number of incident deuterons, N_{Li} is the number of dropped Li, and $\Delta\Omega$ is the solid angle of the detector. Although a pair of α-particles are produced in every reaction, one of them is observed on the detector, while the other is stopped in the Li bulk.

The R_m is compared with the calculated reaction rate R_c;

$$R_c = \int_{E_{in}}^{0} n_{Li} \frac{\sigma(E)}{(dE/dx)} dE. \quad (2)$$

where n_{Li} is the Li density, -dE/dx is the stopping power of the target, and E_{in} is the incident energy of deuterons. Here continuous slowing down of the incident ions is assumed.

The hypothetical reaction rate with a thermodynamic enhancement, R_e, is expressed as follows [2];

$$R_e = R_c \times \exp\left(-\frac{\Delta G}{k_B T}\right), \quad (3)$$

where k_B is the Boltzmann constant, T is the temperature of the metallic Li, and ΔG is the change in Gibbs free energy of activation defined for the intermediate complex of the reacting nuclei, deuteron and Li. The exponential term in eq.(3) is the Arrhenius factor or the enhancement factor defined in ref.[3] .

3. RESULTS AND DISCUSSION

Here we describe the first preliminary run. The 5500 droplets of the liquid Li were exposed to the 0.1-0.2 μA beam of 20 keV deuterons up to a total dose of 7.0×10^{13}.

The energy spectrum recorded with the SSBD throughout the run is shown in Fig.3. The α-particles having about 7.5MeV, *i.e.*, a half of ^{7}Li(d,nα)^{4}He reaction's Q-value, are not appearing in the spectrum. We see only signals of electrical origin and probably those originating in cosmic rays. Similarly, we could find no trace of the reaction products in other detectors, CR-39 and the neutron rem-counter.

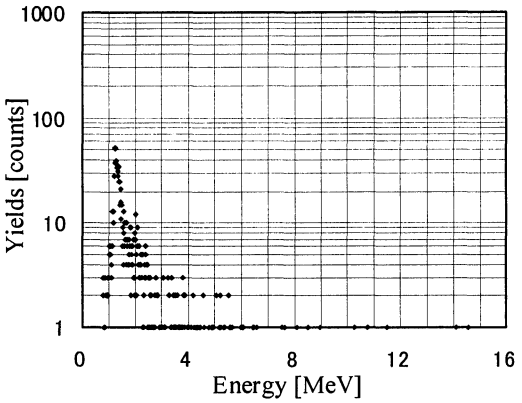

Fig.3. Energy spectrum throughout the first run.

This means that the observed reaction rate R_m calculated with eq.(1) is less than 1.5×10^{-10}. This maximum reaction rate is calculated

assuming that one count in the spectrum is ascribed to the product of the $^{7}Li(d,n\alpha)^{4}He$ reaction.

The reaction rate R_c calculated with eq.(2) is 1.8×10^{-19}. To estimate a modest enhancement for the present experiment, we assume the Li temperature of 570 K. In ref.[3] the value of Gibbs energy change ΔG has been derived to be about ΔG = -1.25 eV for a reacting Li-D atom pair to form a united atom [DLi] from the bond energy of metallic Li liquid. The enhanced reaction rate R_e taking account of the Arrhenius factor results in 1.7×10^{-8}, which is two orders of magnitude greater than the observed one. The present result implies that it is difficult to apply eq.(3) to the reaction under the present experimental condition.

Let us examine change in temperature of the droplets during their free fall. They lose energy as a result of vaporization, while they receive thermal energy from deuterons. The temperature decrease due to the former effect is estimated to be of the order of 0.1 K using a vapor pressure of 10^{-4} Pa at 570 K and a specific heat of 3.5 J/gK. The temperature rise due to the beam heating is estimated to be about 0.3K. Therefore we can expect no substantial change in the temperature of the Li droplets. A fundamental question remains to be solved, however, whether the flow of energy is small enough to keep the droplet in thermal equilibrium.

We should also check the possibility that the number of deuterons bombarding the Li target is much less than the above value derived from the oscilloscope trace. Since the droplets are floating in vacuum, there may be a possibility that effect of deflection due to electric charging-up of the droplet is strong enough to shield itself from succeeding beam particle bombardment. In Fig.4 the observed trace (the solid line) is compared with that calculated as a time-dependent cross sectional area of the d beam overlapped by the Li droplet (the broken line). We find very good agreement between them, which implies that the charging-up of the droplets has no appreciable effect on the deflection or the loss of the succeeding beam particle bombardment. The fact that the trace has a shorter rise time in the leaving phase than in the entering phase is caused by acceleration of the droplet by gravity.

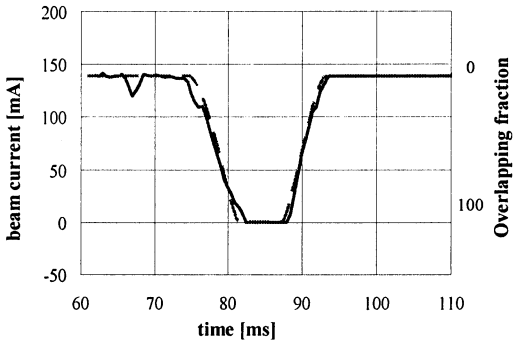

Fig.4. Oscilloscope trace of the Faraday cup signal (solid line) and that calculated as a time-dependent cross sectional area of the beam overlapped by the droplet (broken).

4. SUMMARY

Preliminary results of experiments to confirm the reaction rate enhancement has not necessarily been positive, although it is too early to deduce any conclusion. Regular work under varied conditions is needed.

REFERENCES:

[1] Evidence of Enhanced Nonthermal Nuclear Fusion, H. Ikegami, and R. Pettersson; Bulletin of Institute of Chemistry, BENF No.3 (Uppsala University, September 2002).

[2] Recoilless Nonthermal Nuclear Fusion, H. Ikegami, and R. Pettersson; Bulletin of Institute of Chemistry, BENF No.2 (Uppsala University, September 2002).

[3] Buffer Energy Nuclear Fusion, H. Ikegami; Bulletin of Institute of Chemistry, BENF No.1 (Uppsala University, September 2002); H. Ikegami, Jpn. J. Appl. Phys. 40 (2001) 6092.

(d,p)t Reaction Rate Enhancement and its Dependence on Target Material under Irradiation of D Ions

Y. Awa, T. Minari, S. Awano, R. Nishio, T. Hirao, A. Taniike, Y. Furuyama and A. Kitamura*

Department of Environmental Energy Science, Faculty of Maritime Sciences, Kobe University

5-1-1 Fukaeminami-machi, Higashinada-ku, Kobe 658-0022, Japan

*kitamura@maritime.kobe-u.ac.jp

Abstract: To investigate possible anomaly in nuclear reactions in solids, deuterium ion irradiation of deuterated Au/Pd samples has been performed with extensive measurements of reaction products and simultaneous characterization of the samples including ERDA and RBS. Using a re-regulated beam optics system, we observed the D(d,p)t reaction rate exceeding the calculated one by a factor of about 10 in the Au/Pd mixed layer with a modified composition under 7.5-25 keV D^+, D_2^+ and D_3^+ irradiation.

Keywords: D(d,p) reaction rate enhancement, Au/Pd, deuterium density, *in situ* accelerator analyses

1. INTRODUCTION

A variety of deuterium-induced reaction in metal deuterides with some yield anomaly has been reported in recent years. Three-body reactions, *i.e.*, DD(d,^{4}He)pn, DD(d,^{4}He)d and DD(d,^{3}He)t, have been claimed to take place with great enhancements of the reaction rate in TiD_x [1-3]. Nuclear transmutations in a variety of samples have also been reported by many authors, which includes experiments on forced permeation of D through a multi-layered film of Pd and CaO doped with some amounts of Cs [4].

In these reports, the deuterium densities of the samples have not always been made clear during these reactions. The three-body reaction probabilities were measured for the titanium deuterides. However, the deuterium density under irradiation was assumed. In some experiments of nuclear transmutation, the deuterium densities in the samples reached the saturation value.

Measurements of the local deuterium density in samples should be effective to identify the anomaly and clarify the origin of anomalous enhancements of the reaction rate [5]. In the present paper, we present experimental results on the D(d,p)t reaction rate and deuterium density measured simultaneously with accelerator analyses under deuterium irradiation of gold-deposited palladium (Au/Pd) samples.

2. EXPERIMENTAL PROCEDURE

A schematic of the experimental system is shown in Fig. 1. The sample is irradiated with atomic/molecular deuterium ion beams extracted from a 30-kV duoplasmatron ion source. The beams bombard the front surface of the sample in vacuum whose rear surface is exposed to deuterium gas in a reservoir. The sample can be characterized *in situ* and simultaneously by means of accelerator analyses, *i.e.*, elastic recoil detection analysis (ERDA), and Rutherford backscattering spectroscopy (RBS), during/after irradiation. Four solid state detectors (SSDs) are prepared around the sample to detect products of deuterium-induced reactions at an angle of 110° and scattered/recoil particles for characterization

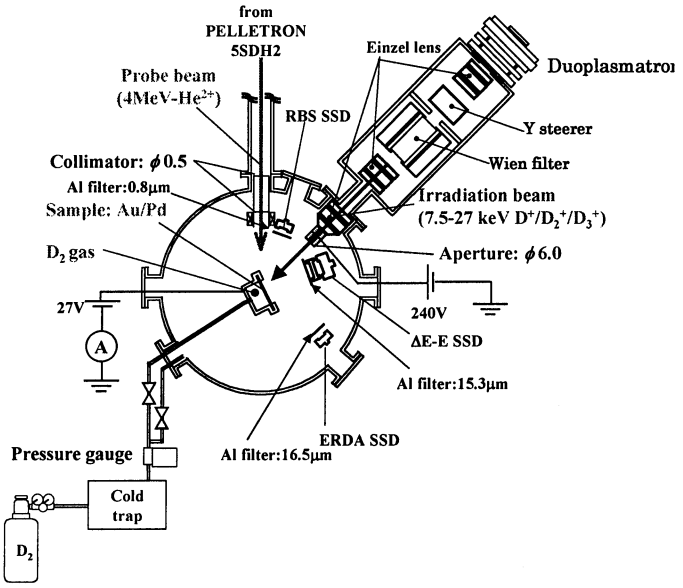

Fig.1. Experimental system.

at angles of 160° and 34° with respect to the analyzing accelerator beam. In particular, the ΔE-E counter telescope technique is employed at the angle of 110° for simultaneous measurements of mass and energy with a dual parameter MCA (DMCA). Thin aluminum films are mounted on all SSDs to shield them from secondary particles and thermal radiation emitted by the sample.

In the present experiments, some Pd samples coated with vacuum-deposited Au layers have been prepared. The Au layer prevents deuterium reemission into vacuum due to recombination on the Pd surface, which is expected to keep the deuterium density high in the Pd bulk. The typical thickness of the Au layer is several tens of nm as measured with ^{4}He-RBS method.

The DD reaction rate in Pd is calculated from the measured yield with use of the ΔE-E counter telescope. Here, we introduce a normalized yield or an enhancement factor, R_r, in order to evaluate the difference between the measured reaction probability and the theoretical one. The enhancement factor R_r is defined as the ratio of the measured reaction probability R_m to the calculated one R_c;

$$R_r \equiv R_m/R_c.$$

The measured one R_m is expressed as follows:

$$R_m = (Y_{ROI}/N_i) \times (4\pi/\Delta\Omega),$$

where Y_{ROI} is the measured proton yield of the D(d,p)t reaction during bombardment of N_i incident deuterons, and $\Delta\Omega$ is the solid angle of the detector. The TRIM85N code [5] is used to calculate the probability of the D(d,p)t reaction for a given composition of target atoms and thickness.

3. RESULTS AND DISCUSSION

The enhancement factor R_r obtained earlier during irradiation of Pd samples having a deposited layer of 70- or 150-nm-thick Au reached 800 [6,7]. The irradiation was done with beams of 15, 20 and 25 keV D_2^+ after deuterium loading by exposure to D_2 gas at a pressure of 1.0×10^5 Pa for 3 hours. However, the reproducibility was rather poor.

The poor reproducibility could be a result of a possible lack of purity in the beam particle species. We re-regulated the beam optics system composed of an einzel lens, a Wien filter, a steerer, an entrance aperture and the current measurement system to find the optimum condition. Figure 2 shows a mass spectrum of the beam emerging from the Wien filter. We expect practically no possibility of contamination of the beam by

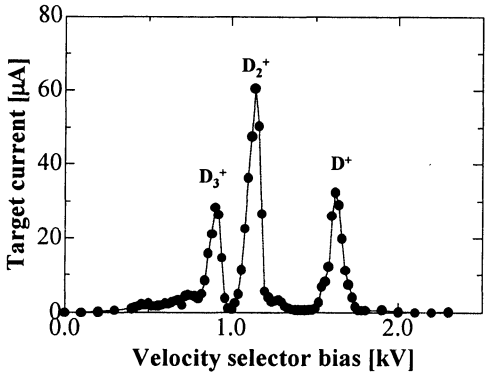

Fig.2. Mass spectrum of the 25 keV irradiation beam emerging from the Wien filter.

species other than that of interest.

During the deuterium ion beam irradiation, the Au/Pd samples were occasionally analyzed by means of RBS and ERDA methods using a 4-MeV ^{4}He beam simultaneously with the deuterium ion irradiation. The irradiation conditions together with the deuterium density and R_r that are averaged over the specified phase of irradiation are summarized in Table 1 for a Au(43nm)/Pd sample. The reaction enhancement with the averaged values of $R_r \approx 1$ - 4 is observed in and after the phase 3, when a mixed layer of Au and Pd is well formed as is analyzed below.

The typical energy spectra of RBS made at the fluence of zero, 4.2×10^{19} cm^{-2} (the beginning of the phase 5) and 7.2×10^{19} cm^{-2} (the end of the phase 5) are shown in Fig. 3. The continuum below 3.3 MeV in the spectrum originates in the α particles scattered by the bulk Pd atoms, while the peak near 3.5 MeV (a) originates in those scattered by the deposited Au atoms. With the progress of the D_2^+ irradiation, the Au(α,α) yield decreases with its spectral shape flattened and the peak energy decreased (b) until finally it almost disappears (c). In addition, the yield near the spectral edge formed by the Pd(α,α) particles decreases, and the edge goes up to the higher energy (b). The decrease in the Au(α,α) scattering yield can be caused either by the sputtering loss of the Au atoms or by formation of a mixed layer of Au and Pd. The peak flattening and the edge modification, however, can be explained only by mixing of Au, Pd and possible other elements.

The deuterium depth profiles are shown in Fig.4, which are deduced from energy spectra measured with ERDA simultaneously with RBS. In the phase 5, the deuterium density decreases with increasing fluence. This might be caused by a reduced blocking effect of the Au/Pd layer with a reduced thickness. The deuterium density of 0.6×10^{22} cm^{-3} at the fluence of 4.2×10^{19} cm^{-2} corresponds to the composition of $PdD_{0.09}$. This composition and those similarly deduced are used for the calculation of R_c and hence R_r in Table. 1.

Table 1. Irradiation condition and measured values of the deuterium density n_D and the enhancement factor R_r that are averaged over each phase of irradiation of the Au(43nm)/Pd sample.

Phase	Energy	Particle species	Flux	Fluence	n_D	R_r
[-]	[keV]	[-]	[10^{14}/cm^2·sec]	[10^{19}/cm^2]	[10^{22}/cm^3]	[-]
1	15	D_2^+	2.0	0.0-1.0	1.25	0.29
2	15	D_2^+	8.2	1.0-2.1	5.08	0.37
3	15	D_2^+	16	2.1-3.2	0.83	1.05
4	7.5	D^+	16	3.2-4.2	0.82	2.13
5	15	D_2^+	16	4.2-7.2	0.40	3.88
6	25	D^+	8.2	7.2-8.3	1.20	2.49

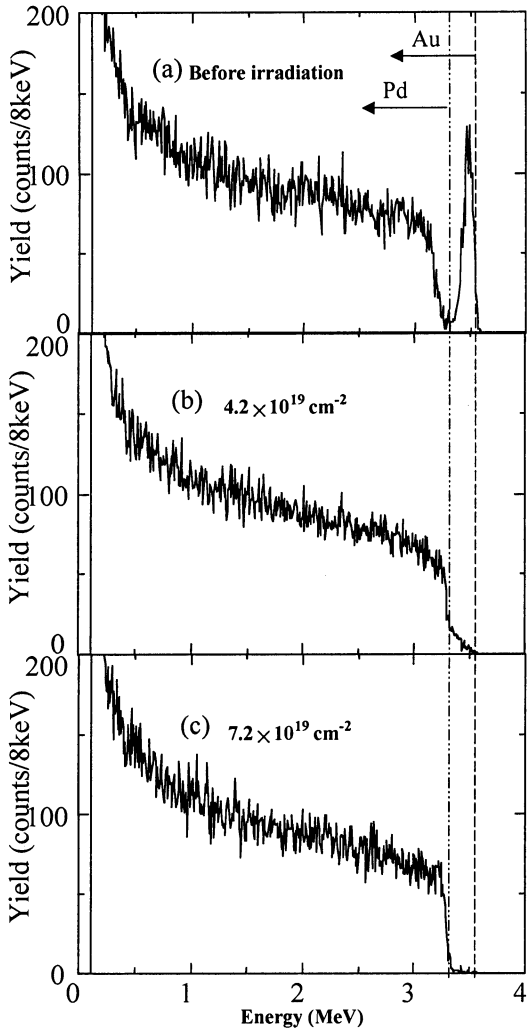

Fig.3. Energy spectra recorded on the RBS-SSD before and during 15-keV D_2^+ irradiation (phase 5) of the Au(43nm)/PdD_x sample.

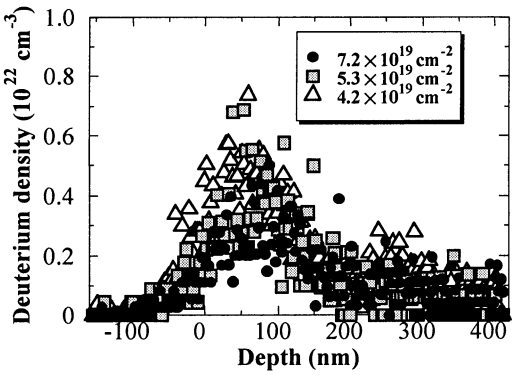

Fig.4. Evolution of the depth profile of deuterium density in the Au(43nm)/PdD_x sample during 15 keV D_2^+ irradiation (phase 5).

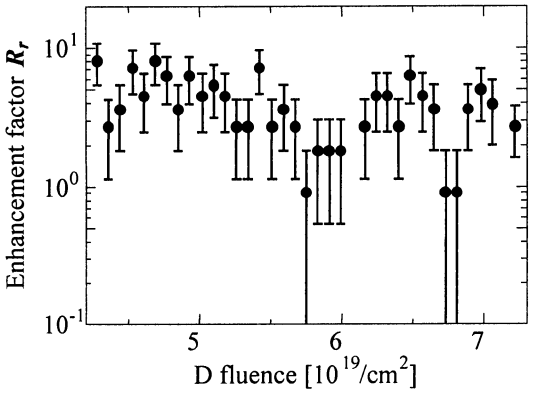

Fig.5. Evolution of R_r obtained during 15-keV D_2^+ irradiation (phase 5) of the Au(43nm)/vPdD_x sample.

The evolution of R_r during the phase 5 is shown in Fig.5. The enhancement factor R_r decreases gradually from about 8 to 3 in correspondence with the decrease in the deuterium density, implying the possibility that the enhancement is closely related to the blocking effect.

The enhancement of the reaction probability was observed only when a mixed layer was formed. However, we couldn't find clear dependence on any parameter. The enhancement factor R_r exceeding unity is plotted as a function of center-of-mass energy of the d-D pair in Fig. 6.

It is sometimes convenient to discuss the screening effect in terms of an effective screening potential U_s [2], a potential energy inside a negatively charged spherical surface. In this model, the cross section $\sigma(E)$ for a given U_s is expressed as;

$$\sigma(E) = \frac{S(E+U_s)}{E+U_s} P_b(E+U_s),$$

where P_b is the penetration probability for bare nuclei. It should be noted that the enhancement is expressed as the ratio of the measured reaction probability to that calculated for the case of

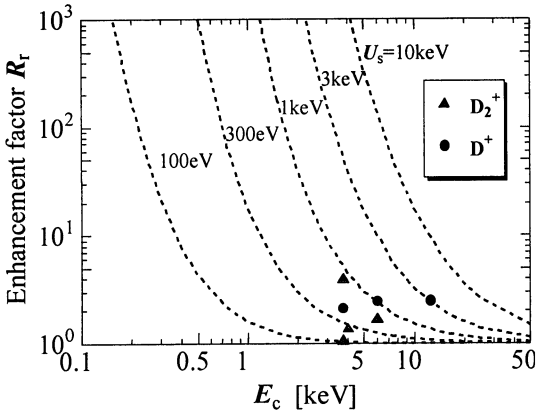

Fig.6. Enhancement factor plotted as a function of the center-of-mass energy of the incident deuteron and the target D atom. The solid lines represent the cross section enhancement for the specified shielding potential.

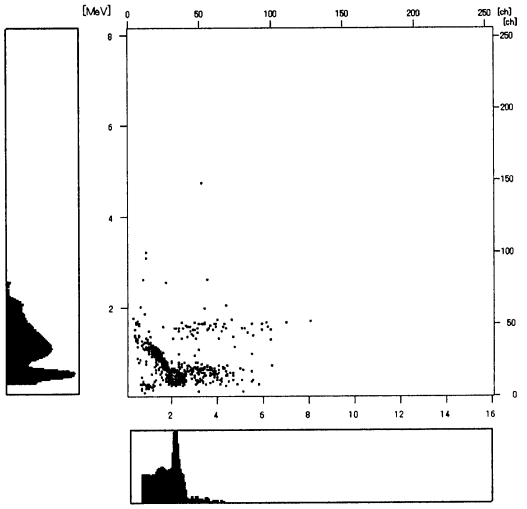

Fig.7. Energy spectra recorded on the DMCA during 25 keV D^+, D_2^+ irradiation of the Au/PdD$_x$ sample.

shielding with the universal potential which is approximately equivalent to U_s = 60 eV [7]; the enhancement factor equal to unity means the screening with U_s = 60 eV.

The experimentally found enhancement factors scatter between the lines for U_s = 60 eV and U_s = 3 keV. There might be another factor governing the reaction enhancing mechanism, or the experimental condition to realize the enhanced reaction might be very sensitive to a factor we have not yet controlled. We need further experimental evidence to confirm the anomaly.

Next we discuss unidentified peaks in the spectra. One of them observed in the DMCA spectra is shown in Fig. 7. It was recorded during 25-keV D^+ irradiation of the Au(100nm)/Pd sample. If we assume that the peak at energies (ΔE, E) = (1.4 MeV, 1.0 MeV) was formed by some charged particles, they are deuterons with energies of about 3.0 MeV before penetrating through the Al filter foil. However, since similar peaks were not observed simultaneously in other detectors, we cannot confirm that any reaction in the sample target is responsible to this peak.

4. SUMMARY

The enhancement of the D(d,p)t reaction probability reaching a factor of about 10 was observed only when a mixed layer of Au and Pd was formed. We need further experimental work to find clear dependence on any parameter.

REFERENCES

[1] A. Takahashi, *et al.*; Fusion Technol., 34 (1998) 256.
[2] J. Kasagi, *et al.*; J. Phys. Society Japan, 64 (1995) 777.
[3] A. Takahashi et al.; Fusion Technol., 34, (1998) 256
[4] Y. Iwamura , *et al.*; J. Appl. Phys. 41 (2002) 4642.
[5] A. Kitamura, *et al.*; Fusion Technol., 29 (1996) 372.
[6] M. Miyamoto, *et al.*; Proc. 4th Meeting of Japan CF Research Society, (Iwate Univ., 2003) 37.
[7] A. Kitamura, *et al.*; Proc. ICCF10, http://www.lenr-canr.org/acrobat/KitamuraAddptreacti.pdf.

Detection of d + alpha channel by 3D fusion

A. Takahashi, H. Miyamaru and T. Dairaku
Osaka University
akito@nucl.eng.osaka-u.ac.jp

To study further the 3D fusion process, experiments were done to observe 15.9 MeV deuterons which would be emitted by a possible branch of 3D fusion. Using a rather thick delta-E detector and a front thick absorption foil, coincidence spectrometry with delta-E&E counter telescope was applied to catch 15.9 MeV deuterons. As a result, [3D]/[2D] yield ratio for the d + alpha channel was observed as on the order of 1E-4 that was on the same order of the t + ^{3}He channel of 3D fusion, and anomalously enhanced with the order of 1E26 compared with the random nuclear fusion theory.
Key words: 3D fusion, 15.9 MeV deuteron, TiDx, d beam, counter telescope

1. Introduction

Why do we study on 3D fusion ? Firstly, if there happens anomalous enhancement of d-d fusion rate in condensed matter, e.g. metal-deuteride lattice, we should have enhanced density of close d-d pairs and therefore by injecting d-beam from outside we may observe enhanced 3D fusion rate as illustrated in **Fig.1**. Secondly, if multi-body deuteron fusion is anomalously enhanced in the condensed matter, we can explain radiation-less reactions with major product of ^{4}He and heat and secondary selective transmutation reactions[1-6] which may be the underlying physics of condensed-matter-nuclear reactions, or so called "cold fusion".

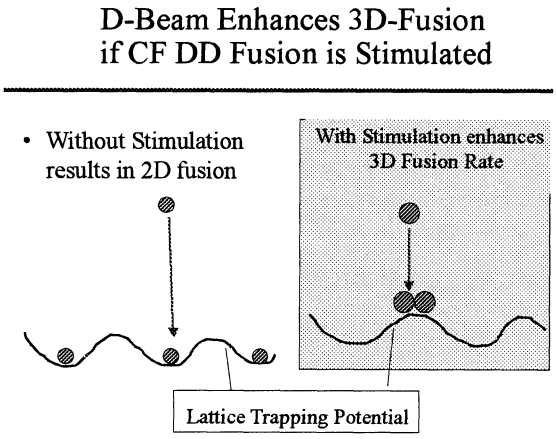

Fig.1: Why is 3D fusion a probe of "cold fusion"?

Possible major outgoing branches of 3D (D+D+D) fusion are as follows:

$$D+D+D \rightarrow {}^6Li^* \rightarrow t(4.75MeV) + {}^3He(4.75MeV) \quad (a)$$

$$\rightarrow d(15.9MeV) + {}^4He(7.93MeV) \quad (b)$$

In the past ten years, we have intensively studied the reaction channel (a) using d-beam implantation technique with TiDx targets[1-4]. A summarized result is shown in **Fig.2**, where the d-beam energy dependence of [3D]/[2D] ratios for the channel (a) is plotted.

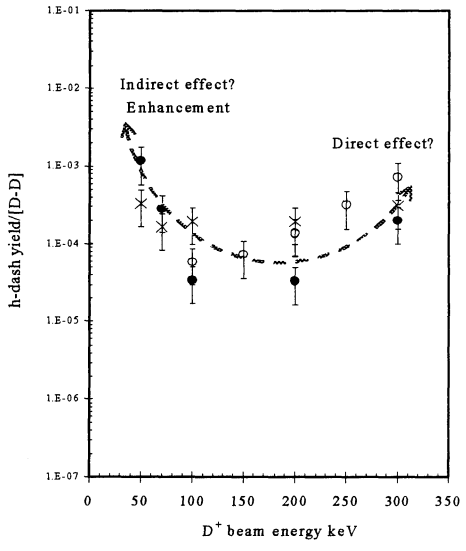

Fig.2: D-beam energy dependence of [3D]/[2D] yield ratios for the 3D to t + ^{3}He channel

In this study, we try to measure the high energy (15.9MeV) deuterons by the channel (b) and to determine the branching ratio between (a) and (b) channels.

2. Experiments

In our preliminary experiment with a single SSD detector with a 500 micron thick Ti absorption foil in front of the detector, we observed unidentified spectrum components as shown in **Fig.3**. Flat spectral component below 2 MeV was discussed to be response of neutrons by 2D fusion. And we considered the "unknown signals" over 3 MeV may be attributed to the high energy deuterons by the channel (b) of 3D fusion. So, we decided to apply a delta-E & E counter telescope coincidence spectroscopy to identify the emission of 15.9 MeV deuterons from the channel (b).

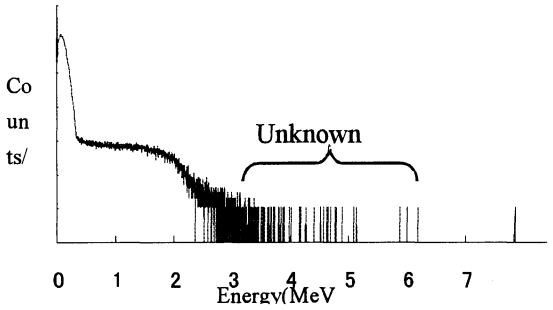

Fig.3: Unknown signals in single SSD Ek detector with 500 micron Ti absorption foil in front, by d-beam implantation experiment with TiDx target

The applied experimental system is shown in **Fig.4**. We adopted a rather thick delta-E detector of 66.5 micron thickness which absorbed 1.5 MeV of 4.9 MeV deuteron energy after 15.9 MeV deuteron passed through a 500 micron thick Ti absorption foil. The original 15.9 MeV deuteron by 3D fusion in TiDx target was estimated to lose 10.9 MeV by passing through the 500 micron Ti foil. The remaining 3.2 MeV of deuteron would be absorbed by the 200 micron E detector of SSD. Two-dimensional coincidence data of charged particle spectra with delta-E and E-detectors were analyzed with MMCA, two-dimensional multi-channel analyzer. Single energy spectrum of either delta-E or E-detector was analyzed with MCA.

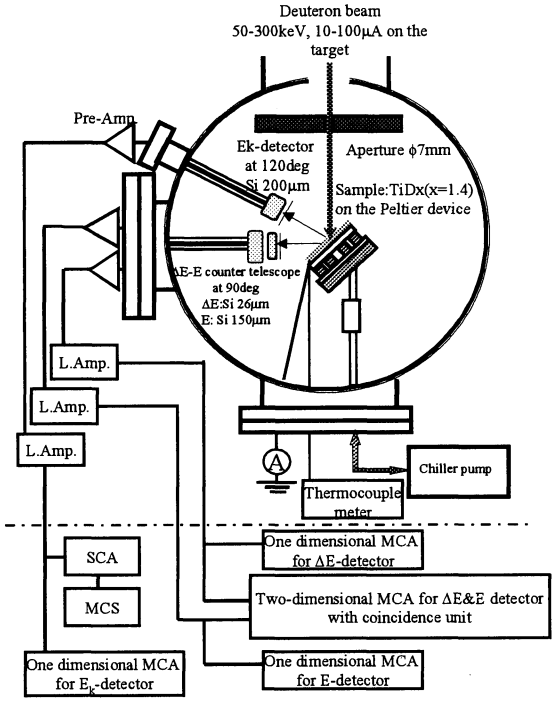

Fig.4: Experimental system: delta-E detector was replaced with 66.5 micron thick SSD and E-detector with 200 micron thick SSD. Used screening (absorption) foil was 500 micron thick Ti plate.

Deuteron beam energy for this experiment was 300 keV. Using the famous TRIM code, energy losses of deuteron by absorption foil and SSD detectors were simulated. To know the energy spread region of 15.9 MeV deuterons in the two-dimensional coincidence spectrum, a simulation calculation of energy straggling was done by the TRIM code. By the simulation, the nominal 4.9 MeV deuteron after the 500 micron Ti foil had an energy spread in the 4.5 to 6 MeV region.

An example of measured two-dimensional coincidence spectra of delta-E & E counter telescope is shown in **Fig.5**. The elliptic domain with broken line shows the region of identification for the 15.9 MeV deuteron by the channel (b) of 3D fusion. We could observe significant counts within the domain.

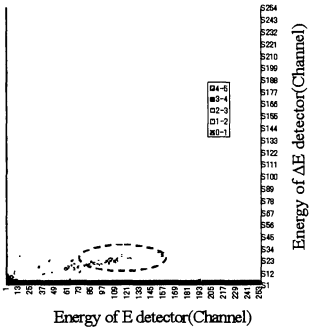

Fig.5: Two-dimensional coincidence data of delta-E & E counter telescope, for 15.9 MeV deuterons appearing within the elliptic broken line zone

3. Results and Discussions

The observed coincidence counts within the elliptic domain of Fig.5 can be regarded as deuterons by the channel (b) of 3D fusion, although we did not detect pairing alpha-particle of 7.93 MeV in the present system. However, increasing trend of counts contour in the region may be due to energy spread by the thick absorption foil. In our previous experiments[1-4], we tried to measure the 7.93 MeV alpha-particles in two ways. One was with the single Ek spectra of SSD set up at backward angle of beam-target geometry: We saw peak at around 7.4 MeV, but we found that the peak was mostly of the alpha-zero channel of ^{14}N(d, alpha) reaction as impurity reaction of nitrogen and incident deuteron in the TiDx target, and it was difficult to separate possible signals of original 7.93 MeV alpha-particles by 3D fusion from the contaminated peak of nitrogen-deuteron reactions. Another trial was to use an about 10 micron thin Ti target and set up two SSD detectors at 180 degree opposite directions in front and back side of the Ti target to take coincidence signals of 15.9 MeV deuteron and 7.93 MeV alpha-particle: We could not observe any meaningful signals in this case, probably due to deuterium diffusion-out of the target sample by elevation of temperature with d-beam irradiation.

Regarding the counts in the elliptic domain of Fig.5 as those of 15.9 MeV deuterons by the channel (b) of 3D fusion, we took the ratio with the 3 MeV proton peak counts of 2D fusion reactions in the Ek-detector set up at backward angle of TiDx target, to define [3D]/[2D] yield ratio. We obtained [3D]/[2D] ratio for the channel (b) to be on the order of 1E-4, which was on the same order of magnitude as that for the channel (a) previously studied[1-4]. From this result, we speculate that branching ratio between (a) and (b) channel is roughly one to one. By the observation of channel (b) in this work, we have again confirmed that 3D fusion rates were anomalously enhanced with the order of 1E25 to 26, compared with the random reaction theory calculation of established nuclear physics[2].

References:

1) A. Takahashi, et al.: Studies on 3D fusion reactions in TiDx under ion beam implantation, Proceedings of ICCF10, August 25-29, 2003, Cambridge USA, see http://www.lenr-canr.org
2) A. Takahashi, et al: Fusion Technology, 27(1998)256-272
3) A. Takahashi, et al.: Physics Letters A, 255(1999)89-97
4) Y. Isobe, et al: Jpn. J. Appl. Phys., 41(2002)1456-1556
5) A. Takahashi: Mechanism of deuteron cluster fusion by EQPET model, Proc. ICCF10, see http://www.lenr-canr.org
6) A. Takahashi: Clean fusion by tetrahedral and octahedral symmetric condensations, Proceedings of JCF5, December 15-16 2003, Kobe Japan (this proceedings)

Observation of Nuclear Reaction in Glow Discharge Experiment Using Deuterated Palladium Electrode

S.Narita*, H.Yamada, A.Arapi, D.Kato, M.Yamamura, M.Itagaki

Department of Electrical and Electronic Engineering, Iwate University

Morioka, Iwate, 020-8551, JAPAN

* narita@iwate-u.ac.jp

ABSTRACT

We performed discharge experiment using Pd deuteride cathode in deuterium atmosphere. Gamma ray emissions in the 80-330keV region were observed during the discharge with certain efficiency. It was assumed that a nuclear reaction took place in the Pd cathode and some short-lived radioisotopes were produced. The low-energy photofission model showed good agreement with the part of our experimental results. Elements on the Pd cathode and their isotopic abundance were analyzed by a time-of-flight secondary ion mass spectroscopy to find the evidence of nuclear reaction.

Keywords : glow(-like) discharge, Pd deuteride, gamma ray, surface analysis, time-of-flight secondary ion mass spectroscopy, low-energy photofission

1. Introduction

We have reported gamma ray emission in the 70-110keV region and the element production on deuterated Pd cathode in DC glow discharge experiment in deuterium atmosphere [1,2]. It has been supposed that a low energy nuclear reaction, producing some elements including radioisotopes, was induced in the experiment. However the reaction efficiency was quite low and the trigger condition for inducing the reaction was not understood. In this study, we attempted to increase the deuterium density in the discharge space, that is, the pressure of atmospheric deuterium gas was changed from ~3Torr to ~1atm expecting the reaction efficiency to be improved. This discharge condition was definitely different from that of the conventional glow discharge, and it was so-called "glow-like" discharge. Moreover, we precisely analyzed the energy of detected gamma rays and nuclear products aiming to specify the reaction occurring during the experiment, considering the existing theoretical model.

2. Experiment

The experiments were carried out by DC glow-like discharge with a deuterated Pd (Pd/D) foil cathode in deuterium atmosphere. The Pd sample used was 10x10x0.1mm^3 in size and >99.95% in purity. At first, the sample was washed with acetone and aqua regia for 100s. Then, it was put in a chamber and loaded with deuterium gas under 10atm pressure for ~48h. The loading ratio was determined by measuring the mass change of the sample, and it was typically 0.6-0.7. After gas loading, the sample was placed in a discharge cell. The cell made of Pyrex glass has a cylindrical shape with an inner diameter of ~12cm and a volume of ~1000cm^3. The thickness of the glass is 5mm. By using Pyrex glass cell instead of metallic one, the contamination to the sample can be minimized and the precise analysis of nuclear products is enabled. The cell consists of two parts connected to each other with silicone grease. It is connected to a vacuum system via a valve on the upper part of the cell so that we can drive out the gaseous impurities in the cell and control the pressure inside the vessel. An Au foil (0.3mm in thickness) hung by an Au wire was used as the anode. The Pd sample was placed as a cathode on an Au stand with a quartz cylinder surrounding it to prevent movement during the discharge. The gap distance between the two electrodes was ~10mm. After closing up the cell, it was evacuated to 10^{-2}-10^{-3}Torr and deuterium gas was supplied until the pressure inside became 1atm. Then, DC voltage was applied to expose the sample to discharge with currents of 2-4mA and voltage of 4000-6000V. The duration time of the discharge was 60min.

A NaI(Tl) scintillation counter (SCIONIX ϕ 25mm x 25mm crystal) was used to detect gamma rays from the experimental system. It was placed perpendicularly ~10mm away from the side wall of the cell. The photons from the scintillation counter were detected by a photomultiplier tube (PMT). The signal from the PMT was amplified and the pulse

height distribution was obtained using a multi-channel analyzer (ORTEC ScintiPack), then it was converted to an energy distribution of the gamma rays. The energy calibration for the counter was executed using ^{57}Co and ^{137}Cs, which emit gamma rays with the energies of 122.1keV and 661.7keV respectively. The energy resolutions were estimated to be ~25keV and ~80keV (FWHM) for both energies.

For some samples, the surface was analyzed by time-of-flight secondary ion mass spectroscopy (TOF-SIMS) (ULVAC-PHI:TFS-2100) after the discharge. TOF-SIMS has good sensitivity for detecting a small amount of elements on the surface, and high mass resolution. In addition, TOF-SIMS was capable of analyzing all the elements including their isotopes. However, it is difficult to evaluate the concentration of the elements quantitatively from TOF-SIMS results alone. Therefore, in this study, we only discuss the possibility of new element production qualitatively and anomaly in the isotopic abundance for the elements detected.

3. Results

3.1 Gamma ray measurement

Figure 1 shows the energy distribution measured in the absence of discharge as a background run. For most of runs with discharge using Pd deuteride cathode, quite similar distributions to that for background runs were obtained. However, the anomalous signals in the gamma ray spectra with energies below 500keV sometimes appeared. Such signals were observed in 13 out of 68 runs, ~20% of total runs. The spectra measured in those 13 runs are shown in Figure 2. Between the runs for sample-5 and sample-6, a trouble happened on the electronic system of the detector, then it was fixed and the recalibration for the system was carried out. This is why the height for the dark current signal, i.e. the peak at the lowest energy in each spectrum, was significantly lower for sample-6 through sample-13. Observing the on-line monitor, we noticed that the anomalous peaks in the spectrum were formed just after the supply of the DC power, continuously growing the discharge. If these signals were caused by the electric noise introduced by the discharge or signals continuously generated in the data acquisition system, they should have appeared in all runs. Thus, it was supposed that radioactive sources were produced during the experiment and they emitted the gamma rays. In anomalous events, some spectra have obviously two peaks and other have apparently single peak. However, if we carefully look at such single-like peak and consider the energy resolution of the detector (see above), it may contain at least two monochromatic peaks. So, in this analysis, a combination of two Gaussian functions and a linear function was chosen to be fitted to the observed spectra to determine the energy of the emitted gamma rays precisely. Table 1 shows the mean value and the standard deviation obtained by fitting the two Gaussians. The emitted gamma ray energies distribute in the range 80-330keV.

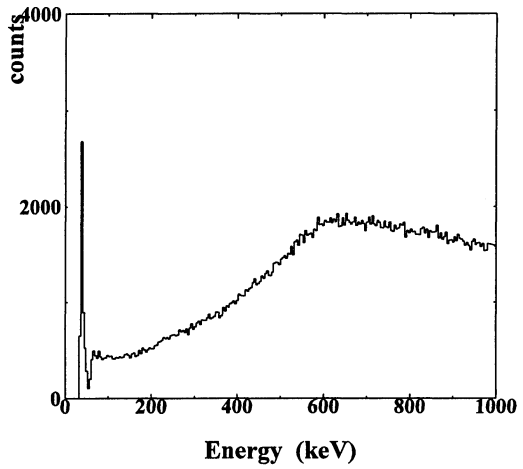

Figure 1: Gamma ray spectrum for the background run.

We also carried out a discharge experiment with hydrated Pd cathode in hydrogen atmosphere in 50 runs, and no anomalous peak in the gamma ray spectrum was observed. This is additional evidence that the anomalous gamma signals in deuterium experiment were not due to a kind of electric noise.

3.2 Surface analysis

For some Pd samples, the surface was analyzed by the TOF-SIMS to search for the symptom of nuclear reaction. As mentioned above, since it is difficult to estimate how much a specified element exists in an analyzed area by TOF-SIMS alone, our analysis was concentrated on checking the existence of some particular elements and the change in their isotopic abundance. In this analysis, we examined 8 samples (4 out of 8 are the samples with which the gamma rays were observed during the discharge) and 5 fresh samples, and compared them. As a result, we did not find clear evidence that any new elements were produced. In our glow discharge experiment (i.e. discharge with deuterium gas at a pressure of ~3Torr), Be had been found to be a candidate for the nuclear reaction product [2], but it was not detected at all. On the sample surface, there are K, Ca, Ni, Cr, Fe and Cu found as impurities. The isotopic abundance for these elements was checked, and no anomaly was found, that is, it was in good agreement with natural one.

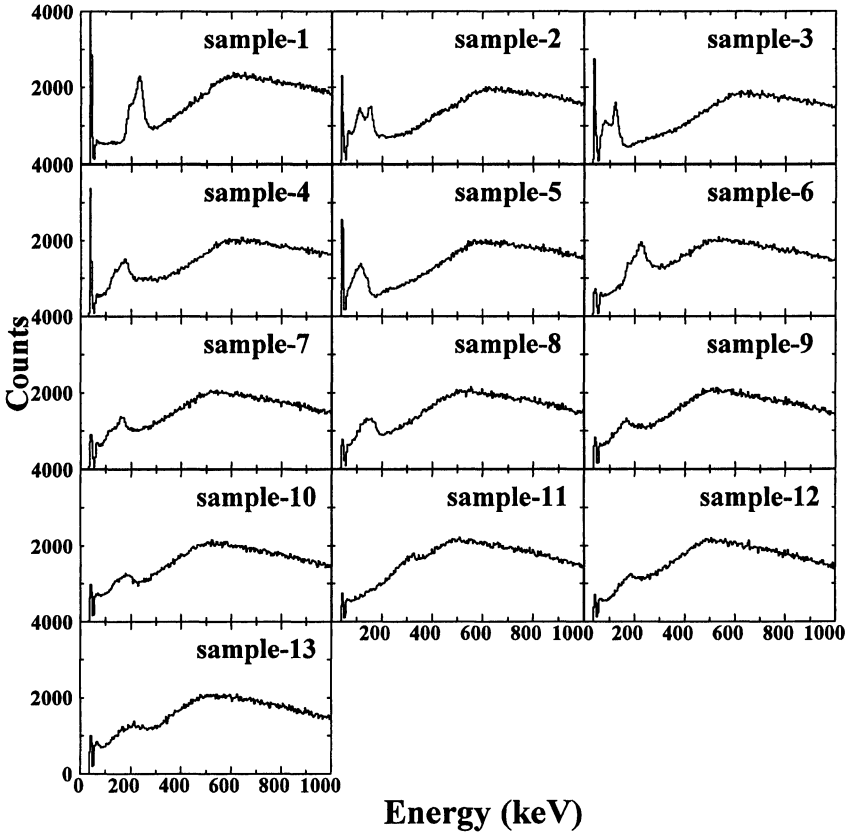

Figure 2: Anomalous signals in gamma ray spectra.

Sample ID	E1 (σ) [keV]	E2 (σ) [keV]
1	193.8 (10.2)	230.2 (16.6)
2	113.3 (15.6)	153.3 (10.6)
3	83.6 (15.2)	124.2 (15.2)
4	134.0 (14.6)	172.2 (17.7)
5	91.0 (25.3)	124.3 (18.5)
6	170.1 (17.0)	219.1 (24.5)
7	117.5 (13.0)	162.6 (19.0)
8	132.1 (23.6)	164.8 (13.1)
9	165.1 (21.5)	215.6 (12.9)
10	137.9 (20.4)	184.5 (20.2)
11	259.0 (22.2)	313.0 (27.6)
12	137.5 (11.2)	179.7 (25.5)
13	153.1 (21.8)	206.6 (29.3)

Table 1: Gamma ray energy from Gaussian fit and the standard deviation.

4. Discussion

Now the trigger condition for inducing the reaction is discussed. Figure 3 shows D/Pd ratio for all samples and the hatched histogram indicates that in the samples with which anomalous gamma ray signals were observed. As is seen in the figure, no clear evidence for the loading ratio dependence was obtained. It has been claimed that there is a strong correlation between the efficiency of the nuclear reaction in the condensed matter and the D/Pd ratio, especially for the case of deuteron fusion [3,4]. Although we have not understood the reaction that occurred in our experiment yet, it is possible that the D/Pd ratio affects the reaction efficiency even in our experiment. If so, the critical threshold of the loading ratio for effectively inducing the reaction may be much higher.

Then, the reaction efficiency can be also related to the discharge condition. In our previous glow discharge experiment with different condition, that is, at a pressure of ~3Torr, we observed similar gamma emissions in 4 out of 105 runs, 4% of total runs. It turns out that the reaction is more likely to take place in glow-like discharge rather than glow one. Therefore, the discharge under a significantly higher density deuterium environment is expected to induce the reaction more effectively. As our current cell is not designed for a discharge in a pressure of greater than 1atm, new type cell will be prepared. Moreover, in order to clarify the trigger conditions for the reaction, other discharge conditions such as current density, distribution of the electric field (shape and arrangement of the electrodes) and so on should be also considered in the future study.

Another interest is what kind of reaction happened during the discharge and how radioactive sources were produced. One of the considerable processes for the formation of radioisotopes in our experimental condition is the low-energy photofission (LEPF) of Pd proposed by Takahashi et al. [5]. They claim that a high peak flux of low-energy photons in a dynamic lattice of Pd deuteride (hydride) can lead to the fission of Pd via a selective channel. The model shows good agreement with the some experimental results on the nuclear products such as Z-distribution, mass distribution and isotopic ratio. According to the model, major fission products are stable isotopes, and there are also reaction channels in which short-lived radioisotopes are produced. Such radioisotopes can emit gamma rays with various energies in their beta decay process. Among them, the isotopes which can emit gamma rays in the 80-330keV range are listed in Table 2. In this table, the radioisotopes, which are produced with relatively lower yield in the LEPF of Pd, are not shown. Because the gamma ray detection was

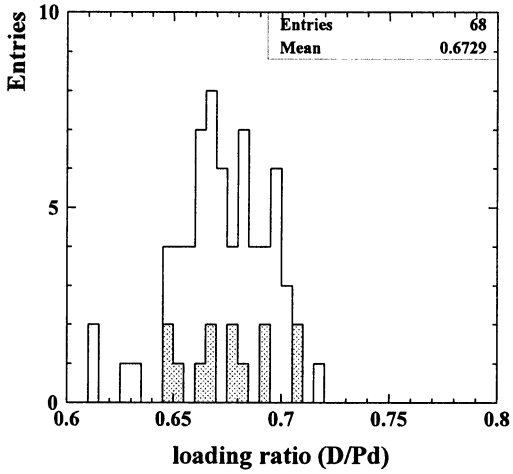

Figure 3: Loading ratio, D/Pd. The hatched histogram is for the sample in which anomalous gamma rays were observed.

Nuclide (half life)	Yield [%]	E_γ [keV] (Release rate [%])
^{50}Ca (87.7s)	1.03	71.6 (52.0)
^{56}Cr (5.9m)	1.50	83.9 (95.3)
^{63}Co (27.4s)	0.57	87.1 (48.7)
^{53}Ti (32.7s)	1.33	100.8 (20.3)
^{57}Mn (87.2s)	1.33	122.1 (13.9)
^{52}Ti (1.7m)	1.50	124.5 (98.6)
^{58}Cr (7.0s)	1.00	126.0 (75.0)
^{53}Ti (32.7s)	1.33	127.6 (46.0)
^{44}Ar (11.9m)	1.06	182.6 (66.0)
^{53}Ti (32.7s)	1.33	228.4 (40.0)
^{50}Ca (13.9s)	1.03	256.9 (98.0)
^{58}Cr (7.0s)	1.00	289.5 (18.8)
^{61}Fe (6.0m)	1.33	297.9 (22.2)
^{51}Ti (32.7s)	1.33	320.1 (93.0)

Table 2: List of major nuclides, which can emit 70-320keV gamma rays [6]. These are predicted to be produced in the LEPF of Pd. The yields were calculated by Dr. M.Ohta (Osaka University)

performed only during the discharge, i.e. 60min, radioisotopes with relatively longer lifetime are also excluded from the list. Some gamma ray energies observed in our experiment look corresponding to the predicted ones in the table. However, some signals, observed in 150~170keV, are not predicted to appear in the model. On the other hand, in Table 2, there are some isotopes emitting gamma rays which we did not observe in the experiment. Actually, on this matter, we should investigate the effective yield of gamma rays, considering the yield of each isotope in photofission process, the release rate of gamma rays, and the energy dependence of the detection efficiency for the gamma rays. In addition, since the model predicts the production of other isotopes which emit gamma rays with higher energy (up to a few MeV), such signals should be surveyed for examining the applicability of the model to the phenomenon observed in the present work.

In order to justify the LEPF model, the origin of low energy photon has yet to be clarified. Takahashi et al. have mentioned that coherent multibody deuteron fusion of deuteron in Pd can be responsible for existence of strong bursts of low-energy photons. If such reaction happens simultaneously, X-rays emission and He production can be observed as the evidence [7]. This is another interest for the future study. Additional consideration is necessary for the results in hydrogen experiment. If high flux low-energy photons are generated around the Pd cathode in the glow(-like) discharge state itself, the LEPF can be induced even in Pd hydride sample, in principle. However, we did not observe any anomalous gamma rays in hydrogen system, as described above. This result suggests that the gamma ray emission is caused by deuteron related reaction. Hence, as far as our experiment is concerned, the low-energy photon burst generated by deuteron fusion can be a candidate for the photon source inducing the LEPF.

In elemental analysis, we did not find any anomalies. If a nuclear reaction took place during the experiment, a symptom such as changes in the isotopic abundance should have been found. The LEPF model predicts that some isotopes of Ca, Cr, Fe, Cu and so on can be produced selectively by the fission of Pd isotopes. It is probable that just a small amount of the elements have been produced with the yield below sensitivity of the TOF-SIMS. For confirming the assumption, we will attempt to make the yield to be enhanced and search out the products carefully with various methods.

5. Summary

We observed anomalous gamma ray signal with 80-330keV in DC glow-like discharge experiment. It suggested that some radioisotopes were produced in the discharge. We found that the efficiency can be improved by changing the discharge condition. The LEPF model is a candidate for the model describing the reactions which may take place in our experimental system and explain the formation of radioisotopes emitting such gamma rays. Some, but not all, of our results agree with the LEPF prediction. Several ideas are considered for future study to understand the trigger condition to induce the reaction and clarify the reaction process.

Acknowledgements

We would like to extend our appreciation to Prof. A. Takahashi and Dr. M. Ohta (Osaka University) for their helpful comments on this work.

References

1. H.Yamada et al., Fusion Technol, 39 (2001) 254.
2. A.Arapi et al., Jpn. J. Appl. Phys., 41 (2002) L1181.
3. M.McKubre, Proc. of 3rd Int. Conf. Cold Fusion, (1993) 5.
4. D.Azzorone et al., Proc. of 8th Int. Conf. Cold Fusion, (2000) 199.
5. A.Takahashi et al., Jpn. J. Appl. Phys., 40 (2001) 7031.
6. R.B.Firestone and V.S.Shirley, "*Table of Isotopes*", (John Wiley and Sons, Inc.) 8th ed., (1996)
7. M.Matsunaka et al., Proc. of JCF4 meeting, (2002) 32.

Measurements of new elements in Pd-H_2 thin films.

A. Lorusso, V. Nassisi, E. Filippo*, M. Di Giulio*, D. Manno*, G. Buccolieri*, F. Celani**

Laboratory of Applied Electronics, Department of Physics, University of Lecce, I.N.F.N.-Lecce, C.P. 193, 73100 Lecce-I.
**Department of Material Science, University of Lecce*
***I.N.F.N.-LNF, Frascati (Roma)*
Tel. 0039 832 297495 Fax. 0039 832 297482 E-Mail: Nassisi@le.infn.it

Abstract: The effects of H_2 absorption in Pd thin films are investigated. 10 nm thickness Pd layers have been deposited by thermal evaporation on Si substrates. Pairs of Pd/Si samples have been loaded in a 250 cm^3 stainless steel cylindrical chambers, which were evacuated down to a 10^{-5} mbar background pressure and then filled with high purity H_2 at a pressure of 5 bar. Only one sample of each chamber has been irradiated by an excimer laser (λ=308 nm, τ_{FWHM}=20 ns, 500 shots), for one day before the opening. The applied fluence has been 20 mJ/cm^2, low enough to avoid film ablation. The chamber have been opened after 1, 2, 4, 8, 16, 32, 90 days. The samples have been analysed by Scanning Electron Microscopy (SEM), Energy Dispersive X-ray Spectroscopy (EDS) and Inductive Coupling Plasma-Optical Emission Spectroscopy (ICP-OES). Several important effects have been noticed; 1) the film surface exhibited cracks just after 4 days of soaking in H_2 atmosphere, irrespective of laser treatment; 2) after 8 days polycrystalline grains with dimensions of 1-2 μm were formed; 3) chemical composition analysis of grains exhibited elements such Al, Ca, S, Fe, Mo; 4) laser irradiation induced the increasing of grain concentration and their dimensions.

Keywords: H_2 absorption, Pd/Si, laser treatment, polycrystalline grains.

1. INTRODUCTION

The controversial phenomenon called "Cold Fusion" (CF), "Low Energy Nuclear Reactions" (LERN) or "Chemically Assisted Nuclear Reactions" (CANR) started in 1989 with the famous discovery of Fleishmann and Pons(1).

Since this work was published, a lot of experiments were performed in many laboratories: the first method to load palladium with deuterium used electrolysis cells(1). Next, the gas loading method became very utilised in many laboratories due to its low grade of contamination(2, 3). The first experiments used deuterium as loading gas because of its large probability to get nuclear reaction inside the Pd lattice, but recent studies have reported interesting results by loading Pd with hydrogen gas(4).

Recently, Iwamura et al. at Mitsubishi Heavy Industry in Japan have evidenced the presence of new elements due to transmutation processes in particular systems. They deposited a thin layer of palladium (40 nm) on a layer of CaO, which had been deposited on a thick palladium substrate. To load the system deuterium gas has been utilised. When the gas molecules diffused through the sandwich, several nuclear reaction effects were observed, including excess energy(5).

In this work we have utilized the gas loading method in Pd/Si systems and we have also observed the morphological modification of the samples on different days of treatment and the presence of different new elements from the Pd which they could be generated by the probable nuclear reactions that were induced by a strong loading of H_2 in the lattice of the samples. Moreover applying an UV laser light, the effects of gas loading marked the experimental results particularly concerning grain concentration and grain dimensions(6).

2. EXPERIMENTAL SET-UP

We have realized, by thermal evaporation technique, Pd thin films deposited on Si (100) wafers of about 1 cm^2 in surface. We have selected films of 110 nm thick because they were very efficient in new elements production(7).

They were placed in cylindrical stainless steel chambers of about 250 cm^3 in volume. Fig. 1 shows a photo of the experimental setup.

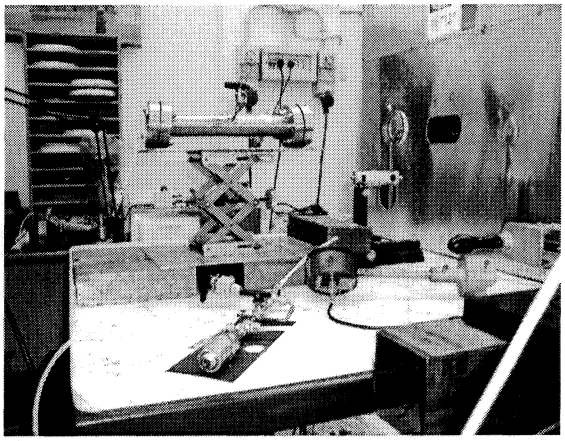

Fig. 1:Photo of experimental setup

The chambers were equipped by two quartz windows in order to allow the laser beam to go until the samples. To avoid contaminations, the chambers were carefully cleaned with acetone and dried in nitrogen flux before the experiment. Subsequently a pair of Pd/Si samples have been placed to the inside of the chambers; these last were filled with H_2 gas to maximum pressure of the exercise of 5 bar. In Fig. 2 we have a schematic drawing of a chamber: one can see as the samples are fixed to the inside of the chamber by stainless steel supports.

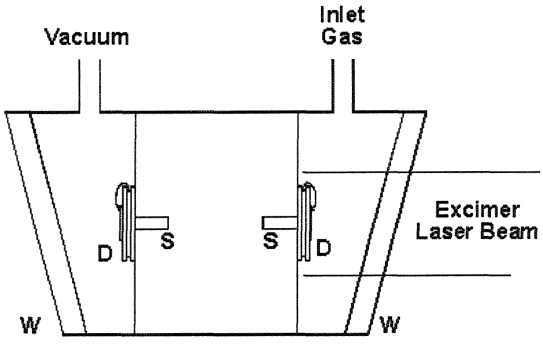

Fig. 2: Schematic drawing of a chamber. W: quartz windows; S: supports where the samples are fixed; D: film samples

The samples were loaded with H_2 for 1, 2, 4, 8, 16, 32, 90 days and only one sample from each chamber was irradiated by an XeCl home-made excimer laser (λ=308 nm, 20 ns) one day before opening the chamber, with 500 shots.

After the treatment has ended, the samples were analysed by a Scanning Electron Microscopy (SEM) and an EDX analyser. Some of these samples were analysed by ICP-OES technique too.

3 NUMERICAL RESULTS AND DISCUSSIONS

After the above protocol has executed the chambers have been opened and the samples were observed by the SEM. Different behaviours were revealed for samples kept in air, laser treated and no-treated: thus, for samples kept in air, the film surface was smooth, with mirror like aspect; instead, the samples treated and no-treated by laser showed morphological modification of the films just after 4 processing days. The morphological modifications consisted in formation of cracks just after 4 days of soaking in H_2 atmosphere and in polycrystalline grains with dimension of 1-2 μm which resulted after 8 treatment days. Fig. 3 shows an example of grains after 10 days of gas loading.

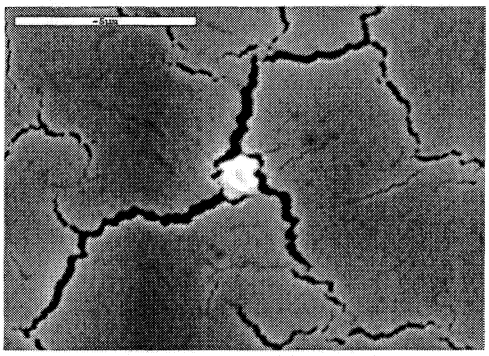

Fig. 3:Cracks and grains are evident after 10 days of treatment

By EDX analyser, we have investigated inside the grains and found the presence of new elements such as Na, S, Ca, Fe, Mo for the samples with more than 4 days of H_2 loading treated by laser irradiation. In addition, in the course of this treatment up to 32 days we have found a large number of cracks and grains and an increase of the kinds of new elements (see Fig. 4). So we can say that, for the H_2 loading experiments, the time duration of treatment was very important for the formation of elements different from Pd.

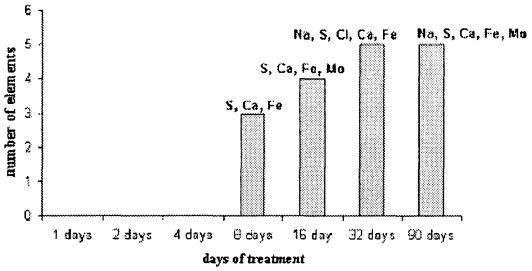

Fig. 4: Number of new elements in relation to the number of the days: no new elements before 8 days of treatment by loading in hydrogen and laser irradiation.

During a 90 days of treatment we have that the samples were very damaged because of the high gas loading.

For the samples only treated through the H_2 loading for the different days, we have revealed an increase in the number of the elements in relation to the increase of the number of treatment days.

Analysing the samples treated by both gas loading and laser radiation by SEM we have observed that the laser effect increased the density and dimension of cracks and grains. In the Fig. 5 we have an example of the film of palladium with and without the laser treatment for over 32 days.

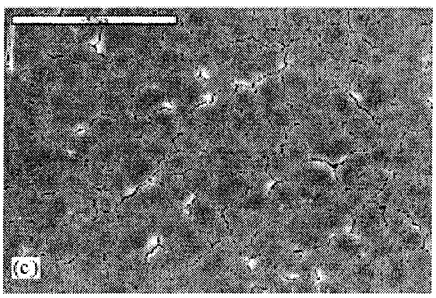

Fig. 5 c: Surface without laser treatment

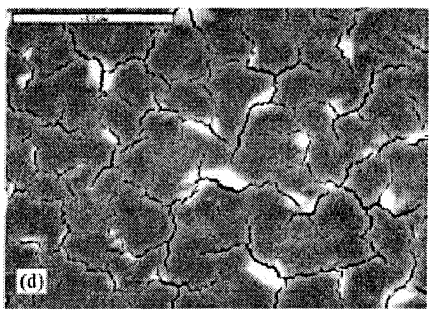

Fig. 5 d: Surface with laser treatment

Calculating the density of grains of the samples, we have found that for the samples loaded H_2 for different days with laser radiation much more grains have been produced as compared with those without laser radiation (see Fig. 6).

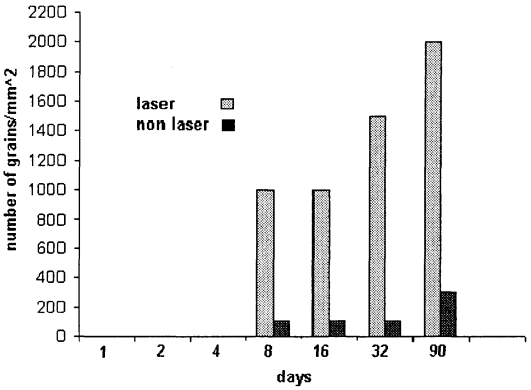

Fig. 6: Laser effect: the grain density increases stronger respect to non-laser samples

Finally we have analysed quantitatively the amounts of some new elements produced by loading of H_2 gas and laser irradiation with use of ICP-OES technique. The results are listed in Table 1. The amount of Al increases with increasing the number of days, while the amount of Fe changes in an irregular way but in any case its percentage is higher that that of the virgin sample.

Samples	Al (μg/g)	Fe (μg/g)
32 days no laser	3.2	2.3
16 days laser	1.8	21.1
16 days no laser	0.0	4.3
Virgin	0.0	2.1

Table1- Results of ICP-OES technique

However, we can say that the amount of Fe found in the samples could be due to contaminations because of the presence of the stainless steel spring used in order to fix the samples to the inside of the chamber.

Acknowledgments

The authors are pleased to acknowledge the excellent technical support of A. De Bartolomeo and V. Nicolardi.

References

1 M. Fleischmann, S. Pons and M. Hawkins, *Electrochemically induced nuclear fusion of deuterium*,J. Electroanal. Chem., **263**, p. 301 (1989).

2 F. Scaramuzzi, *Survey of Gas Loading Experiments, in Second Annual Conference on Cold Fusion,* "The Science of Cold Fusion", Como, Italy (1991)

3 Y. Arata and Y.C. Zhang, *A new energy caused by "Spillover-deuterium"*, Proc. Jpn. Acad., Ser. B, **70 ser. B**, p.106 (1994).

4 M. Di Giulio et al., *Performance study of hydrogen effect in Pd thin films irradiated by an UV irradiation*, Proc. ALT-02, Adelboden, Switzerland (2002)

5 Y. Iwamura et al. Detection of Anomalous Elememnts, *X-Ray and Excess Heat Induced by Continous Diffusion of Deuterium Through Multi-layer Cathode (Pd/CaO/Pd)*, in The Seventh International Conference on Cold Fusion, Vancouver, Canada (1998)

6 V. Nassisi, *Transmutation of elements in saturated palladium hydrides by an XeCl excimer laser*, Fusion Technol., **33**, p.468 (1998)

7 A. Castellano et al., *Nuclear Transmutation in Deutered Pd Films Irradiated by an UV Laser*, in 8th International Conference on Cold Fusion, Lerici, Italy (2000).

Heating of Heavy Water by Acoustic Wave Propagation in Magnetic Field and Phonon Maser Action of Deuteron

(Experiment)

Kohji Kamada[1] and Isao Yoshizawa

Faculty of Education, University of Ibaraki
Bunkyou 2-1-1, Mito-shi, Ibaraki Prefecture, 310-8512 Japan

Heating of heavy water of up-to 10℃ at room temperature was observed under the propagation of acoustic wave of 6 MHz with intensity of about 2 Watt / cm^2 during the scanning of the magnetic field from 800 to 1000 mT. Control experiment with light water did not show the heating. Spin-flip phonon maser action of deuteron nucleus is presumed to be the cause of heating. The 6 MHz acoustic waves produce the pumping transitions of the nuclear spin system of deuterons.

Deuteron, Heavy water, Heat evolution, Acoustic wave, Phonon maser

The experiment presented in this paper was intended to explain the heat evolution mechanism in deuteron implanted Al, which contains precipitation of the implanted deuterium in the sub-surface area, on high energy electron bombardment in electron microscope as reported before (1,2,3). The mechanism is presumed to be based on the phonon-maser action of deuterium precipitates in Al, as briefly discussed in (4).

Spin-flip phonon maser action using unpaired electron of magnetic ions in solid had been studied in the 1960's. However, the amplification of the ultrasonic wave was not effective enough because of its short wave length of sub-μ m, reflecting large magnetic moment of electron.

If we can use the nuclear spin-flip, instead of the electron spin-flip, for the phonon maser action, the wave length of the emitted phonons will be sub-mm or more, and further, the amplification of coherent phonons is presumed to be much easier. In the present paper, we employed deuteron as a candidate of the nucleus and transmitted acoustic wave into heavy water in order to induce pumping transition between energy levels of the deuteron spin system in scanning magnetic field and observed the temperature rise of up-to 10 ℃ at room temperature.

In this experiment, we transmitted 6 MHz acoustic waves into heavy water in scanning magnetic field at room temperature. However, it should be emphasized here, that the intensity of the acoustic wave used in this experiment was about 2 $Watt / cm^2$ as will be calculated later. This intensity is well below that of the threshold intensity for cavitations to occur in water. The threshold is larger than $10^4 Watt / cm^2$ for 6 MHz acoustic waves in water (5). Therefore, the present experiment is quite different from that done recently by Teleyarkhan et al. (6) under the condition of the cavitations.

In the following, we will describe only the experimental results of the heat evolution and

1) Professor Emeritus of National Institute for Fusion Science.
Permanent Adress: 173-74 Naganuma-chou, Inage-ku, Chiba-shi, Chiba-ken, 263-0005 Japan. E-mail address; kohji.kamada@nifty.com

defer its theoretical explanation to the following paper (Part 2), in which it is shown that the spin-flip maser action of deuterons in heavy water, due to the thermal Raman process under 6 MHz acoustic wave pumping, explains almost quantitatively the present results..

Figure 1 shows the experimental apparatus for charging the heavy water, into which the acoustic wave is emitted from the bottom of glass tube toward stainless steel block situated at the top of it. About 20cc of heavy water fills the glass tube which has the internal diameter of about 20 mm. No thermal insulation was provided for the glass tube. The ultrasonic transducer was set at the bottom of the glass tube. The diameter of active area of the transducer emitting the ultrasonic wave was 6 mm. The emitted acoustic wave was reflected at the bottom of the SUS block, about 68 mm distant from the transducer. Therefore, the volume of the region through which the acoustic wave propagates, which is cited as " acoustic wave road " in Fig.1, is about 2 cm^3. An insulated Type K thermocouple of 0.075 mm of diameter, covered with Cu sheath of 1.5 mm and 1.0 mm of outer and inner diameter, respectively, was inserted into the heavy water through the SUS block. The Cu sheath was thin enough to bend easily so as to be able to change the position of the thermocouple junction in the heavy water. Whole assemblies were placed between pole pieces of electric magnet. The thermocouple was connected to a digital multi-meter, via ice point reference temperature, then to a personal computer to record automatically the change of temperature throughout the experiment. Time interval of the temperature measurement was 1 second. The temperature was measured during the scanning of the magnetic field from about 800 to 1000 mT. The change of temperatures, detected by thermocouple (T.C.), was measured by the digital voltmeter. The wave form of the emitted acoustic waves were detected by the digital oscilloscope. Ultrasonic transducer worked as emitter and the receiver of the acoustic wave at the same time. The acoustic waves were emitted in burst form. The number of waves in a burst (burst count) was 100 and the repetition of the bursts was 200 μ sec . The reflected burst waves were observed in between the emitted burst at a position satisfying two times of the distance between the transducer and the reflector, namely 2 x 68 cm, with sound velocity, with the same burst count and repetition as the emitted wave, but with reduced intensity.

Figure 2 illustrates the diagram of measuring circuit. The signal generator supplies the acoustic wave with frequency of 6 MHz into the heavy water vessel which is illustrated in Fig.1. The change of temperature, detected with thermocouple (T.C), is measured by digital voltmeter. The output voltage of the digital voltmeter is recorded by the personal computer. The wave form of the emitted acoustic wave is observed by the digital oscilloscope.

The acoustic transducer was made of ceramics, $PbNbO_3$, with thickness 0.42 mm and nominal resonant frequency of 10 MHz. However, the Fourier decomposition of the emitted acoustic wave showed that the main component was of about 6 MHz, accompanied with higher harmonics up to more than 70 MHz, with intensities reduced down to less than 30 % of the main component, which is seen in Fig.3.

Figure4 shows an experimental result showing the temperature change of heavy water on the

acoustic wave propagation during the scanning of the magnetic field from about 800 to 1000 mT in 32 minutes.

Two kinds of the temperature change are seen in this figure. One is that of rather gradual and continuous temperature rise of about 1℃ which looks like "back ground" temperature rise as seen in Fig.4. Another temperature changes are very abrupt showing sharp peaks like those in Fig.5, which are details of the two groups of relatively large temperature peaks observed near 890 mT, (a), and 1000 mT, (b), in Fig.4.

The ordinate and abscissa of these figures are thermocouple output voltage and the magnetic field strength, respectively. The magnetic field strength was measured with proton NMR during the scanning and showed almost linear increase with the scanning time. The temperature was measured at the center of the region through which the acoustic wave propagates from the ultrasonic transducer toward the reflector.

These temperature rises were considered to be a result of the heat evolution caused by the phonon-maser action, namely, the induced emission and amplification of the coherent phonons due to the spin-flip of deuteron nuclei. The maximum temperature rise observed in this experiment was about 10 ℃ as shown in the figure, and the duration of the temperature rise was one to ten seconds or so for larger peaks and several minutes for some of the smaller temperature rises.

The reason of these apparently abrupt, but not continuous, behavior of the temperature rise may be presumed as follows; (1) because the heavy water was not thermally insulated at all, and, at the same time, the heated region was surrounded by un-heated heavy water with 20 mm of outer diameter, heat generated in the central region close to the junction of the thermocouple may rapidly diffuse away resulting in the peak of temperature, and (2) since the temperature was measured by only one thermocouple, the temperature change occurred at places distant from the junction of the thermocouple could not be measured accurately. The thermocouple junction used in the experiment was naked so as to be sensitive as possible to the temperature change. The observed amount of the temperature change would depend on the distance of the heated place, where the phonon maser action takes place, from the junction of the thermocouple. Therefore, one of the reasons for observing the smaller temperature changes in between the larger peaks in Fig.4 can be presumed to correspond to the phenomena occurred at places distant from the junction. The "back ground" like temperature rise of about 1 ℃ mentioned above would reflect the more frequent heat evolutions at places more distant from the junction.

Other than the experimental reasons for observing many temperature peaks described above, more fundamental reason peculiar to the maser action in liquid, but not in crystalline solid, will be mentioned in Part 2.

Control experiment using light water, H_2O, is shown in Fig.6 (a). It is clearly seen that no temperature change occurred in light water.

Noise measurement was done with the same procedures described above, but without the acoustic emission. The result is shown in Fig.6 (b), which was measured under the noise source working. The main noise source in the present experiment was the instrument called ICAP (Inductively Coupled Argon Plasma Emission Spectro-Photometer), which is situated in the

same building with the present experimental site. The noise caused by this instrument was avoided by providing Al foil over the circuit of the thermocouple.

Finally, we will estimate the energy gain obtained in this experiment. In the experiment described above, the input energy into the heavy water is the sum of energy of the acoustic wave, W_u, and that of the magnetic field, W_H. Thee intensity I_u of the acoustic wave propagating in heavy water is given by $I_u = P^2 / \rho S$, where P is the amplitude of acoustic pressure. P =2eV/t was calculated with piezoelectric constant e = 3.5 Coulomb/m^2, which is a nominal value for the material $PbNbO_3$ used in this experiment, and the thickness of the piezoelectric film t = 0.42 mm. The applied voltage was about 10 volt. The The acoustic impedance of water $\rho S = 1.5 x 10^6$ *Newton* · sec *ond* · m^{-3} with its density ρ and sound velocity $S = 1.5 x 10^5$ *cm* / sec . Therefore, $P = 1.7 x 10^5$ *Newton* · m^{-2} and I_u = 1.9 Watt · cm^{-2} was obtained, and further the energy of the acoustic wave $W_u = I_u / S$ = 130 erg · cm^{-3}. The energy of the magnetic field is given by W_H = 10 erg cm^{-3} when H = 1000 mT.

On the other hand, specific heat of heavy water is 4.2 joule/gm / K at 20 ℃, giving W_{heat} = 4.2 x10^8 erg cm^{-3} for the temperature rise of 10 ℃. After all, the energy gain is given by

$$W_{heat} / (W_u + W_H) \sim 3 x 10^6$$

This energy gain is unexpectedly large in comparison with other nuclear process such as nuclear fusion. This is clearly an evidence of the fact that the heat evolution observed in this experiment is not due to the nuclear fusion caused by the cavitationsuch as observed in (6).

The present experiment should be observed as a measurement in a transient process between the heat generation, due to the phonon maser action of deuterons, and the escape of the generated heat into surrounding heavy water. For more exact measurement of the temperature rise, thermal insulation of the heavy water is requisite. By improvement of the experiment, we can expect higher temperature rise and higher energy gain to be obtained. Further, if we superpose another acoustic wave of frequency different from that for the pumping, much more temperature rise would be expected.

As conclusions, the temperature rise up-to 10℃ was observed in heavy water under the propagation of 6 MHz acoustic wave. The experimental energy gain of more than 10^6 was obtained experimentally, which could be larger if experiment was properly designed.

The present research is supported by the REIMEI Research Resources of Japan Atomic Energy Research Institute. The authors acknowledge Dr.M.Sakaki of the Ibaraki University for his suggestions and co-operations in the course of the experiment

The authors also acknowledge Prof.Y.Kogure of Teikyou Science University for his suggestions on the ultrasonic experiment.

References

(1)K.Kamada, H.Kinoshita and H.Takahashi,

Jpn.Jr.Appl.Phys. **35**, 738 (1996).

(2) K.Kamada, H.Kinoshita, H.Takahashi and H.Kakihana, J.Atom.Energy.Soc.Japan, **A426** (1996) (in Japanese).

(3) K.Kamada, Y.Katano, Y.Enokido, N.Ookubo and I.Yoshizawa, Rad.Eff.Def. in Solid, **159**,275 (2002).

(4) K.Kamada, Fus.Eng.Des. **60**, 219 (2002).

(5) T.J.Mason and J.P.Lorimer, "Sonochemistry Theory, Application and Uses of Ultrasound in Chemistry", John Wiley & Sons, New York.

(6) R.P.Taleyarukuhan, C.D.West, Jr.,R.I.Nigmaturin, nd R.C.Block et al.; Science **295**, 1868 (2002)

.

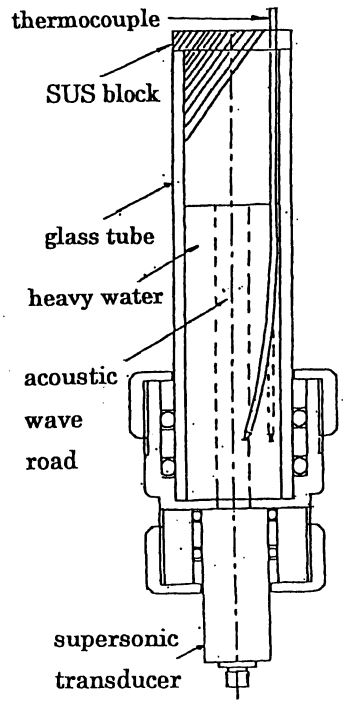

Fig.1. Illustration of heavy water vessel equipped with ultrasonic transducer and thermocouple.

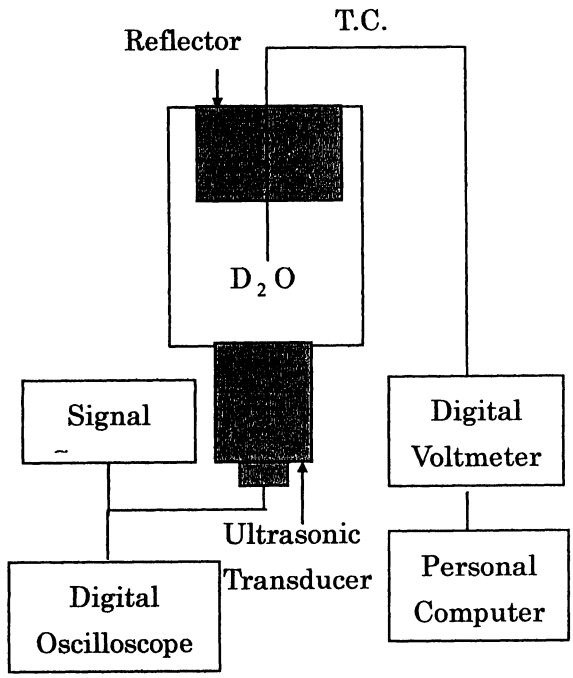

Fig.2. Diagram of measuring circuit used in the experiment

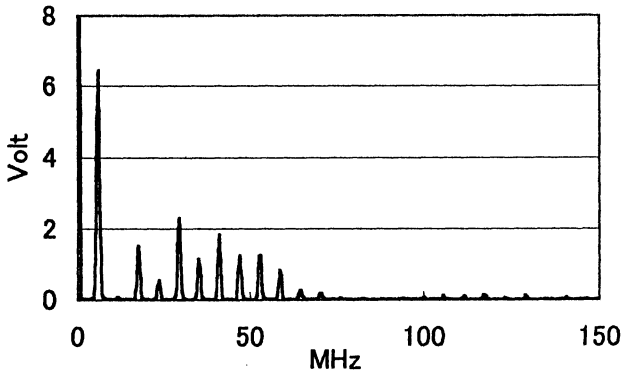

Fig..3. Fourier decomposition of the acoustic waves emitted for the pumping.

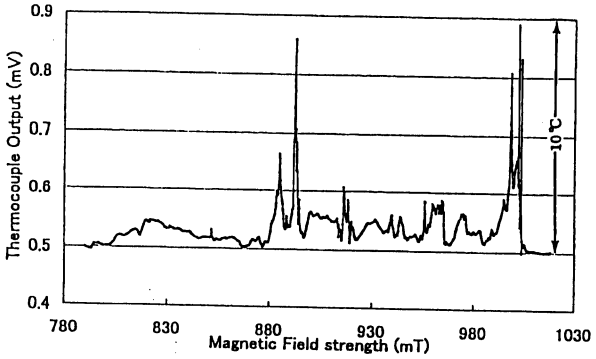

Fig.4 The Temperature rise observed in heavy water 6 MHz acoustic wave was applied for the pumping during the scanning of magnetic field..

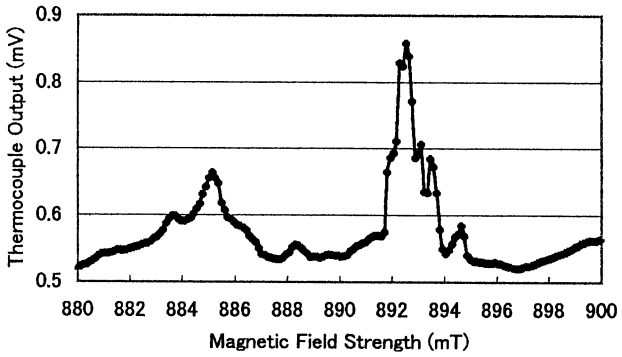

Fig.5(a) Detail of a part of the temperature rise in Fig.4..

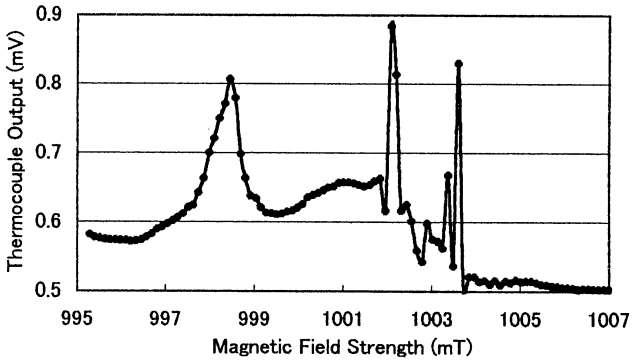

Fig.5(b) Detail of a part of the temperature rise in Fig.4

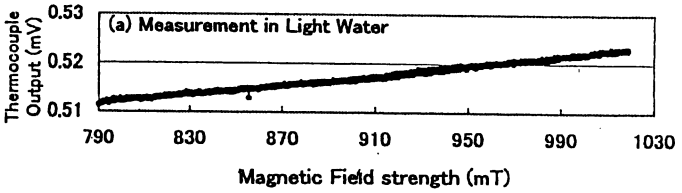

Fig.6 (a) Temperature change in light water, H_2O .

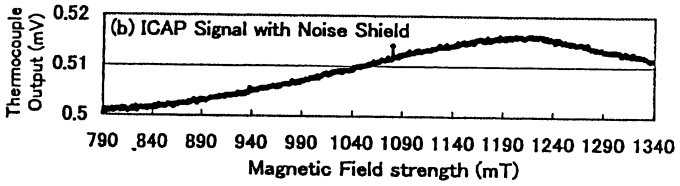

Fig.6 (b) Noise level measurement during ICPA operation .

Neutron emission from D_2 gas under magnetic field at low temperature

Tadahiko Mizuno, Kenichi Himoro, Tadashi Akimoto,
Tadayoshi Ohmori, Yoshiaki Aoki[1]

Division of Quantum energy engineering, Graduate School of Engineering,
Hokkaido University, Kita 13 Nishi 8, Kita-ku, Sapporo 060-8628, Japan
1: Center for advanced Research of Energy Technology,
Hokkaido University, Kita 13 Nishi 8, Kita-ku, Sapporo 060-8628, Japan
mizuno@qe.eng.hokudai.ac.jp

Abstract

We observed neutron emissions from pure deuterium gas after cooling in liquid nitrogen followed by compression under a magnetic field. The neutron count, and duration of the release, and the time of the release after treatment was initiated all fluctuated considerably. Neutron emissions were observed in ten test cases out of ten. Compared to the experiments in which neutrons were observed with electrolysis in a heavy water solution, repeatability was highly good and the neutron count was high.

Keywords; neutron, D_2 gas, magnetic field, Low temperature

1. Introduction

In 1989, Fleischmann and Pons [(1)] reported that excess heat from palladium cathode electrolyzed in heavy water, so-called cold fusion reaction. However, reproducibility and control of the phenomenon have been difficult, and although many researchers attempted to replicate, most failed. If we assume the reaction is some form of a normal d-d reaction, there should be a much higher neutron flux. However, there are few reports of the neutron observations in the literature of [(2,3,4,5,6,7,8)]. The authors have examined many of the reports made until now of neutrons and have reached the following conclusions.

First, neutrons and excess heat are rarely observed, but when they are observed, they occur suddenly after electrolysis and discharge have continued for a long time. Second, many instances have been reported in which these effects began when some triggering reaction occurred. Third, it is well known that almost all cold fusion experiments have been performed by absorbing the deuterium into the reaction system at first; the electrolyte contains almost pure deuterium gas.

Based on these considerations, we conclude the cold fusion reaction must be something quite different from conventional d-d fusion. Furthermore, the reaction must involve factors other than absorption of deuterium. Especially after electrolysis and discharge of deuterium has continued for a long time and the deuterium has been replenished, some trigger is very likely to be added in with it. Also, in view of these considerations, we predict that certain triggers will be needed to give rise to the reaction.

We produced an anomalous neutron burst, using what seems to be a rather simple method. We introduced pure D_2 gas into a glass tube, keeping the pressure at several atmospheres. The glass tube was cooled to the temperature of liquid nitrogen. Then a magnetic field was formed around the tube. At that point, we observed the strong neutron burst.

2. Experiment

Figure 1 shows schematic representation of the measurement system. We used pure D_2 gas for the reaction material. The reaction cell was a Pyrex glass tube of 6mm diameter,

3 mm inner diameter and 100mm in length. Another Pyrex glass vessel of 50mm diameter was put around the reactor tube, and filled with liquid nitrogen. A coil wound in a spiral around the reaction tube produced a magnetic field. The magnet coil is 1.5mm diameter of copper wire, 300m long, and the turn number was about one thousand. The entire system was put inside a stainless vessel with the outer surface insulated by Styrofoam insulation, which in turn was covered with outer stainless steel plates, 1.5mm thick, to prevent electromagnetic noise from reaching the neutron measurement system. Liquid N_2 gas was supplied into the vessel to cool the reactor tube.

The maximum magnetic field was

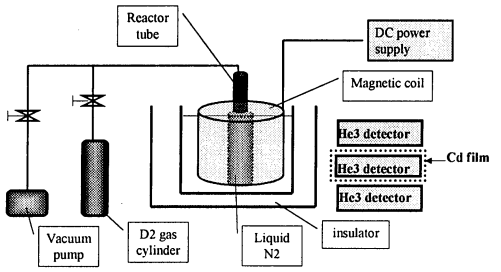

Fig. 1 Schematic representation for the experimental system

10kG in the center of the reaction tube. The current for the magnetic coil was supplied by a stable direct current power supply through a resistive wire. The magnetic field passes through the reaction tube along the length. The height of the magnetic coil is 100mm, that is, the same as tube length. The current passing through the coil was changed from 0 to 100A; the intensity of the magnetic field was changed from 0 to 10kG.

Neutrons were measured with three external He3 detectors, each 2cm diameter and 10cm in length, placed around the cell, separated 20cm from the cell. All the detectors were surrounded by cylindrical plastic neutron moderators, 12cm diameter and 15cm high. The detectors were placed inside cylindrical moderator, with the open end of the cylinder facing the cell. To reduce noise, the detectors were covered by electromagnetic shielding. After calibration, neutrons and noise were distinguished by covering one of the detectors (C-Cd) with 0.5-mm thick Cd film. A neutron entering through the plastic moderator will lose energy and be absorbed by the foil, while electromagnetic noise easily passes through the Cd material. The detectors were calibrated with a standard Cf252 neutron source (2.58 x 10^4 decay/s).The background count was estimated as under 0.008 $\pm$ 0.003c/s. A typical count under these conditions was 5 $\pm$ 1c/s from the standard neutron source. This means the total counting efficiency is estimated as 0.0002.

3. Result

The reaction was triggered by a dynamic change in experimental conditions. A particularly striking example is shown below. Fig. 2 shows the background counts after the reactor tube was cooled with liquid N2, but before deuterium gas into the tube or a magnetic field was imposed. The background count for each 10min was 1.61

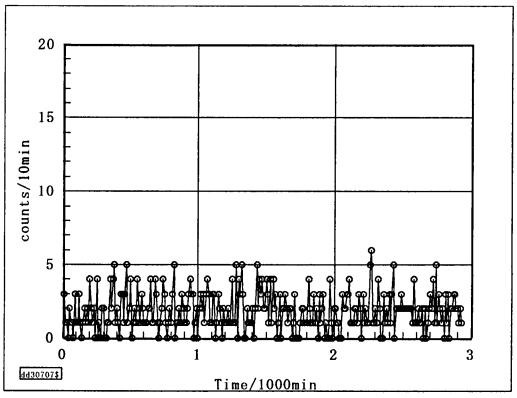

Fig. 2: Background neutron count

+/- 0.5 counts.

The number of the background count and the fluctuation were same in the absence of one or two of the three factors: the deuterium gas in the reactor tube, the magnetic field and cooling by liquid nitrogen.

Figure 3 shows the typical neutron counting rate in 10min after 3 atmospheres of D_2 gas filled the tube, a magnetic field of 8kG was imposed, and the cell was cooled in liquid nitrogen. The magnetic field was changed to 10kG at 1200s, by increasing the current. About 20 seconds, a low-level

neutron emission began, and after 50 seconds, a sudden neutron burst was observed. In this experiment, the reactor tube was filled with the pure deuterium gas up to 3 atmospheres, and the liquid N_2 was put into the vessel holding the reactor tube, and the magnetic field was imposed in the last step. In other experiments, these steps were taken in a different order. In this example, cooling of the deuterium gas was continued for a considerable time and neutron emission was

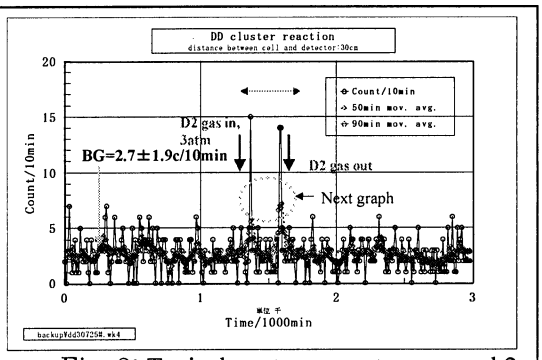

Fig. 3: Typical neutron counts averaged 2 counters for 10min, D_2, 8kG and liq. N_2 temp. C-Cd showed no increase. of neutron.

sporadically observed when the electromagnetic field was changed. However, in other runs, neutron emissions were observed immediately after liquid N_2 was added.

Figure 4 shows the neutron count that was calculated from Fig. 3. Here, the neutron emission occurred in a few seconds. Fig. 3

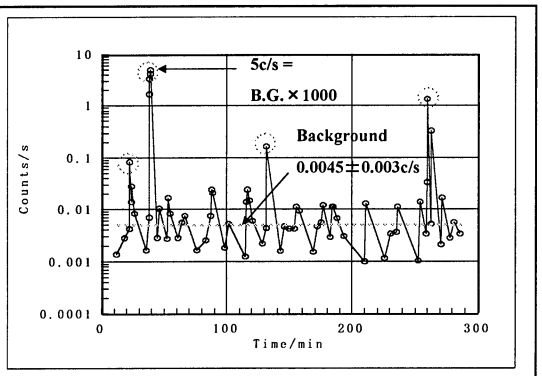

Fig. 4: Recalculated neutron count for Fig. 3.

was not exact because the count rate was averaged in 10min segments. Fig. 4 shows the burst that occurred from 1300s to 1600s in Fig. 3. The neutron burst of 5.5c/s is 1000 times higher than the background counts. Bursts occurred twice within 300 seconds. The total neutron emission can be estimated from the counting efficiency of 1.7% and geometrical factor of 1.18%, and it is 27500c/s.

Figure 5 shows another typical result of neutrons emitted when the tube was first supplied the magnetic field and then cooled by liquid N_2. Here, the neutron emission occurred immediately after liquid N_2 was added. The count rate increased up to a peak within a few seconds and decreased a few seconds later. Total neutron emission for this brief period is estimated as 5×10^5. However, no more neutron emissions were observed after that, even when the input magnetic current was increased up to 100A for 4000s. In other examples, the total neutron count ranged from 10^4 to 10^5, and emissions lasted 1 ~ 4000 s. All cases were marked by a characteristic high level of neutron emissions at first, which gradually declined.

Figure 6 shows the neutron count that was calculated in the burst time from Fig. 5. Here, it shows the neutron burst during 0s to 120s in Fig. 5.

Figure 7 shows the case of hydrogen gas under 8kG of magnetic field at –196℃. First, the tube was evacuated and the magnetic field was fixed at 8kG. After that, at 220s, hydrogen gas was introduced into the tube, and the hydrogen gas was removed at 3430s. No neutron burst was observed during the time hydrogen gas was present in the tube.

Figure 8 shows an example where the temperature was kept at room temperature, 20℃. Deuterium gas was kept in an 8kG magnetic field.

The neutron emission measurements under various conditions are shown in Table 1. The necessary condition to make the neutron burst was deuterium gas, magnetic field and temperature. Neutrons were not generated when one of these conditions was not met. The generation of the neutron when the intensity of magnetic field was changed has not been examined systematically. We usually kept the intensity of the magnetic

field constant to avoid noise from the current change and magnetic influence on the measurement system. We cannot reach a conclusion about correlation between the magnetic field intensity and the neutron emission. However, when a magnetic field was not imposed at all, neutrons were not emitted. We conclude that deuterium gas, a magnetic field, and a low temperature are all necessary for the neutron generation.

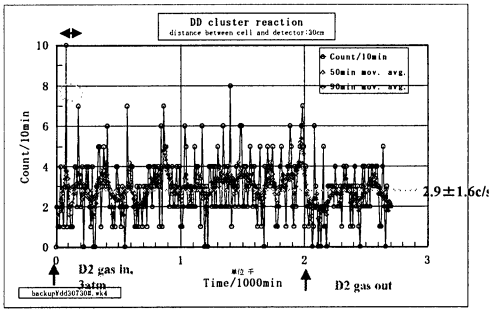

Fig. 5: Averaged neutrons count for 10min.

Neutron emissions from the cooled D_2 gas following a change in a magnetic field are very difficult to explain by the models proposed heretofore, which involve d-d fusion reactions. These models assume that neutron emissions occur when deuterium gas alone is present; they suggest nothing about a magnetic field or low temperature; and they predict that emissions must be accompanied by excess heat and tritium production.

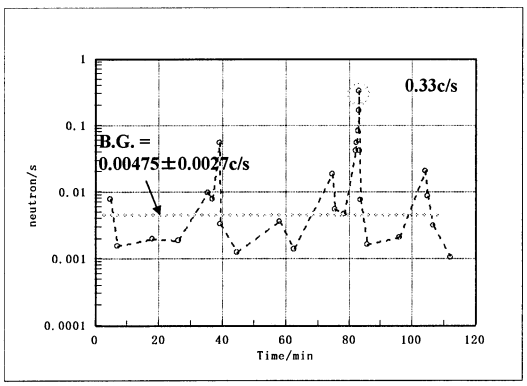

Fig. 6: Recalculated neutron count after supplied the magnetic field of 5kG; the tube was filled with 3 atmospheres D_2 gas under room temperature and cooled to liquid N_2 temperature. After tube was cooled by liquid N_2, the neutron emissions suddenly occurred.

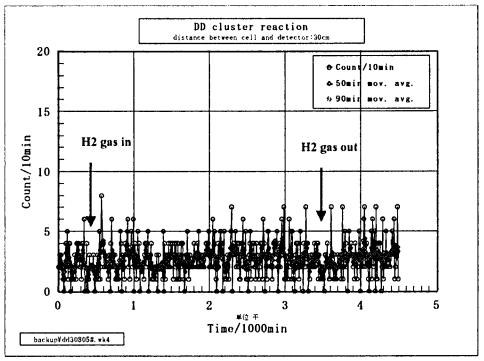

Fig. 7: Neutron count for H_2

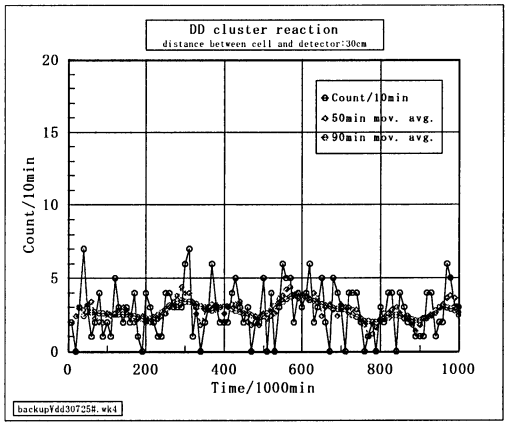

Fig. 8: Neutron count for D_2 gas at normal temperature.

The reaction we observed came about after cooling by liquid temperature in the magnetic field, and the reaction appears to be highly reproducible. We conclude that the models proposed heretofore based upon d-d reactions are inadequate to explain our present results, which must involve the magnetic field for the nuclear reactions.

4. Discussion

Many theoretical models have been proposed to explain anomalous results from cold fusion or LENR (Low Energy Nuclear Reactions) as it is now sometimes called. That no observable fusion rates (e.g., d+d fusion rates) can take place in stationary states of metal deuterides is almost proved. Possibilities may exist in transient states of deuteron motion in solids [9,10,11]. If we require a very drastic enhancement of any fusion rates that can reach the observed heat level, the following three conditions should

simultaneously be fulfilled:
1. A dynamic mechanism should exist for forming close clusters of more than two deuterons within 0.02-nm (comparable to a de Broglie wavelength of 1-eV deuteron) space in solids.
2. Quantum mechanical tunneling through the Coulomb barrier, i.e., barrier penetration probability should be enhanced very much, should be more than 10^{-6}. In other words, we need super screening. To depress the Coulomb repulsive potential this much, squeezing of quasi-free electrons in metal deuterides during the transient dynamics should occur in local points where deuteron clustering is taking place.

The present LENR experiment result can be explained by the following mechanism. The deuterium atom that was coherent in a metal forms a cluster, and it induced the nuclear transmutation, and generated heat and other products. Deuteron causes the D-D nuclear reaction under a specific condition and formed the D-cluster in the metal. The cluster generated a nuclear reaction by a collapsing reaction and then generated a light element (atomic weight 3-12). At the time, a magnetic flux was spontaneously emitted from the reaction and caused a nuclear transmutation on the host metal atom. The generation of excess heat is considered followed product of the nuclear fission of a metal atom by a nuclear collapsing of D-cluster and the transmutation.

Neutrons are assumed either to be present in the lattice within a stabilizing structure [12] or to be created by collapse of an electron [13,14,15,16,17,18,19,20,21,22] into the nucleus of a hydrogen or deuterium. The latter collapse makes a di-neutron [23,24] The importance of a neutron presence is suggested by the unusual effects observed when an external neutron flux is applied to electrolyte cell. [25,26,27,28,29] Apparently, the environment acts like a neutron amplifier. In addition, one might ask why more neutrons are not detected, as they are being released or created within the cell, especially when thin cathodes are used?

Fisher [30,31] has proposed that large, stable neutron clusters can form and that these can attach themselves to normal nuclei to produce super-heavy atoms. A small concentration of such atoms is proposed to be present in all matter. Under the right conditions, these neutron clusters are released, thereby causing novel nuclear reactions. The work of Oriani [32] supports the existence of super-heavy carbon in electrodes subjected to chemical assisted nuclear reaction processes.

5. Conclusion

We have confirmed clear neutron emissions from pure deuterium gas after cooling in the liquid nitrogen followed by compression by the magnetic field. The neutron count and duration of the emission and the time during test was fluctuated considerably. The repeatability of the phenomenon was excellent and the neutron count was high.

Table 1. Neutron counts in various conditions

Gas	Magnetic field	Temperature	Neutron counts
Air	8kG	20℃	0.60c/min
Air	8kG	-196℃	0.58c/min
Vac.	5kG	20℃	0.59c/min
Vac.	8kG	-196℃	0.54c/min
H2	8kG	20℃	0.52c/min
H2	8kG	-196℃	0.82c/min
D2	8kG	-196℃	5c/s

References

1. M. Fleischmann and S. Pons: J. Electroanal. Chem. 261 (1989) 301.
2. Chicea, D. and D. Lupu, *Low-intensity neutron emission from TiDx samples under nonequilibrium conditions.* Fusion Technol., 2001. **39**: p. 108.
3. Choi, E., H. Ejiri, and H. Ohsumi, *Application of a Ge detector to search for fast neutrons from DD fusion in deuterized Pd.* Jpn. J. Appl. Phys. A, 1993. **32A**: p. 3964.
4. Mizuno, T., et al., *Neutron Evolution from a Palladium Electrode by Alternate Absorption Treatment of Deuterium and Hydrogen.* Jpn. J. Appl. Phys. A, 2001. **40**(9A/B): p. L989-L991.
5. Klyuev, V.A., et al., *High-energy Processes Accompanying the Fracture of Solids.* Sov. Tech. Phys. Lett., 1986. 12: p. 551.
6. Dickinson, J.T., et al., *Fracto-emission from deuterated titanium: Supporting evidence for a fracto-fusion mechanism.* J. Mater. Res., 1990. 5: p. 109.
7. Preparata, G., *A new look at solid-state fractures, particle emission and 'cold' nuclear fusion.* Nuovo Cimento A, 1991. 104: p. 1259.
8. Fateev, E.G., *Possibilities for establishing the mechanism of neutron generation in deuterated materials under mechanical loading.* Tech. Phys. Lett., 1995. 21(5): p. 373.
9. A. Takahashi et al.: J. Appl. Electromag. Mat. 3 (1992) 221.
10. A. Takahashi et al.: Fusion Technology, 19 (1991) 380.
11. A. Takahashi et al.: Fusion Technology, 27 (1995) 71.
12. Kozima, H., K. Kaki, and M. Ohta, *Anomalous phenomenon in solids described by the TCNF model.* Fusion Technol., 1998. 33: p. 52.
13. Mayer, F.J. and J.R. Reitz, *Nuclear energy release in metals.* Fusion Technol., 1991. 19: p. 552.
14. Russell Jr., J.L., *Plausibility argument for a suggested mechanism for cold fusion.* Ann. Nucl. Energy, 1990. 17(10): p. 545.
15. Yang, J., L. Tang, and X. Chen, Dineutron model research of cold fusion. Acta Sci. Nat. Univ. Norm. Hunan, 1996. 19(2): p. 25.
16. Swartz, M., *Possible deuterium production from light water excess enthalpy experiments using nickel cathodes.* J. New Energy, 1996. 1(3): p. 68.
17. Pokropivnyi, V.V., *Bineutron theory of cold nuclear fusion.* Dokl. Akad. Nauk. Ukr., 1993(4): p. 86 (in Russian).
18. Timashev, S.F., *Possible mechanisms for nuclear-chemical transformations in a palladium matrix during heavy water electrolysis.* Zh. Fiz. Khim, 1989. 63: p. 2283 (in Russian).
19. Cerofolini, G.F. and A.F. Para, *Can binuclear atoms solve the cold fusion puzzle?* Fusion Technol., 1993. 23: p. 98.
20. Conte, E., *Theoretical indications of the possibility of nuclear reactions at low energy.* Infinite Energy, 1999. 4(24): p. 49.
21. Phipps Jr., T.E., *Neutron formation by electron penetration of the nucleus.* Infinite Energy, 1999. 5(26): p. 58.
22. Schultz, R. and J.P. Kenny, Electronuclear catalysts and initiators: *The di-neutron model for cold fusion.* Infinite Energy, 1999. 5(29): p. 58.
23. Andermann, G. A., *Theoretical Model (Nu-Q) for Rationalizing Electrochemically Induced Nuclear Events Observed in Deuterium Loaded Pd Cathodes.* in The First Annual Conference on Cold Fusion. 1990. University of Utah Research Park, Salt Lake City, Utah: National Cold Fusion Institute.
24. Moon, D., *Addendum to "Mechanisms of a disobedient science".* Infinite Energy, 1996. 1(5/6): p. 89.
25. Lipson, A.G. and D.M. Sakov, *Increase in the intensity of the external neutron flux in the irradiation of a KD_2PO_4 crystal at the point of the ferroelectric transition.* Tech. Phys. Lett., 1994. 20: p. 954.
26. Roussetski, A.S. *Investigation of Nuclear Emissions in the Process of D(H) Escaping from Deuterized (Hydrogenised) PdO-Pd-PdO and PdO-Ag Samples.* in Sixth International Conference on Cold Fusion, Progress in New Hydrogen Energy. 1996. Lake Toya, Hokkaido, Japan: New Energy and Industrial Technology Development

Organization, Tokyo Institute of Technology, Tokyo, Japan.
27. Stella, B., et al. *Evidence for Stimulated Emission of Neutrons in Deuterated Palladium.* in Third International Conference on Cold Fusion, "Frontiers of Cold Fusion". 1992. Nagoya Japan: Universal Academy Press, Inc., Tokyo, Japan.
28. Lipson, A.G. and D.M. Sakov. *Amplification of the Neutron Flux Transmitted Through KD_2PO_4 Single-Crystal at the Ferroelectric Phase Transition State.* in 5th International Conference on Cold Fusion. 1995. Monte-Carlo, Monaco: IMRA Europe, Sophia Antipolis Cedex, France.
29. Oya, Y., et al. *Hydrogen Isotope Effect Induced by Neutron Irradiation in Pd-LiOD(H) Electrolysis. in Sixth International Conference on Cold Fusion*, Progress in New Hydrogen Energy. 1996. Lake Toya, Hokkaido, Japan: New Energy and Industrial Technology Development Organization, Tokyo Institute of Technology, Tokyo, Japan.
30. Fisher, J.C., *Polyneutrons as agents for cold nuclear reactions.* Fusion Technol., 1992. 22: p. 511.
31. Fisher, J.C., *Liquid-drop model for extremely neutron rich nuclei.* Fusion Technol., 1998. 34: p. 66.
32. Oriani, R.A., *Anomalous heavy atomic masses produced by electrolysis.* Fusion Technol., 1998. 34: p. 76.

Anomalous Isotopic Distribution of Palladium Generated during the Light Water Critical Electrolysis on Palladium Electrodes

T.Ohmori, T.Mizuno (Department of Quantum Energy Technology, Hokkaido University) H.Yamada, and S.Narita (Department of Electrical and Electronic Engineering, Iwate University)

ABSTRACT

The appearance of the anomaly of the isotopic distribution of Pd on the surface layers of Pd electrode after the light water critical electrolysis was confirmed for all of the electrodes investigated. In particular, the increase in the content of ^{108}Pd was found for all of the electrodes, whereas the contents of the isotopes with relatively small mass numbers, i.e. ^{104}Pd, ^{105}Pd and ^{106}Pd, were decreased for most of the electrodes. This result supports strongly that some nuclear transmutation reaction involving hydrogen atoms, palladium atoms and electrons takes place during the critical electrolysis.

INTRODUCTION

As have reported at the last meeting in Morioka [1], we found that the isotopic distribution of Pd in the surface layers of Pd electrode material caused marked deviation from its natural isotopic abundance, when the Pd electrode was electrolyzed at a current density very close to the plasma electrolysis condition [2] for a long period of time (this electrolysis is referred to as critical electrolysis). This result verifies that some nuclear transmutation reaction participates in this electrolysis process. From this point of view it is of utmost importance to confirm as to whether the anomaly of the isotopic distribution of Pd is always observed with sufficient reproducibility under above electrolysis condition. This is the purpose of the present study.

EXPERIMENTAL

In this study two types of electrodes were used. One is untreated Pd sheet and the other is cold worked Pd sheet prepared by way of scraping its surface with a cleaned Pyrex-glass fragment. The apparent electrode surface area is ca. 0.8 cm^2. The counter electrode is Pt gauze (1cm×7cm, 80 mesh). The electrolytic cell is made of fused quartz glass (240 ml). Electrolyte solution is 1 M or 2 M K_2CO_3 prepared from Merck sprapur reagent and Milli-Q water. The volume is 220 ml at maximum. Electrolysis was conducted galvanostatically at a current ranging from 2.5 to 3.0 A for 20 days. During the course of the electrolysis the volume of the solution was gradually reduced by the decomposition and evaporation of water, hence Milli-Q water was added every nearly 12 hours to restore the solution to the initial volume. The

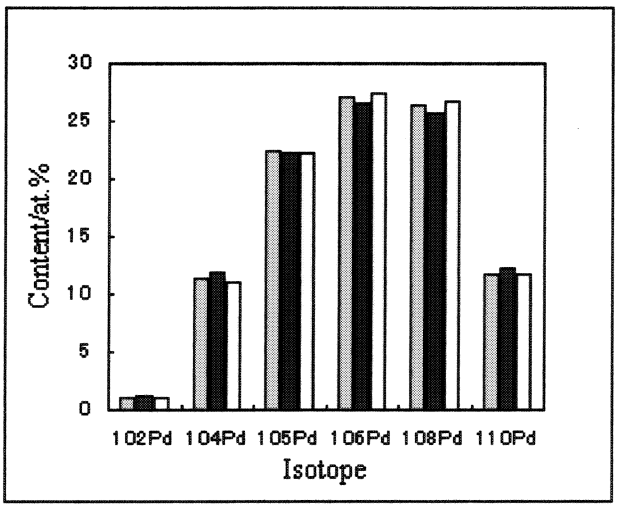

Figure 1. Isotopic distribution of Pd atoms of the electrode before electrolysis. In each of three sets of bars the left and middle bars show found values at the different spots of the electrode and the right bar shows natural isotopic abundance.

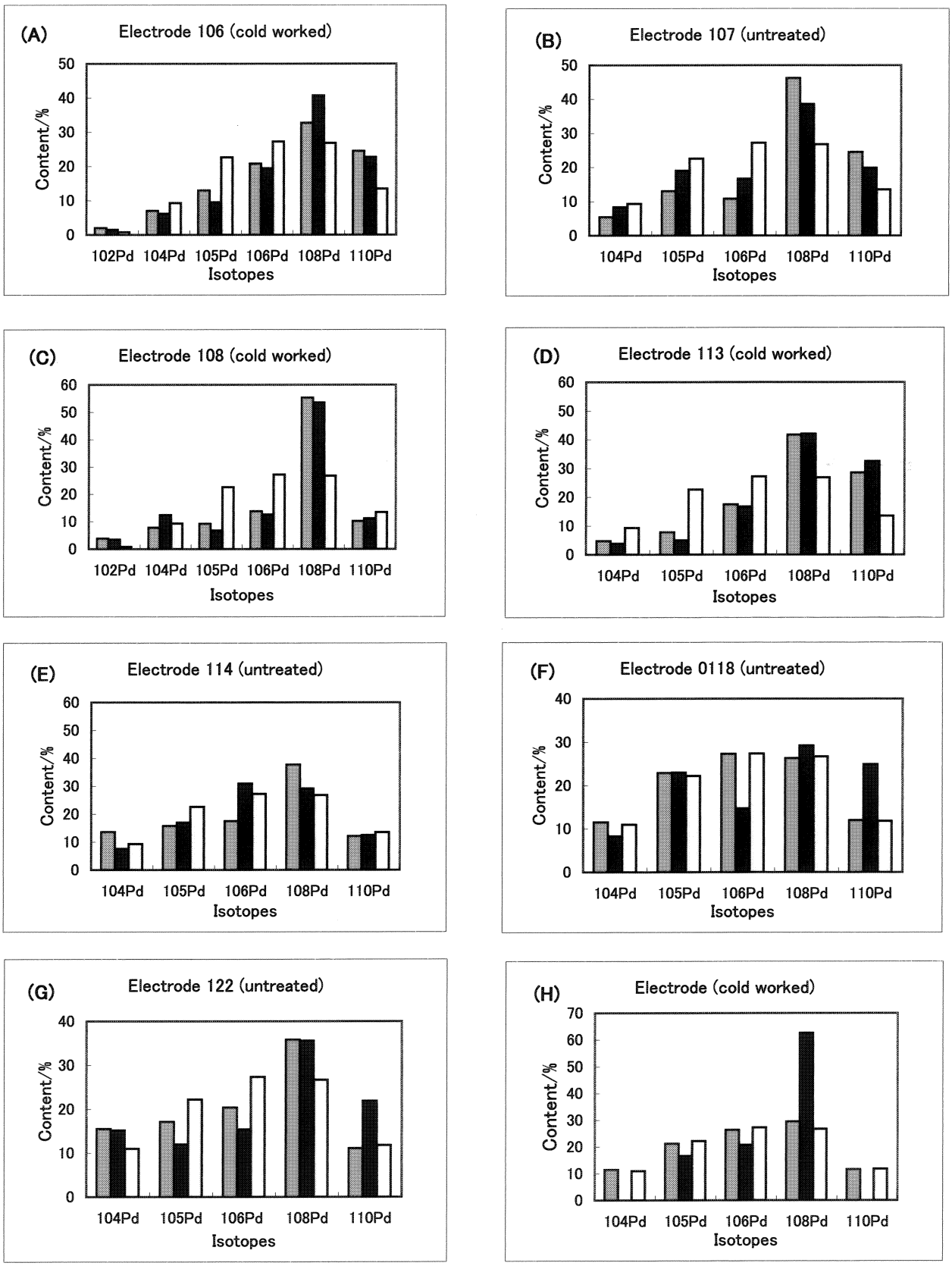

Figure 2. Isotopic distribution of Pd on the face exposed after sputtering for 30 s for eight kinds of the electrodes after critical electrolysis. (A)-(E) in 2 M K_2CO_3 solution, (F)-(H) in 1 M K_2CO_3 solution.

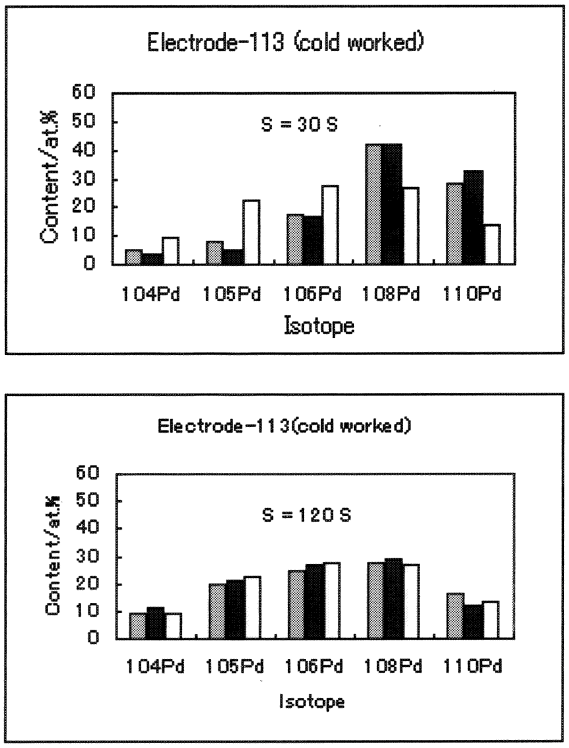

Figure 3. Isotopic distribution of Pd on the faces exposed by sputtering for 30 s and 120 s.

isotope analysis of Pd in the surface layers of the electrode after the electrolysis was carried out by time of flight-type secondary electron mass spectroscopy (TOF-SIMS). The TOF-SIMS measurement was made by the Ga^+ ion irradiation using a ULVAC-PHI, TFS-2100 TOF-SIMS spectrometer with 40μm ×40μm raster size and 0.01 amu resolution. By use of the TOF-SIMS it is possible that the signals of ^{104}Pd, ^{105}Pd, ^{106}Pd, ^{108}Pd and ^{110}Pd isotopes are detected separately from those of organic or inorganic compounds other than palladium hydrides with nearly the same mass numbers. Typical isotopic distribution of Pd in the surface layers of the electrode before the electrolysis is shown in Fig. 1. Naturally, the isotopic distribution of Pd agrees with its natural isotopic abundance.

RESULTS

Figure 2 shows the isotopic distribution of Pd on the face exposed after sputtering for 30 s for eight kinds of Pd electrodes after the critical electrolysis. This is the results obtained for all of the electrodes we have made TOF-SIMS analysis in the present study. Without exception the isotopic distribution of Pd is anomalous, markedly deviating from its natural isotopic abundance. It is seen from this figure that there are some common characteristics as is pointed out in the following: (i) Isotopic content of ^{108}Pd exceeds significantly its natural isotopic abundance for all of the electrodes investigated, reaching ca. 2 times for Electrode-108 and partially for Electrode-127. (ii) Isotopic content of ^{110}Pd also exceeds its natural value in many cases. (iii) In contrast, for other lighter isotopes isotopic content is generally below their natural isotopic abundance. Consequently, it seems that the isotopic contents of the heavier Pd isotopes increase, whereas the isotopic contents of lighter ones decrease throughout the critical electrolysis. As long as the anomaly of the isotopic distribution of Pd is concerned, the intrinsic difference between cold worked and untreated Pd electrodes is not discerned.

Of course the anomaly of the isotopic distribution of Pd appears only in the layers within the limited depth from the surface of the electrode after the critical electrolysis. Figure 3 shows the isotopic distribution of Pd on the faces exposed after sputtering for 30 s and 120 s. As seen from this figure, the anomaly observed on the face after sputtering for 30 s completely disappears on the

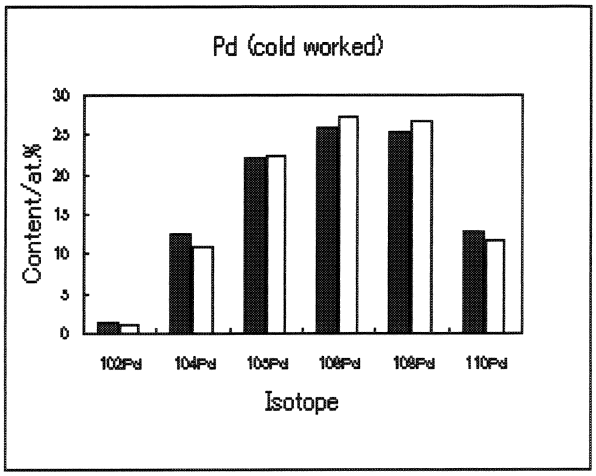

Figure 4. Isotopic distribution of Pd on the surface layers of cold worked Pd electrode after the electrolysis at a current density of 0.2 A/cm^2 in 0.5 M K_2CO_3 solution.

Table 1

Signal intensities of SIMS of the particles with mass numbers ranging from 105.9 to 110

Electrode sample	Mass amu	Intensity counts	Candidate particles
122	105.9144	6910	^{106}Pd
	106.9144	95	^{107}Ag, ^{106}PdH
	107.9044	11260	^{108}Pd, ^{107}AgH
	108.9193	231	^{109}Ag, ^{108}PdH
	109.9119	3501	^{110}Pd, ^{109}AgH
127	105.9054	5768	^{106}Pd
	106.9059	262	^{107}Ag, ^{106}PdH
	107.904	17397	^{108}Pd, ^{107}AgH
	108.9116	269	^{109}Ag, ^{108}PdH
	109.9214	9090	^{110}Pd, ^{109}AgH

face after sputtering for 120 s. This result shows that the depth where the anomaly of the isotopic distribution of Pd appears is limited to the extent of 100-200 layers from the surface.

In order to verify that the signal intensities exhibited in Fig.2 is those of Pd isotopes alone it is essential to ascertain whether the signals are free from overlapping of the signals of Pd hydrides. Table 1 shows signal intensities of SIMS of the particles with mass numbers ranging from 105.9 to 110 measured on the faces exposed after sputtering for 30 s for two different electrodes. From the inspection of this Table it is found that the signal intensities corresponding to ^{107}Ag and ^{106}PdH, and ^{109}Ag and ^{108}PdH, are much smaller than the signal intensities of Pd isotopes, hence, it is seen that the influence of the Pd hydrides on the signals of Pd isotopes can be ignored.

The anomaly of the isotopic distribution of Pd appears only when the electrolysis is conducted at a very large current density, i.e. a critical electrolysis condition. Figure 4 shows the isotopic distribution of Pd on a Pd electrode after electrolysis at a current density of 0.2 A/cm^2 for 7 days. Any anomaly of the isotopic distribution of Pd is scarcely found under this electrolysis condition.

CONCLUSIONS

In this study we revealed that the anomaly of the isotopic distribution of Pd appears in the surface layers of the electrode after the critical electrolysis for all of the Pd electrodes investigated without exception. This result is enough to verify the validity of the previous observation of the anomaly of the isotopic distribution of Pd, which can never be explained without introduction of the idea of nuclear transmutation. The mechanism still remains unknown. Judging from the characteristic that the anomaly appears only under the critical electrolysis condition hydrogen density and/or electron density in palladium electrode may play an important role. The tendency of the increase in the contents of the heavier Pd isotopes seems to support this supposition. We infer that either hydrogen directly interacts with Pd atom or interacts via the formation of neutron or quasi-neutron particles with Pd atom. To clarify this issue further detailed investigation would be necessary.

REFERENCES

1) Ohmori, S.Narita, H.Yamada, T.Mizuno and Y.Aoki, Proc. of JCF-4, Morioka, p.22 (2002).

2) T.Ohmori and T.Mizuno, Proc. of ICCF-7, Vancouver, p.279 (1998).

FURTHER TESTS ON COMPOSITION AND ISOTOPIC ANOMALIES WHEN PD THIN CATHODES ARE ELECTROLYZED IN ACIDIC C_2H_5OD/D_2O MIXTURES ADDED WITH TH-HG SALTS AT MICROMOLAR CONCENTRATION.

Francesco Celani[(1)], A.Spallone[(1)], P.Marini[(2)], V.di Stefano[(2)], M.Nakamura[(2)], A.Mancini[(3)], P.G.Sona[(4)], E.Righi[(1)], G.Trenta[(1)], C.Catena[(1)], G.D'Agostaro[(1)], P.Quercia[(1)], V.Andreassi[(1)], F.Fontana[(5)], L.Gamberale[(5)], D.Garbelli[(5)], E.Celia[(6)], F.Falcioni[(6)], M.Marchesini[(6)], E.Novaro[(6)], U. Mastromatteo[(7)].

INFN-LNF Via E.Fermi 40, 00044 Frascati (Rome)- Italy; (2) EURESYS, Via Lero 30, 00129, Rome-Italy; ORIM SrL, Via Concordia 65, 62100 Piediripa (Macerata)- Italy ; (4) Via S. Carlo 12, 20090 Segrate (Milan) Italy; (5) Pirelli Labs SpA, Viale Sarca 222, 20126 Milan-Italy; (6) Centro Sviluppo Materiali SpA, Via di Castel Romano 100, 00129 Rome-Italy; (7) STMicroelectronics, Via Tolomeo 1, 20010 Cornaredo (Milan)- Italy.

Abstract: Following the recent ICCF10 Conference held at Boston (USA) on August 2003, we made a new experiment aimed to confirm our previous data[1, 2] showing production of new elements sometimes with non-natural isotopic composition. During the experiment a long (~60 cm) and thin (diameter 0.05mm) Pd wire is (over)loaded and unloaded several times with Deuterium (D). The materials of cell (i.e. Pd and Pt wires, solution and salts) were analysed by a high resolution ICP-MS. As already detailed in the http://www.iccf10.org report by the same Authors, the composition of electrolyte (C_2H_5OD/D_2O slightly acidic mixtures with addition of Th-Hg salts at micromolar concentration) and electrolytic current density ($10mA/cm^2$) were quite unusual.
Moreover, the D/Pd-loading ratio is estimated by measuring the Pd wire resistance. In order to measure the resistance, an AC current flows through the Pd wire (square wave at 10KHz, of quite large intensity ~ $800A/cm^2$ and, for about 30minutes every day, up to $5000A/cm^2$).
We realised that such large electromigration-like current can be efficient also to increase the D flux through the surface, similarly (and perhaps in a quite "stronger" way in some very successful experiments) to gas loading methods, at least from the point of view of "transmutation". In our "best experiment", following the calculation procedure introduced by Iwamura[3], we calculated the "equivalent cross section" of $^{232}Th \rightarrow {}^{208}Pb$ as large as 600barn in Th-Hg experiment. Obviously, we had to adapt such calculation procedure to our experimental set-up conditions: we suppose that all D, produced by electrolysis, cross the Pd wire surface, electro-migrate through the whole wire and is "expelled" at wires end.
A completely new, transparent borosilikat (3.3) glass cell thermal insulated by a vacuum chamber was built. The most recent experimental results, after one month of operations, were reported and the general description of our procedure is discussed.
Our studies by ICP-MS analysis followed both the experimental results of Y. Iwamura[3] (Mitsubishi Heavy Industries, Yokohama) -with replication[4] at Osaka University- and the theoretical model developed from A. Takahashi (University of Osaka[5]) of a "multi-body resonance fusion of deuterons" related to specific element "transmutation" in a proper multi-layers of Pd-CaO-Pd-Sr (or Cs) subjected to prolonged deuterium gas flow (according to Y. Iwamura procedures).

Keywords: PdDx, electrolytic hydro-alcoholic solution, Pd thin-long wire, Sr-Hg and Th-Hg "transmutation".

1. INTRODUCTION

During the overloading experiments (Pd-Deuterium) we changed from usual water based electrolyte to hydro-alcoholic solution since 1999. The scientific explanation for the use of such an unconventional electrolyte are stated in detail in our previous Reports at JCF (3, 4) and ICCF(8, 9, 10) series and related papers.
We used a (*very unconventional in all their aspects*) main solution made of heavy ethyl alcohol (C_2H_5OD) and heavy water (D_2O) with a ratio 90—95% to 10—5%. The main dissolved cations were Strontium (as $SrCl_2$) and Mercury (as $HgCl_2$), at a typical concentration as low as 10 micromolar and 1 micromolar respectively. The pH was kept around 4.
For the sake of comparison, most of the electrolytic "Cold Fusion" experiments (several thousands) performed in the world use pure D_2O and LiOD at a concentration of 0.1÷1 molar, i.e. giving strong basic solutions (pH $\simeq$ 13 ÷ 14). This kind of solutions follow the "teachings" of Martin Fleischmann and Stanley Pons (Utah University-USA) who in 1989 first showed the possible "nuclear" origin of some anomalous heat in their electrolytic cell.
Moreover, we use as cathode Pd electrodes consisting of wires 50 to 100 cm long with diameter as thin as 50μm instead of the most diffused rods (according to M. Fleischmann and S. Pons) or plates (according to Akito Takahashi, Osaka University-Japan, 1992). We experienced that some suggestions from Giuliano Preparata and Emilio Del Giudice (University and INFN Milan, 1994) about the peculiarity of long-thin wires are substantially effective.
As referred in detail in the papers quoted, we found excess heat (see ref. 22 in Ref. 1) and tritium well above background (see ref. 24 in Ref.1) in a series of experiments with hydro-alcoholic solutions

containing small amounts of Sr salts and Hg ions. Moreover, we found that in the hydro-alcoholic environment, during the anodic phases (that is for some hours every 1-3 days) of our loading cycles, the Pd electrode is eroded. Significant amounts of very fine Pd particles are found at the bottom of the cell at the end of the experiments. ICP-MS analysis after electrolysis showed the presence of Pd in this black powder (see ref. 26 in Ref.1).

Moreover, after several electrolytic loading-deloading cycles, the Pd wire eroded surface could absorb the deuterium dissolved in the solution (whose maximum overpressure is only 50mbar in our experimental apparatus), quickly and with no electrolysis current so as to yield a mean D/Pd ratio up to 0.75. Such a behaviour could result from an increase of the catalytic activity of the Pd surface. We would like to point out that Yoshiaki Arata[6] (University of Osaka- Japan) has stressed the importance of *nano-structures* in order to get loading of Deuterium in Pd (even over 1/1 loading ratio). Accordingly, very large amounts of "anomalous excess heat" and ^4He were observed in some of his experiments when a proper "trigger" was applied. It is reasonable to suggest that the increased activity exhibited by our Pd wires is caused by the formation of *nano-structures* on its surface, similar to those obtained by Y. Arata in a more elaborated way.

We recall that Y. Iwamura, at Mitsubishi Heavy Industries in Yokohama-Japan (see ref. 25 in Ref. 1) **first showed that Sr is apparently transmuted into Mo (molybdenum),** or Cesium (Cs) into the rare heart Praseodymium (Pr) when a proper multilayer of Pd/Pd-CaO/**Sr** or **Pr** is forced to be flown by deuterium gas for enough long time (several hundred of hours). We tried to check whether such a "transmutation" could occur also after the repeated D-Pd loading/deloading/loading cycles in our experimental set-up. In July 2002 we were ready to perform an independent variant of the Iwamura experiment.

Before starting, we analysed by ICP-MS all the components present in the cell (C_2H_5OD, D_2O, $SrCl_2$, DCl, $HgCl_2$), and pieces of both the Pd cathode and the 2 Pt wires (used as anode and reference electrodes).

At the end of the repeated D-Pd loading/deloading experiment, the electrolytic solution was vacuum dried, the residue was collected and again analysed by ICP-MS together with the Pd. Molybdenum was found in excess of any conceivable contamination, the isotopic composition of the Mo was different from the natural one (see ref. 26 in Ref. 1).

It appears that the phenomenon first discovered by Y. Iwamura in a flowing deuterium gas system also occurs in our electrolytic cell when it is operated according to loading-deloading-loading procedure for a time length of the order of 500-1000 hours.

The main improvement performed during the 2003 was the use of Thorium (Th) as main electrolyte instead of Strontium, again in a very low concentration range (of the order of a few tenths of micromoles/liter).

1.1. Experiment: Thorium salts as electrolyte

In January 2003, we substituted Th salts for the Sr salts used previously.

The reason for such kind of experiments were mainly two:

1) based on some results (published also from our group) on 1997-1998, indicating possible Th "transmutations" during high-electric power (and high-temperature, high-pressure) AC (50Hz) electrolysis with massive zirconium electrodes (both anode and cathode, see ref. 28 in Ref.1), we decided to test whether something similar could happen in our new experimental apparatus based on thin Pd wires and a very strict control of impurities;
2) like Sr, Th ions can form an inorganic precipitate on the cathode surface as $Th(OH)_4$ (solubility product $Ks = 10^{-50}$), by action of the current density. Another similarity to Sr^{+2} is that Th^{+4} ions cannot be galvanically deposited because of the highly negative value of their standard potential ($E_0 = -1.899V$). Moreover, even if Th is co-deposited on Pd surface through some unknown process, it can form a stable hydride-deuteride compound with supposedly no incompatibility with the aim of our specific experiment. According to such chemical-physical characteristics, it is possible to deposit the proper $Th(OD)_4$ and/or ThD_x layer(s) on the Pd cathode surface at a value of the current density lower than that required for Sr salts: the input power to the cell is reduced and anomalous excess heat, if any, can be more easily detected.

Accordingly, with the present work we intended to essay the following:

a) the occurrence of excess heat,
b) the presence, if any, of foreign elements in both the cathode and the cell after electrolytic loading.

The operations were performed with electrolytes containing small amounts of Th and Hg salts.

1.2. Experimental set- up: electrolytic cell and flow calorimeter

The cell configuration is shown in Fig. 1 of Ref.1. The sample holder, a PTFE tube, is placed in a 1000ml borosilikat glass (type 3.3) cylinder (diameter 67mm, height 460mm). The cathode and anode are both "U" shaped and are located on the opposite walls of the holder, facing each other. The cathode is a thin (diameter 0.050mm) long (60cm) Pd wire (total surface about $1cm^2$; resistance about 30 Ohm with no Deuterium inside). In the lower part of the "U", at its center, a small weight (6g PTFE cylinder) keeps the wire tense during the Pd loading so as to compensate its 4--6% elongation. The anode is a Pt wire (diameter 0.250mm, length 60 cm, purity 99.99%). A

third Pt wire (diameter 0.250mm, length 30cm) is put exactly in the middle of the "U" shaped cathode for reference purposes.
To measure the cathode resistance, an AC current (16mA, 10KHz, square wave: equivalent to a current density along the wire as high as 800A/cm^2) is superimposed to the (low intensity) electrolysis DC current (2—20mA): the resistance value is continuously monitored using the resulting AC voltage drop.
A high quality LM135H thermometer (sensitivity 0.05°C), inserted in a PTFE tube, is placed in the middle of the cell. A Joule heater (max. 20W) is used to calibrate the calorimeter and is located between the electrodes in a peripheral position. It consists of a chain of 20 resistors inserted in a PTFE tube (diameter 8mm, length 30cm) filled with thermal conducting grease.
The cell is pressurised (50mbar) and thermally insulated. The electrolysis gases and vapours flow through a twin cold-traps and a silicon oil bubblier before reaching the atmosphere. Corrections for these losses of energy are not yet applied, consequently all the data about excess heat are under-estimated.
The heat exchanger within the cell consists of a 500cm long PTFE pipe, outer/inner diameter 4/2mm, wound around the PTFE holder through which distilled water flows. Temperature of the distilled water flowing in the pipe is continuously measured at the inlet and outlet of the heat exchanger with two LM135H thermometers. A computerised peristaltic pump (Masterflex 7550-62) provides a constant flow of distilled water (0.200ml/sec, with day-to-day stability of ±1%, routinely measured every 12 hours). Water is picked up by the pump from a 2-liter reservoir to which it returns from the cell. The cell, water reservoir, and pump are placed in a container held at a constant temperature of 24°C. In other words, we continue (since 1992) to use the, very reliable, flow calorimetric measurement method.

2. COMPOSITION OF THE ELECTROLYTE, CLEANING PROCEDURE

A 93 to 7 % by volume mixture of ethyl alcohol (C_2H_5OD) and heavy water (D_2O) respectively was used as the electrolyte, having a total volume of 750 ml.

- The ethyl alcohol was previously vacuum distilled at 35°C (by a vacuum distillation system Buchi 134) in order to eliminate mainly sodium and iron and ultra-filtered on-line using a 100nm, MILLIPORE PTFE filter: distillation system deeply modified in our Frascati laboratory. The density was routinely measured (Mettler Toledo DA-110M) before and after distillation, to confirm that no significant H_2O contamination occurred during the operations.
- The heavy water, 99.97% isotopic purity (reactor grade from Ontario Hydro, Canada), was distilled at 45°C under vacuum and ultra-filtered before use, similarly to alcohol. Density was measured before and after distillation.
- $Th(NO_3)_4$, (5 ÷ 15mg) was added to the electrolyte and the pH of the resulting hydro-alcoholic solution was adjusted to a value of about 3 by adding few drops of concentrated HNO_3, in order to avoid uncontrolled precipitation of $Th(OD)_4$.
- The cell was cleaned after each experiment using repeated cycles of water/organic solvents/water/nitric acid/water in an ultrasonic warm bath. After Experiment #2 (Feb. 14, 2003; see Table 1a), we increased the duration of the immersion in concentrated (65%) warm (60°C) HNO_3 from 2 minutes to 14 hours because we suspected that a residual amount of Cs might be hidden somewhere in the cell. As a consequence, the final washing cycles with distilled water were increased from 4 to over 10 because we experienced that warm, long time lasting, HNO_3 is absorbed by the non-glass parts of the cell.

.

3. EXPERIMENTAL RESULTS

We got both excess heat (best result was an energy gain of about 10 for several days) and several strong indications of the "production" of new elements, some of these with an isotopic composition different from the natural one.
Some of the new elements "produced" (Cu, Zn) are the same as those obtained by using Sr as the main electrolyte, others are peculiar respectively of Strontium (i.e. Mo) or of Thorium (i.e. Pb)
Surprisingly, we found that the electrolyte consumption was much larger than could be expected according to the Faraday's law. We suspect that this loss is caused by the heat being generated in a few hot spots at wire surface, where the temperature might raise to rather high values. This local over-heating could evaporate the solution so that gaseous D_2O and C_2H_5OD are lost in addition to D_2 and O_2.
We plan to build a new cell made out of PTFE, quartz, HDPE, and mylar, and use a thermo-camera in order to detect the IR radiation that might issue from the deuterated Pd wire surface.

3.1. ICP-MS Measurements.

ICP-MS measurements were performed in a chemistry laboratory operating under the ISO 9001 quality control protocol. The laboratory is located in the Interdisciplinary Research Area of Castel Romano (Rome), in the "Centro Sviluppo Materiali" building. The ICP-MS used is HP & YOKOGAWA Analytical Systems, model 4500. It has been in operation since 1996. Calibrations with Atomic Absorption Standards are made every day before starting analysis. Sensitivity is about $6{\cdot}10^{10}$ Atoms/count. Typical background is 10 - 80 counts, depending both on the mass analyzed and the "overall condition" of the instrument (mainly high voltage

setting and the Ar carrier gas flow intensity). Background is higher for well known sources of interference, due to Ar, Cl, O, N, C, H, and impurities dissolved in the deionised "Milli-Q" water and reagents used. Because of our specific experimental constraints, we almost always use hot, concentrated Aqua Regia (4cc used for about 10-20mg of material) to dissolve the materials in glass beakers (borosilikat 3.3). A nominal concentrations of 2% and 0.2% (to avoid instrumental saturation) is submitted to the instrument for analysis of the main elements in the electrolyte (Pd, Sr, Th, Hg). In other words, we have about 10--20mg of unknown elements diluted in 50cc (or 500cc) of acidic water. We make 2 runs, from mass 2 to 260 with a resolution of 0.2 AMU. Each run takes about 200 seconds and sample uptake is 0.5ml/min. Blank and mass tuning runs (^{7}Li, ^{89}Y, ^{206}Tl) are made at the beginning of the analysis, after 3 hours of operation, and at the end of the study. Calibration is done more frequently if an element is at a particularly high concentration. After each measurement there is a washing cycle of about 10 minutes using HNO_3 at 5% concentration or Aqua Regia if needed. A blank measurement is always performed.
Data are analyzed according to the general recommendation of ICP-MS manufacturer applied to our specific operating conditions. We especially want to avoid spurious results caused by double mass and half-mass signals adding to the masses of interest. To solve such problems, we performed a large number of analyses using standard solutions of the elements of interest to calibrate the apparatus. Obviously, D_2O and C_2H_5OD were also carefully characterized.

3.2. Comments on ICP-MS experimental result

The ICP-MS results are shown in Tab.1 and Tab 2.
We studied 3 main reactions: Sr-->Mo, Cs-->Pr, Th-->Pb (+other).

Sr-->Mo

Results using Sr within the electrolyte were reported in ref.26 of Ref.1. We observed that some of the Sr was transmuted to elements with mass 94 and 96, qualitatively in agreement with the Y. Iwamura results. Moreover, the total amount of Mo atoms we found ($1\text{-}2\cdot10^{15}$), normalized to Pd electrode surface (about $1cm^2$), is very similar to the Iwamura gas experiments.

Cs-->Pr

Transmutation of Cs to Pr (according to Y. Iwamura) was not observed in our experiments when we used concentrated Cs solutions, because in the ensuing conditions we were not able to achieve a sufficiently high deuterium concentrations within the cathode. Much to our surprise, results were better when a Th salt, at very low concentration, was used with a "proper mixture" of Ca and Sr salts. Using these mixtures, we apparently transmuted Cs and Pr, although in smaller amounts in respect to Iwamura procedure. We noticed that the Th salt did not contain measurable impurities of Cs or Pr, according to both the assay from the chemical company (Aldrich) and our analysis by ICP-MS. In the best experiment in which apparent transmutations have been detected, the signal is nine times the background.
Later (in experiments #5 and #6) we used only Th and Hg salts to increase the deuterium concentration in Pd. Surprisingly in experiment #6 we observed for Pr a signal to background ratio as large as 21. Experiment #4 did not achieve the necessary deuterium concentration, making it a very useful blank for ICP-MS analysis.
In other words, apparent transmutations of Th to Cs (like "fission") and later Cs to Pr (like "fusion" of $Cs+2^4He$) occurred in an electrochemical environment, similar to those reported by Y. Iwamura in a gaseous environment[3] (see also ref. 25 in Ref.1) and recently confirmed by A. Takahashi[4] *et. al.* about the speculated reaction $Cs+2^4He$-->Pr. Such kind of, very surprising, 2 step reactions need to be confirmed by more experiments and cross-checked with other kind of analysis.

Th-->Pb(+other)

We performed a total of 4 experiments with Th salts, in amounts ranging from $8x10^{-6}$ to $6.5x10^{-5}$ moles in the total volume of electrolyte. The pH for the Th solution was $\simeq$ 3 compared to $\simeq$ 4 for the Sr containing solution.

3.2.1. Details on ICP-MS results shown in Tab.1 and 2.

A list of masses relatively easy to identify is reported in Tab. 1 and Tab. 2. For this masses reproducible results were obtained. We observed several other anomalies not yet fully understood. We anticipate that most of such anomalies are in the range of masses 46 - 60, 107 - 116, along with some isotopic anomaly for Pd.

4. Conclusions

After a large number of experiments performed during 14 years of research work aimed at finding anomalous effects in systems forced to a high concentration of deuterium, we are confident that most of the observed effects occur at the interface between the solution and the Pd bulk. ***A properly formed layer of a third element is necessary. Non-equilibrium situations are also necessary to trigger the effects***. Recently, we found that deuterated hydro-alcoholic, slightly acidic solutions, work very well in producing the so called "anomalous effects". Additions of Th and Hg salts within the micromolar concentration range improve the effects even at very low electrolytic current density ($<10mA/cm^2$).

The so-called "transmutations" seem real and not an artifact. Moreover, the amount and type of new elements seem related to:

a) value of overloading and its time duration;
b) intensity of D "flux" at its interface (in our case improved because "bulk" electromigration along wire and repeated cycles of cathodic-anodic stripping);
c) the type of main electrolyte (e.g. Sr, Th);
d) a proper "third" element at Pd surface , i.e. CaO according to Ywamura, Hg in our experiment.

We think that the model developed by Akito Takahashi[5] about multi-body resonance fusion of deuterons can explain most of the thermal and isotopic anomalies, including foreign elements that we have recently observed.
Further work is necessary to fully characterize the system and increase the magnitude of the effects.

Table 1: Results of ICP-MS analysis. Please note that overloading means D/Pd>0.9.

Exp	Date: begin→ end [dd/mm/yy]	Electrolyte composition: [moles]	Comments: OVL=Overloading S/N=Signal/Noise Pr=1count=$6\cdot10^{10}$ Atoms;
#1	20/12/02 → 16/01/03	$CsNO_3[5\cdot10^{-5}]$ - $SrCl_2[1\cdot10^{-5}]$ LiOD $[1.5\cdot10^{-5}]$ - $H_2SO_4[5\cdot10^{-6}]$ NH_3OH $[1\cdot10^{-4}]$	Almost No OVL ; Anode=Pd wire 250□m Pr=80=>S/N=2
#2	17/01/03 → 14/02/03	$CaCl_2$ $[21\cdot10^{-5}]$ - $SrCl_2$ $[1\cdot10^{-4}]$ $HgCl_2$ $[2\cdot10^{4}]$ – H_2SO_4 $[1\cdot10^{-5}]$	2 times OVL, - Residual Cs?? Pr=170=>S/N=4
#3	18/02/03 → 05/03/03	$CaCl_2$ $[1\cdot10^{-5}]$ - $SrCl_2$ $[1\cdot10^{-4}]$ $HgCl_2$ $[2\cdot10^{-4}]$ -H_2SO_4 $[1\cdot10^{-5}]$ $Th(NO_3)_4$ $[8\cdot10^{-6}]$	3 times OVL R/Ro=1.706 Pr=370=> S/N=9
#4	04/04/03 → 14/04/03	$HgCl_2$ $[1\cdot10^{-5}]$ -Hg_2SO_4 $[1\cdot10^{-4}]$ $Th(NO_3)_4$ $[2.1\cdot10^{-5}]$	No OVL
#5	15/04/03 → 19/05/03	$Th(NO_3)_4$ $[2\cdot10^{-6}]$ Hg_2SO_4 $[2\cdot10^{-6}]$	Several times OVL; Excess heat; Pr=300=>S/N=6
#6	24/05/03 → 14/07/03	$Th(NO_3)_4$ $[2\cdot10^{-6}]$ Hg_2SO_4 $[5\cdot10^{-6}]$	Several times OVL - Excess heat. Pr=1.4E3=>S/N=21 - 208Pb anomaly
#7	31/10/03 → 08/12:03	$Th(NO_3)_4$ $[21\cdot10^{-6}]$ Hg_2SO_4 $[3\cdot10^{-6}]$	Few times OVL (contamination Na)

Table 2: The counts of main mass found are shown. In parenthesis the natural abundance. See Ref. 26 for composition of solution.

Exp	^{31}P(100)	^{39}K(93.3)	^{63}Cu(69.2) ^{65}Cu(30.8) 63/65=2.25	^{64}Zn(48.6)^{66}Zn(27.9) ^{67}Zn(4.1)^{68}Zn(18.8)	^{133}Cs(100)	^{206}Pb(24.1) ^{207}Pb(22.1) ^{208}Pb(52.4) 206/208=.46
#1	$7\cdot10^{3}$	$2.2\cdot10^{6}$	$2.4\cdot10^{6}$	$2.7\cdot10^{6}$	$>3\cdot10^{8}$	$1\cdot10^{4}$
#2	0	0	$2.1\cdot10^{6}$ 63/65=1.94	$1.8\cdot10^{6}$	$6\cdot10^{5}$	$4\cdot10^{5}$
#3	$4\cdot10^{5}$	$2.7\cdot10^{6}$	$6.1\cdot10^{6}$ 63/65=1.93	$1.7\cdot10^{7}$	$1\cdot10^{6}$	$9.5\cdot10^{5}$
#4	$2.5\cdot10^{4}$	$1.4\cdot10^{6}$	$2.9\cdot10^{6}$ 63/65=2.05	$7.5\cdot10^{3}$	$1.94\cdot10^{5}$	$6.9\cdot10^{5}$
#5	$1.8\cdot10^{6}$	$2.3\cdot10^{6}$	$2.4\cdot10^{7}$ 63/65=2.07	$1.2\cdot10^{7}$	$9\cdot10^{4}$	$1.5\cdot10^{6}$
#6	$2.72\cdot10^{7}$	$6.4\cdot10^{6}$	$9.3\cdot10^{8}$ 63/65=2.08	$5.1\cdot10^{8}$	$2.2\cdot10^{5}$	$2\cdot10^{8}$ 206/208=.39
#7	0	0	$3.9\cdot10^{6}$ 63/65=2.0	$3.6\cdot10^{6}$	$2\cdot10^{4}$	$1.25\cdot10^{6}$

References

1) F. Celani, et al. Proceeding - JCF4, October 17-18, 2002, pp.17-21. Iwate Univ. (Japan).
2) F. Celani, et al. Proceeding - ICCF10, Cambridge (USA), August 23-29, 2003; publishing.
3) Y. Iwamura, et al. Proceeding - ICCF10, Cambridge (USA), August 23-29, 2003; publishing.
4) T. Higashiyama,...A. Takahashi, Proceeding - ICCF10, Cambridge (USA), August 23-29, 2003; publishing
5) A. Takahashi, Proceeding - ICCF10, Cambridge (USA), August 23-29, 2003; publishing.
6) Y. Arata, Y. Chang Zhang, Proceeding - ICCF10, Cambridge (USA), August 23-29, 2003; publishing.

Search for Neutrons from Palladium Cathodes during Alternate Electrolysis of Heavy and Light Water

Takayoshi AOKI and Nobuharu YOSHIKAWA*

Isotope Center, The University of Tsukuba, Tsukuba-shi, Tennoudai 1-1-1, 305-8577 Japan
*KEK, Tsukuba-shi, Ouho 1-1, 305-0801 Japan

Abstract

Preliminary tests of searching for neutrons were made with expectation that neutron would generate from Pd cathode during alternate electrolysis of heavy and light water. Total of 12 experimental runs were made up to now. Clear evidences of generation of neutron bursts were not obtained.

Keywords: alternate electrolysis, D2O, H2O, neutrons

1. Introduction

Highly reproducible neutron detection experiments with certain statistical accuracy were reported by Mizuno et.al.[1] They found neutrons generated from palladium cathode electrode by applying alternate deuterium and hydrogen absorption treatment. Soon after that, another group tried similar experiments and obtained partly positive results[2].

Mizuno pointed out that amount of light water impurity contaminant in heavy water might affect the neutron generation and that the impurity contaminant should be least as possible.

The neutron generation mechanism in these experiments was not clear. However, thinking of the fact that the neutron generation is one of direct evidence of so called cold fusion, it may be urged to evaluate the reproducibility of the experiment of this type.

2. Experimental Setup

2.1 Electrolysis cells

A cylindrical quartz glass vessel and a plastic vessel (390 mm in height and 60 mm in diameter) were used D_2O and H_2O electrolysis, respectively. Reagent K_2CO_3 from Kanto Chemical Corp. was dissolved in 400 ml fresh heavy water, 99.9 atom % D, from ISOTEC Corp., to form D_2O electrolyte. The concentration was 0.2 M. Before dissolution, the reagent was heated up to 130℃ to release water in it. The same reagent was dissolved in 1000 ml water to form 0.2 M light water electrolyte. Platinum coated titanium cylinder meshes, 60mm in diameter and 330 mm in length, were worked as anodes. The cathodes were made of palladium wires, 1 mm in diameter and 30 mm in length. The palladium wires were spot-welled with long Teflon coated copper wires.

The anodes and the electrolytes were set in the vessels. The cathode and a thermocouple were bound each other and were set in the heavy water vessel at first stage. The vessels were plugged by silicon rubbers.

2.2 Paraffin neutron moderator blocks

Two Helium-3 filled proportional counters from Reuter-Stokes Corp. were used to detect neutrons. The detectors had sensitive length of 25.4 cm and outer diameter of 2.54 cm, filled

with 10 atmospheres pressure Helium-3 gas. Intrinsic sensitivity is approximately 43 cps/nv for thermal neutrons. One detector, B, was covered with a 1.0 mm Cadmium sheet, which played as a thermal neutron absorber. The detectors A without Cd absorber and the detector B with absorber were inserted into two set of rectangular paraffin neutron moderator blocks. Cross-sectional dimension of the block was 10 cm × 12.5 cm and the length was 40 cm. The purpose of employing the detector B with the Cd absorber was to identify whether or not the observed event was due to the neutron itself. If external strong electric impulse noise would come to the detectors A and B, both the detectors would make signals simultaneously. If the neutron burst come to both the detectors, only detector A would make signals. The detector B would never give signals because the neutrons were decelerated by the moderator and absorbed by the Cd absorber. The detector B worked as an external electric noise watcher.

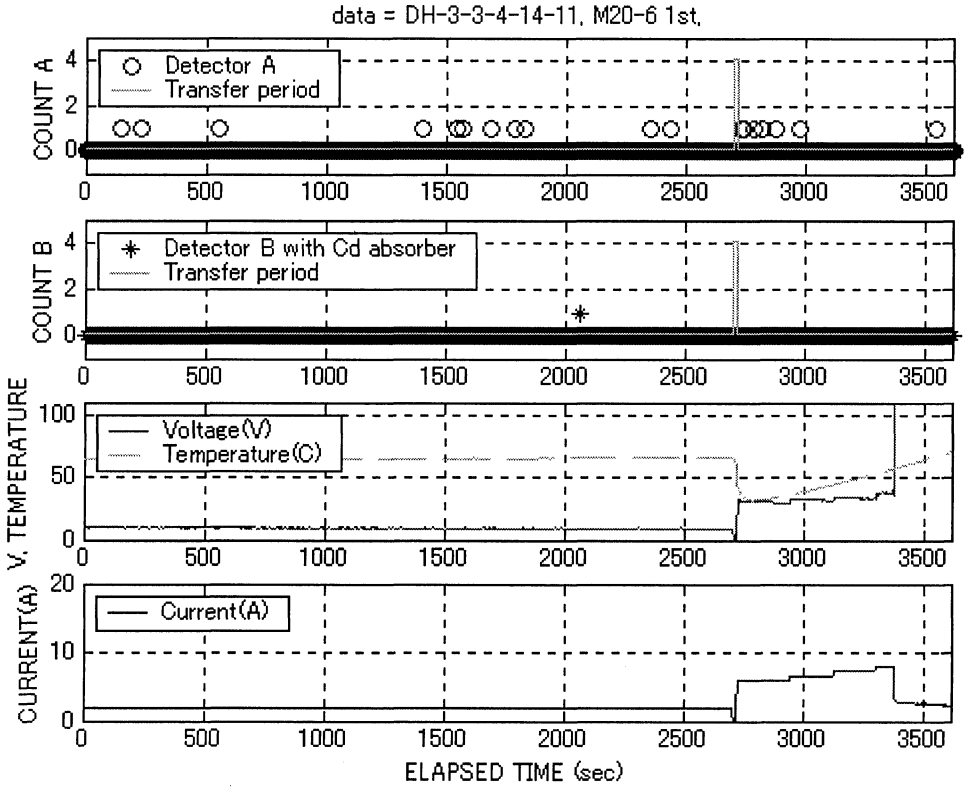

Fig 1. Preliminary test run. Typical neutron counting data and cell parameters of as a function of time. Monitors were made for every successive 2 seconds.The detector B equipped a Cd absorber and showed only one count. The square line indicated the transit time when the cathode was moved from the heavy water to the light water.

2.3 Shielding paraffin box

A shielding paraffin box was constructed from many standard paraffin bricks. The box accommodated the heavy water vessel, the light water vessel and two neutron moderator blocks. The box shielded external BKG- neutrons and electric impulse noise.

Dimension of the inner space of the box was 45 cm in length, 30 cm wide and 60 cm in height. Minimum wall thickness of the box was 10 cm. Upper open space was covered with a lid that was a 10 cm thickness paraffin brick with 0.5 mm Cd sheet. Similarly, 0.5 mm Cd sheets were put on all 5 inner walls of the inner space

to reduce back-ground neutrons. These 6 sheets were connect to each other by wires, which were led to electronic earth ground point to reduce external electric impulse noise.

The moderator A was put horizontally at the bottom of the inner space. The moderator B was set on the moderator A. Two electrolytic vessels were set vertically side by side and come in touch with the two moderators. Vertical position of the Pd cathode in the vessel was adjusted to coincide with central position of the two moderators. The other smaller spaces in the inner space were occupied with many polyethylene bricks.

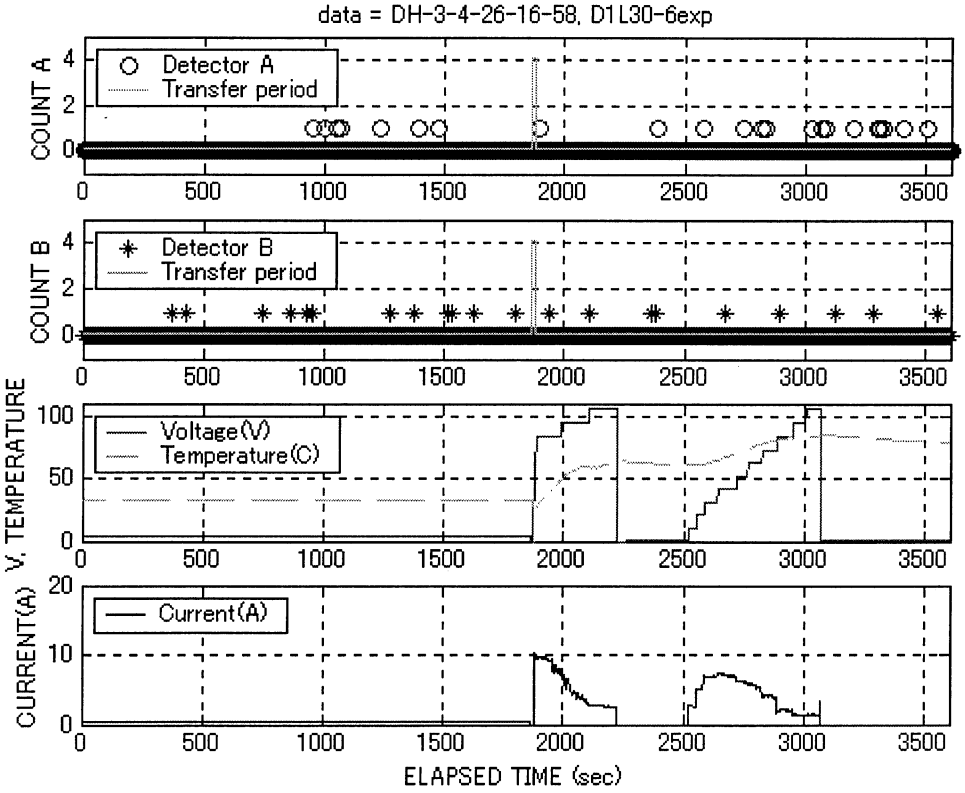

Fig.2 Formal run. Typical neutron counting data and cell parameters. The detector B did not equip the Cd absorber and showed the same counts as that of detector A. Neutron burst was not seen.

2.4 Precautions aginst discharge electric noise

It was worried that electric discharge might happen at certain critical electrolytic voltage. The discharge would generate intense electric noise, which would affect the neutron detectors. The detectors would generate false pulses that would look like true neutron signals. Much attention had been paid for these false signals. It was found effective to shield preamplifiers and detector cables. Fastening the connection between electronic ground loops was particularly important. At the final stage, the false signals were completely suppressed during the discharge in preliminary test runs.

2.5 Electronics

The preamplifier signals of neutron detectors, A and B, were lead to main amplifiers. The amplified signals were led to multi-parameter PHA (pulse height analyzer, Laboratory equipment Corp.) to record sum energy of recoil proton and tritium, and also were fed to single channel analyzer (SCA) modules to generate logic signals, that were led to counter modules

to count neutron events. Windows of SCA were set between 574 to 1765 keV of the recoil sum energy, for further safety of rejection of false pulses, although no false pulses were observed in low energy side of the spectra. The window setting corresponded to the neutron energy of 0 to 1000 keV.

Effective efficiencies of the detectors were determined using a calibrated Cf-252 neutron source and a Am-Be source. The sources were put in the light water cell at position where the cathode was set. The cell was filled with pure light water this time. The averaged efficiency of the detector A was $(1.6\pm0.1)\times10^{-2}$, and the detector B with the Cd absorber was $(1.1\pm0.3)\times10^{-4}$. The efficiency of the detector B without absorber was also measured and was the same as that of detector A within the error. Long-term (one day measurement) background count rate of the detector A was about 4.9×10^{-3} cps, and that of the detector B with the absorber was 4.1×10^{-4} cps. Short-term (less than one hour) background rates showed great fluctuations. They were 2 or 3 times more or less than that of long-term values.

2.6 Control and data taking

For data taking, a personal computer and a GPIB network were used. Cell parameters (cell voltage, current and electrolyte temperature) and the neutron counts, A and B, were monitored for every successive 2 sec. The neutron energy spectra were accumulated for all experimental period. Cathode voltage supplied by a DC power supplier was controlled manually.

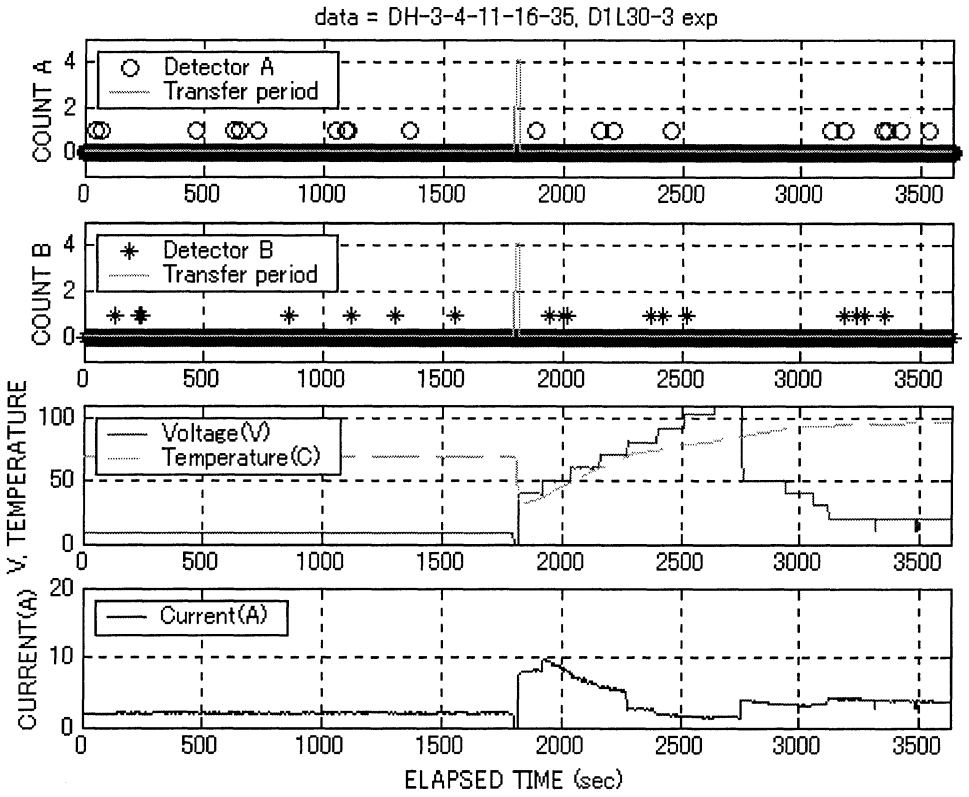

Fig3. Formal run. Detector B had no Cd neutron absorber. Neutron burst was not seen.

3. Experimental procedure

3.1 Preparatory electrolysis

Preparatory electrolysis using a fresh Pd cathode in the heavy water vessel elapsed for several hours to 24 hours. At the first, the electrolytic voltage was set at 5 V and the

current was 0.5 A typically. Then the voltage was increased stepwise up to 8 V and the current was typically 2 A. At the final stage, D-Pd ratio was expected to be almost 1.

3.2 Data taking and light water electrolysis

At the time about 30 minus before preparatory electrolysis was ended, the data taking was started to monitor the cell parameters, the neutron counts and the neutron spectra. When about 30 minutes passed after the data taking was started, the cathode was transferred to the light water vessel and then the light water electrolysis began. It took about 16 seconds for the transfer. The cathode voltage was increased stepwise and was several times as big as the preparatory voltage. The generation of the neutron burst was expected just when the voltage was increased abruptly[1]. The light water electrolysis continued for 30 minutes varying the voltage. The data taking lasted totally for about 60 minutes.

3.3 preliminary test runs

Preliminary test runs were made six times to see whether the electric discharge affected the detectors. At low electrolytic voltage, the current was proportional to the voltage. On the contrary when the voltage was large more than 50 V, the current was inversely proportional to the voltage and the discharge occurred. Lights and sounds caused by the discharge were observed. Typical data was shown in Fig.1. At the time of near 3500 sec when the voltage was raised up to 100 V from 40 V, rapid current dropping was seen. At this moment, both the detectors, A and B, showed no counts. This was direct evidence that the discharge did not affect the detectors.

3.4 Formal runs

The Cd absorber was removed from the detector B, because the false pulse due to the electric discharge had been eliminated and also because total counts of the detector B with the absorber was too low. Formal experimental runs were made 6 times employing the detector A and the detector B without the Cd absorber. By this detector configuration, both the detector would generate true signals simultaneously for the neutron burst. The background neutrons would come to the detectors randomly so that there would be a little chance for both the detectors to count the neutrons simultaneously because the long term background rate was small (4.9×10^{-3} cps) and the monitoring time period was short (2 seconds). Therefore one would be able to distinguish the neutron burst events from the background events by watching simultaneous counting numbers recorded by both the detectors in some short time period. Typical data taken in the formal run were shown in Fig.2 and Fig.3.

4. Results

In order to conclude that the neutron burst was surely happened, it was necessary to point out particular short time period where both the detectors made the counting signals simultaneously and the voltage was increased abruptly.

Much effort had been paid in vain for seeking the particular time period which fulfilled the conditions of neutron burst. The neutron signals were equally distributed and showed no localization of the distribution in the particular short time range. The three figures suggested no correlation between the neutron distribution and the steep voltage rises. Any of the runs including the preliminary test ones and the formal ones showed no neutron burst.

Additional formal runs are in progress using fresh heavy water.

References:

(1) Tadahiko MIZUNO, Tadashi AKIMOTO, Tadayoshi OHMORI, Akito TAKAHASHI, Hiroshi YAMADA and Hiroo NUMATA: Jpn. Appl. Phy., Vol.40(2001), p. L989-L991

(2)Takayuki Ohya, Yuji Isobe and Akito Takahashi:JCF4 ABSTRACTS, p. 15

HEAT MEASUREMENT DURING LIGHT WATER ELECTROLYSIS USING MULTILAYER CATHODES

M.Fujii, H.Inoue, S.Mitsushima, N.Kaıniya and K.Ota

Department of Energy and Safety Engineering, Yokohama National University
76-5 Tokiwadai Hodogaya-ku, Yokohama 240-8501 JAPAN

ABSTRACT

We have conducted heat measurement during light water electrolysis using cathodes, which were made by Al_2O_3 balls sputtered by Pd and Ni with the change of thickness. In 3 of 6 runs, small excess heat (less than 5%) was observed. However, we could not observe a clear excess heat in those runs.

1. INTRODUCTION

15 years has past since the first announcement of the cold fusion by Fleischmann and Pons[(1)]. Many reports claimed excess heat. However, the amount of excess was very small and the reproducibility was very poor in most of the reports. Patterson claimed large excess heat with high reproducibility in light water electrolysis using multi layer beads electrode [(2)(3)]. In this study, we aimed to measure the heat balance using Pd and Ni sputtered Al_2O_3 balls in light water electrolysis to investigate the reproducibility of excess heat generation and establish the conditions of reproducibility using Patterson type power cell [(2)-(5)].

2. EXPERIMENTAL

Fig.1 shows the cylindrical electrolytic cell made of acrylic resin. Ni mesh (3cm ϕ, 55mesh) and Al_2O_3 balls sputtered by Pd and Ni of different thickness were used for the cathode, and Pt mesh (3cm ϕ, 55mesh) was used for the anode.

The Pd and Ni layers were sputtered in the order of Pd and Ni on Al_2O_3 balls under Ar atmosphere ($3.0 \cdot 10^{-1}$ Pa) after evacuation to 10^{-4} Pa. The purity of Al_2O_3 balls was 99.9%. The diameter of Al_2O_3 ball was 1mm. The Al_2O_3 balls were set in a spherical and mesh basket and the sputtering was performed on the power of

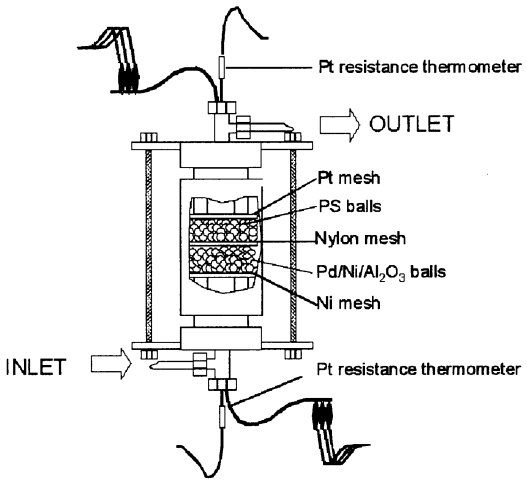

Fig.1 Electrolytic cell

200W, rotating the basket with 1 rpm. The electrolyte was circulated in this system passing through a reservoir. The temperature of electrolyte in the reservoir was kept at 296K. The temperature of electrolyte at cell inlet was kept at 296K. The cell was immersed in water bath whose temperature was controlled at 296K. The plastic balls were put on the upper part of the cathode to prevent the cathode from floating under circulation of electrolyte. The electrolysis was conducted at the constant current of 40 ~ 500mA. The flow rate of electrolyte was fixed at 11 ml min^{-1}. Hydrogen and oxygen that generated during electrolysis were collected in the reservoir and measured the rate of gas

generation. The energy that was used water electrolysis reaction was calculated from the rate of gas generation. The temperature difference of electrolyte was measured by a Pt resistance thermometer placed at the inlet and outlet of the cell. The data was recorded every 20 seconds in a personal computer through a data logger. The heat recovery and heat balance were calculated by the following equations.

$$W_0 = I \cdot V \quad (1)$$

$$W_1 = FR \cdot \Delta T \cdot Cp \cdot d \quad (2)$$

$$W_2 = (2/3) \cdot Q \cdot FR' \quad (3)$$

$$HR = W_1/W_0 \quad (4)$$

$$HB = (W_1+W_2)/W_0 \quad (5)$$

,where W_0 is the input power, W_1 is the heat output that was measured from temperature increase of the electrolyte through the cell, FR is the flow rate of electrolyte, Δ T is the temperature difference between the cell inlet and outlet, Cp is the heat capacity of electrolyte (296K) that was estimated 0.91(J K^{-1} g^{-1}) for 1M Li_2SO_4 solution and d is the density of electrolyte that was estimated 1.087 (g cm^{-3}). W_2 is the energy that was used for water electrolysis, Q is the reaction enthalpy of water electrolysis, FR' is the rate of gas generation, HR is heat recovery when output power is only W_1, HB is heat balance when output energy is the sum of W_1 and W_2.

In measurement of the heat capacity, we used DSC. The bottom of the silver vessel was polished by emery paper (#1500) to improve heat conduction between the holder and the vessel. This measurement was conducted between 273K and 323K with a heating rate of 1K min^{-1}. Fig.2 shows a DSC change with temperature, where Ys is the difference of DSC between the empty and the sample vessels and Yr is the difference of DSC between the empty and the standard sample containing ultra pure water. On the basis of these data, we obtain the heat capacity of 1M Li_2SO_4-H_2O at 296K using the following

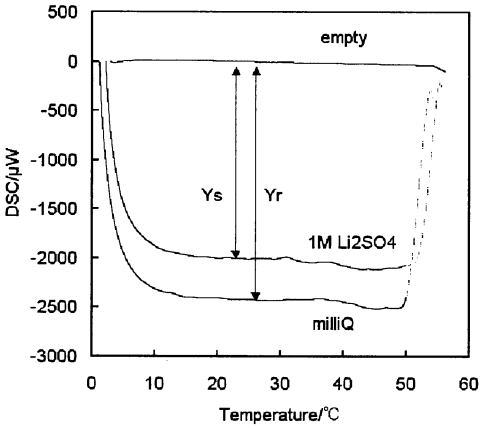

Fig.2 Heat capacity measurement of 1M Li_2SO_4 light water solution by DSC.

equation,

$$C_{ps}=C_{pr} \cdot (mr \cdot Ys)/(Yr \cdot ms) \quad (6)$$

,where Cps is the heat capacity of the sample (1M Li_2SO_4-H_2O), Cpr is the heat capacity of the standard sample (ultra pure water), ms and mr are the weight of a sample and a standard sample, respectively. From this calculation, the heat capacity of 0.91 J K^{-1} g^{-1} was obtained for 1M Li_2SO_4 –H_2O solution at 296K.

3. RESULTS AND DISCUSSION

In order to obtain the heat recovery, a nichrome covered Cu wire (0.35mm ϕ) was used for heat source. Fig.3 show the heat recovery

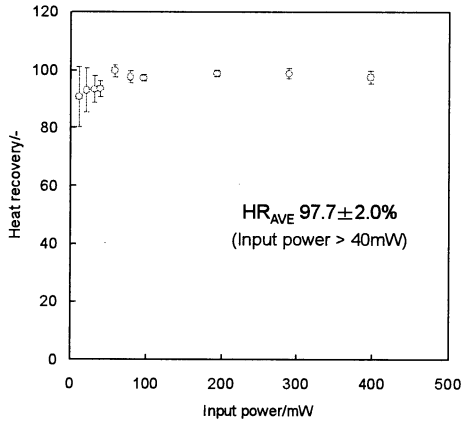

Fig.3 Relationship between heat recovery and input power during calibration using 1M Li_2SO_4-H_2O and resister for heat source.

using nichrome covered Cu wire for heat source in 1M Li_2SO_4-H_2O. The heat recovery was stable when the input power was more than 40mW. Averaged heat recovery was 97.7±2.0%.

Table.1 show the summary of experimental results in electrolysis using Pd and Ni sputtered Al_2O_3 balls for cathode in 1M Li_2SO_4-H_2O. The heat recovery was obtained from only temperature difference between cell inlet and outlet. The Heat balance was obtained from the temperature difference and the energy that was used for water electrolysis. In 3 runs, small excess heat (less than 5%) was observed.

Fig.4 shows trend of cell voltage and temperature difference during electrolysis in 1M Li_2SO_4-H_2O using multi layer cathodes (Pd:1500 Å, Ni:1500 Å) at 100mA. This change of trend was stable. This typical change was observed in most runs. Fig.5 show the trend of heat recovery and heat balance that was calculated from these data. Heat recovery was 74%. Heat balance was99%. In this run, the excess heat was not observed.

Fig.6 show trend of cell voltage and

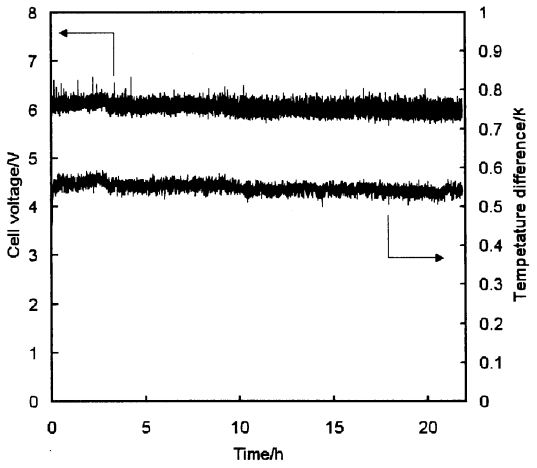

Fig.4 Trend of cell voltage and temperature during electrolysis in 1M Li_2SO_4-H_2O using multi layer cathodes(Pd:1500 Å, Ni: 1500 Å) at 100mA

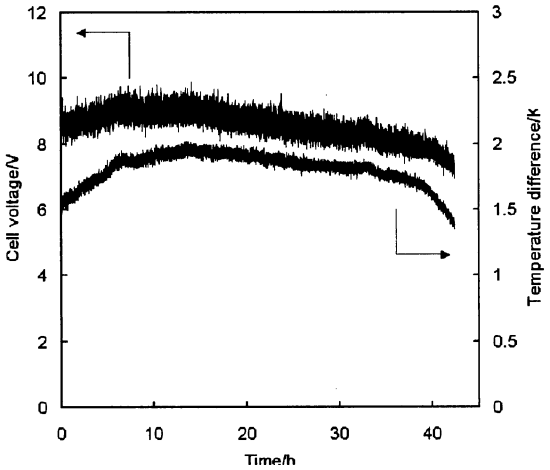

Fig.6 Trend of cell voltage and temperature during electrolysis in 1M Li_2SO_4-H_2O using multi layer cathodes(Pd:1500 Å, Ni: 1500 Å) at 200mA

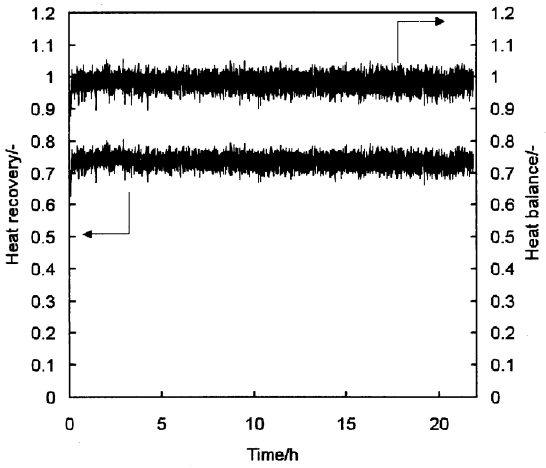

Fig.5 Trend of heat recovery and heat balance during electrolysis in 1M Li_2SO_4-H_2O using multi layer cathodes(Pd:1500 Å, Ni: 1500 Å) at 100mA

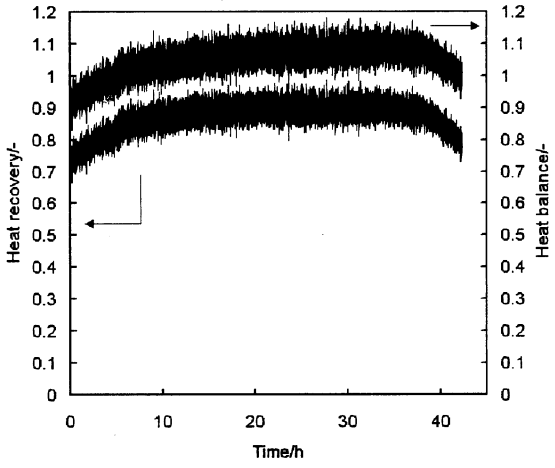

Fig.7 Trend of heat recovery and heat balance during electrolysis in 1M Li_2SO_4-H_2O using multi layer cathodes(Pd:1500 Å, Ni: 1500 Å) at 200mA

temperature difference during electrolysis in 1M Li_2SO_4-H_2O using multilayer cathodes (Pd:1500 Å, Ni:1500 Å) at 200mA. The cell voltage showed a peculiar behavior. This behavior was observed only in this run, although the reason was not clear. Fig.7 show the trend of the heat recovery and the heat balance that were calculated from these data. Input power W_0 was 1.7W. W_1 was 1.48W. Heat recovery was 87%. W_2 was 0.31W. Heat balance was 105%. Small excess heat (less than 5%) was observed in this run. However, we could not observe a clear excess heat in this runs.

4.CONCLUSION

In this study, we observed the small excess heat (less than 5%) using Pd and Ni sputtered Al_2O_3 balls in 3 runs out of 6 runs. However, we could not observed a clear excess heat in those runs.

REFERENCES

[1] M. Fleischmann, S. Pons et al, J. Electroanal. Chem., 286,293 (1989).

[2] James A. Patterson, U. S. Patent, 5318675.

[3] James A. Patterson, U. S. Patent, 5676816.

[4] G. H. Miley et al, Proc.ICCF6, 629 (1996).

[5] D. Cravens, Proc.ICCF4, 79 (1995).

Table.1 Summary of experimental result in electrolysis using two layer (Ni/Pd) on Al_2O_3 balls for cathode in 1M Li_2SO_4-H_2O.

Sample	Cell curent (mA)	Cell voltage (V)	Heat recovery	Heat balance
Pd(2000 Å)	40	3-3.6	0.5	0.96
Ni (1000 Å)	60	3.7-4	0.57	0.91
	80	4-4.3	0.6	0.93
	100	4.2-4.6	0.63	0.96
	200	5.7-6.6	0.7	0.95
Pd(1500 Å)	40	3.3-4.4	0.63	0.89
Ni (1500 Å)	60	4.4-5	0.66	0.93
	80	5.1-5.8	0.7	0.95
	100	5.7-6.6	0.74	0.99
	200	6.9-9.9	0.87	1.05
Pd(2500 Å)	40	2.7-3.3	0.57	0.87
Ni (500 Å)	60	3.3-3.6	0.56	0.9
	80	3.4-3.9	0.57	0.93
	100	3.9-4.3	0.59	0.96
	200	4.9-5.9	0.65	0.92

Sample	Cell curent (mA)	Cell voltage (V)	Heat recovery	Heat balance
Pd (1000 Å)	40	2.9-3.5	0.56	0.8
Ni (2000 Å)	60	3.6-3.9	0.6	0.86
	80	4-4.3	0.63	0.9
	100	4.2-4.7	0.66	0.93
	200	6-6.7	0.71	0.93
Pd (500 Å)	40	2.8-3.4	0.64	0.89
Ni(2500 Å)	60	3.5-3.9	0.64	0.9
	80	3.8-4.2	0.65	0.93
	100	4.1-4.5	0.67	0.95
	200	5.5-6.6	0.81	1.03
Pd(1500 Å)	300	7.3-9.2	0.85	1.04
Ni (1500 Å)	400	8.3-10.3	0.87	1.03
	500	9.4-11.7	0.88	1.03

Confirmation of Transmuted Elements on Pd Complexes using D_2 Gas Permeation Method

Mitsuru SAKANO, Satoshi SAKAI, Takehiko ITOH,
Yasuhiro IWAMURA and Shizuma KURIBAYASHI

Advanced Technology Research Center, Mitsubishi Heavy Industries, Ltd.
1-8-1, Sachiura, Kanazawa-ku, Yokohama, 236-8515, Japan

ABSTRACT

We have already reported on the observation of low energy nuclear reactions induced by D_2 gas permeation through Pd complexes, which consist of a thin Pd layer, alternating CaO and Pd layers and bulk Pd[1-4]. The Pd complex was located in a vacuum chamber and the elemental analysis was performed using an X-ray photoelectron spectroscopy (XPS) apparatus mounted on the chamber. When Cs was added on the surface of a Pd complex, Pr emerged on the surface while Cs decreased after the Pd complex was subjected to D_2 gas permeation at 343K and 1atm for about one week. In the case of adding Sr on the surface, Mo emerged on the surface while the added Sr decreased after D_2 permeation for about two weeks[1-4].

In this paper, recent progress of our research is described. The experimental set-ups and the procedures are basically the same in the following references 1-4. The detected Pr was confirmed by various methods such as TOF-SIMS, XANES, X-ray Fluorescence Spectrometry and ICP-MS.

1. INTRODUCTION

Anomalous elemental changes have been observed on the Pd complexes, which consist of a thin Pd layer, alternating CaO and Pd layers and bulk Pd, after subjecting the Pd complexes to D_2 gas permeation as we reported at ICCF-9[3] and in the paper[1] in the Japanese Journal of Applied Physics (JJAP). In this paper, we describe recent progress; Pr was identified by XPS, TOF-SIMS, XANES, X-ray Fluorescence and ICP-MS.

Our experimental method can be characterized by the following two main features. The first is the permeation of D_2 gas through the Pd complex, as shown in Figure 1(a). Permeation of deuterium is attained by exposing one side of the Pd complex to D_2 gas while maintaining the other side under vacuum conditions. On the D_2 gas side of the Pd complex, dissociative absorption causes the D_2 molecules to separate into D atoms, which diffuse through the metal toward the vacuum side, where they emerge from the metal, combine and are released as D_2 gas.

The second feature is a structure of the Pd complex deposited with elements subjected to transmute. Our sample is a Pd complex composed of bulk Pd on the bottom, alternating CaO and Pd layers, and a Pd thin film on top. After fabricating a Pd complex, Cs or Sr is deposited on the surface of the top thin Pd layer, as shown in Figure 1(b). This Cs or Sr is transmuted. In other words, with this composition, we can provide a deuterium flux through the Pd complex on which a target element is placed as a target to be transmuted. We perform elemental analyses of the given elements after D_2 gas permeation by exhausting the D_2 chamber (by making it into a vacuum chamber). Our experimental method is superior in that it clearly discriminates transmutation products from contamination because we analyze the products by XPS (X-ray Photoelectron Spectroscopy) in vacuum, in situ during the experiment, without moving the sample or opening the chamber.

2.EXPERIMENTAL

The experimental method and setup are basically the same as before[1-4]. Therefore we shall omit a detailed description, and describe only the changed and improved aspects of the experiment. Cs is now added to the surface by the electrochemical method.

Figure 2 shows a schematic of the experimental apparatus. One chamber (Chamber A) is filled with D_2 gas, and the other chamber (Chamber B) is evacuated by a turbo-molecular pump. These two chambers are divided by a Pd complex test piece. D_2 gas is supplied at 1 atm on the Pd film side of the test piece and dissolves in D atoms at the surface. The D atoms intrude into the Pd thin film and diffuse through the Pd complex

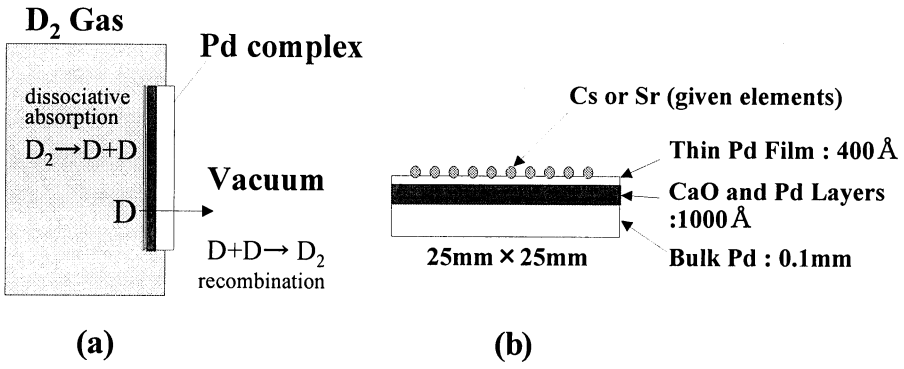

Figure 1. Schematic of the present method: (a)D2 gas permeation of the Pd complex, (b)Structure of the Pd complex deposited with Cs or Sr .

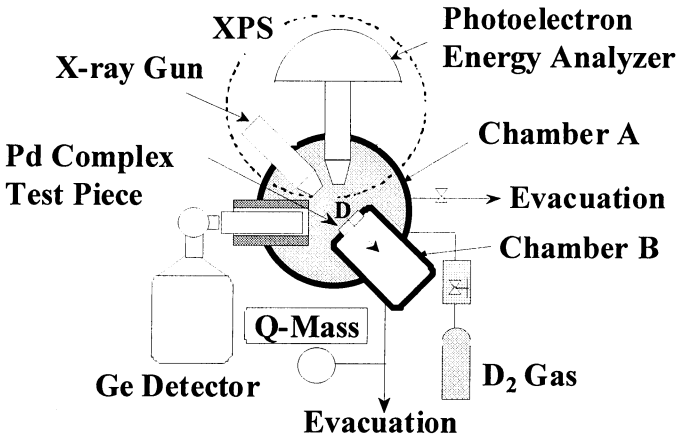

Figure 2. Experimental Setup

and then reach the surface of the bulk side, where they combine and are released as D_2 molecules. One advantage of this newly developed apparatus is that we can analyze the surface of a Pd complex sample by X-ray photoelectron spectroscopy (XPS) without removing it from the vacuum chamber, thereby preventing contamination of the test sample. Another advantage is that we can detect the time dependence of the elements on the Pd complex surface. Repeating D_2 gas permeation and XPS analyses, we can obtain information on time variation of the detected elements.

3. RESULTS

Let us briefly describe the experimental results presented at ICCF-9. A transmutation reaction converting Cs into Pr is shown in Figure 3. Results for two runs are shown as examples. The number of Cs atoms decreased while the number of Pr atoms increased over time. No Pr was detected at the beginning of the experiments. At 120 h, the number of Pr atoms exceeded that of Cs atoms.

The experimental results for Pd complex test pieces with added Sr are shown in Figure 4. We observed that Sr decreased while Mo increased over time. Experiments were performed three times and all data are plotted here. At the beginning of the experiments, no Mo atoms were detected. However, Mo atoms increased gradually while Sr decreased correspondingly. It should be noted that runs with Sr take longer to convert a given mass of Sr into Mo than it takes to convert that mass of Cs into Pr.

Figures 5(a)-(c) show the results of SIMS analysis for the three samples. The intensities of mass number 96 were the largest for each sample, although the intensities were different. The SIMS mass spectrum for a Mo layer (400 Å thickness) that was deposited on a Pd disk is shown in Figure 5(d). This spectrum reveals the natural abundance of Mo. Comparing these figures; we can easily recognize that the isotopic compositions of the detected Mo are different from the natural isotopic abundance of Mo.

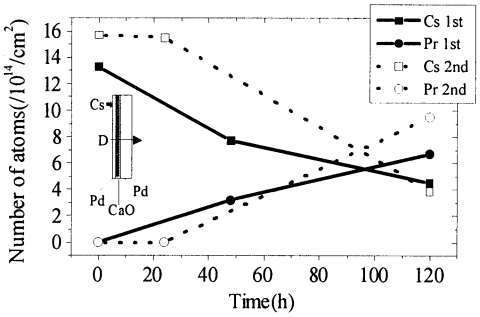

Figure 3. Time variation in the number of Cs and Pr atoms during D_2 gas permeation through Pd complex (Pd/CaO/Pd) deposited with Cs

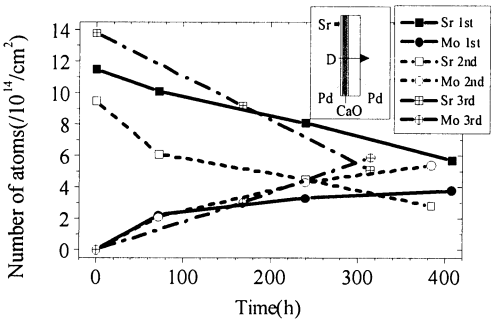

Figure 4. Time variation in number of Sr and Mo atoms induced by D_2 gas permeation through Pd complex(Pd/CaO/Pd) deposited with Sr

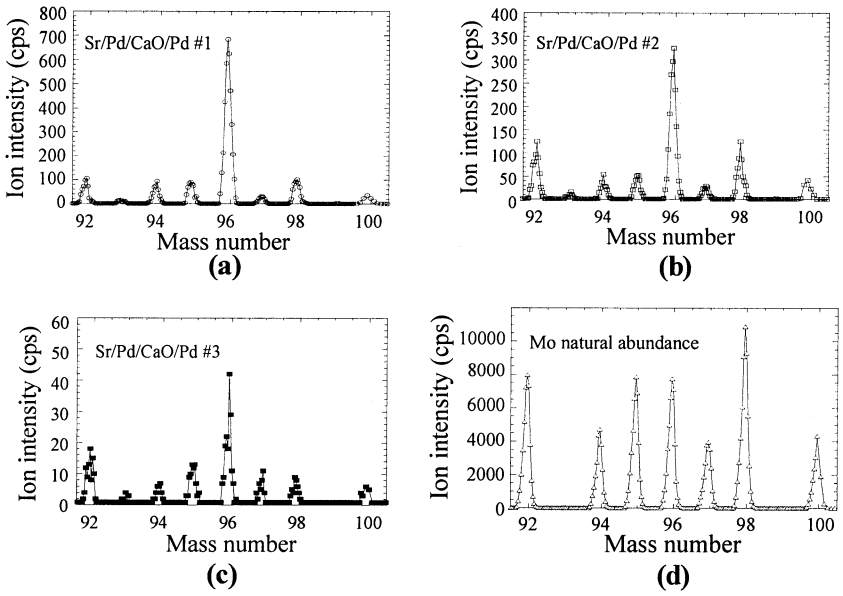

Figure 5. Anomalous isotopic composition of detected Mo: (a)Isotopic composition of detected Mo for run #1, (b)Isotopic composition of detected Mo for run #2, (c)Isotopic composition of detected Mo for run #3, (d) Natural abundance of Mo analyzed by SIMS.

Let us move on to new experimental results. Pr, the transmuted product from Cs, was confirmed by many element analysis methods. The first example is the identification of Pr by TOF-SIMS (Time of Flight Secondary Ion Mass Spectrometry) shown in Figure 6. The TOF-SIMS device is a model TRIFTTM II made by ULVAC-PHI. The upper figure shows the mass

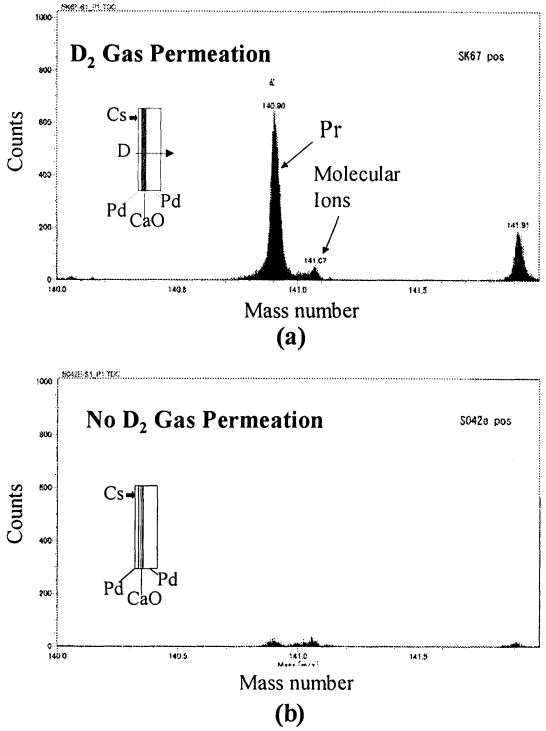

Figure 6. Identification of Pr by TOF-SIMS: (a) Mass number distribution of the sample after D_2 gas permeation, (b) Mass number distribution of the sample without D_2 gas permeation

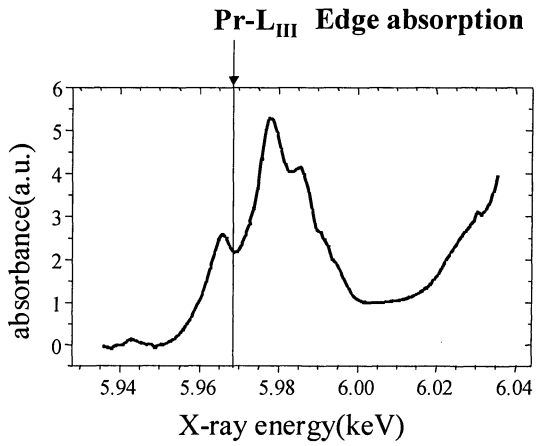

Figure 7. Identification of Pr by XANES (X-ray Absorption Near Edge Structure)

number distribution of the Pd complex (Pd/CaO/Pd) after D_2 gas permeation, and the lower figure is for the Pd complex without D_2 gas permeation. The TOF-SIMS can distinguish small mass difference so that Pr and molecular ions can be clearly separated, as shown in the upper figure. It is confirmed that Pr is detected only for the foreground sample.

Confirmation of Pr by XANES (X-ray Absorption Near Edge Structure) is shown in Figure 7. This spectrum was obtained at the BL-9A Line at the High Energy Accelerator Research Organization (KEK), located in Tsukuba, Japan (www.kek.jp). A Pd complex sample after D_2 gas permeation, on which Pr was detected by XPS, was examined by XANES. Pr LIII Edge absorption was clearly recognized in Figure 7.

Furthermore, Pd complex samples after D_2 gas permeation were examined by X-ray fluorescence spectrometry and ICP-MS (Inductively Coupled Plasma Mass Spectrometry). Although the X-ray fluorescence spectrometry is a bulk analysis method, Pr was detected using strong SOR X-rays. The sensitivity of ICP-MS is so high

that quantitative analysis of Pr is performed for all the experiments. We obtained the data that Pr existed from 1 to 100ng.

We would like briefly touch on a few points, starting with the problem of discriminating contamination and transmutation products. Since the detected material, Pr, is a rare earth element, it is difficult to imagine that Pr accumulated on the Pd complex test samples by any ordinary process. As mentioned in reference 5, Cs atoms do not diffuse and migrate by D_2 gas permeation. Therefore it can be postulated that Pr atoms also do not migrate. The purity of our D_2 gas is over 99.6% and the most of the impurity in it is H_2. Other impurities detected by a mass spectrometer are N_2, D_2O, O_2, CO_2, CO and hydrocarbons; they are all under 10ppm. We analyzed Pd complex test pieces deposited with Cs by ICP-MS mass spectrometry and confirmed that Pr in the test samples was below the detection limit (0.1ng). On the other hand, the detected Pr ranges from 1ng to 100ng. The amount of the detected Pr exceeds the maximum possible contamination of Pr. Therefore we conclude the detected Pr was transmuted from Cs.

Our next point is that the isotope ratio of the synthesized elements is anomalous. The isotopic anomaly of the Mo is particularly strong evidence that some nuclear processes produced this Mo. Some might speculate that the anomalous isotope ratios were caused by Mo contamination undergoing some sort of isotopic separation process, leaving only ^{96}Mo to be detected. (See Figure 5). However, such efficient isotope separation would not be possible.

We noticed that a certain rule exists between starting and produced elements[1-3]. The increase in mass number is 8, and the increase in atomic number is 4 in the case of Cs and Sr. It appears that 4d addition reactions occur. We also observed 2d and 6d addition transmutation reactions[4].

At present, we do not have a complete theory that can explain the experimental results without a few assumptions. The EQPET model[6,7] proposed by Prof. A.Takahashi can basically explain our experimental results, by assuming that a short-lived quasi-particle electron pair like Cooper-pair can be generated. The observed transmutation processes must belong to a new category of nuclear reactions in condensed matter. Therefore much more theoretical investigation is necessary.

4. SUMMARY

Nuclear transmutation of Cs into Pr and Sr into Mo can be observed by D_2 gas Permeation through Pd Complexes. Pr was identified by various methods such as XPS, TOF-SIMS, XANES, X-ray fluorescence spectrometry and ICP-MS.

REFERENCES

[1]Y.Iwamura, M.Sakano and T.Itoh, *Elemental Analysis of Pd Complexes: Effects of D_2 gas permeation.* Jpn. J. Appl. Phys. **41** (2002), pp. 4642-4648.

[2]Y.Iwamura, T.Itoh, M.Sakano, S.Sakai and S.Kuribayashi, *Low Energy Nuclear Reaction in Condensed Matter induced by D_2 Gas permeation through Pd Complexes: Correlation between Deuterium Flux and Nuclear Products.* Proc. of ICCF-10 24-29 August 2003 Cambridge(USA) to be published. (see http//www lenr-canr.org/)

[3]Y.Iwamura, T.Itoh, M.Sakano and S.Sakai, *Observation of Low Energy Nuclear Reactions induced by D_2 gas permeation through Pd Complexes.* Proc. of ICCF-9, 19-24 May 2002, Beijing (China); pp.141-146.

[4]Y.Iwamura, T.Itoh and M.Sakano, *Nuclear Products and Their Time Dependence Induced by Continuous Diffusion of Deuterium through Multi-layer Palladium Containing Low Work Function.* Proc. of ICCF-8, 21-26 May 200 Lerici (Italy), SIF Conf. Proc.Vol.70, pp.141-146.

[5]Y.Iwamura, T.Itoh, M.Sakano, S.Sakai and S.Kuribayashi, Proc. of JCF-5

[6]A.Takahashi, *Tetrahedral and octahedral resonance fusion under transient condensation of deuterons at lattice focal points.* Proc. of ICCF9 19-24 May 2002, Beijing (China); pp.343-348.

[7]A.Takahashi. *Mechanism of Deuteron Cluster Fusion by EQPET model.* Proc. of ICCF-10, 24-29 August 2003 Cambridge(USA) to be published (see http//www lenr-canr.org/).

[8]Y.Iwamura, T.Itoh, M.Sakano and S.Kuribayashi; SOLID STATE PHYSICS, Agne, Vol.39 (2004), p.p.203-210

Correlation between Deuterium Flux through Pd Complexes and Quantity of Nuclear Products using D_2 gas Permeation Method

Yasuhiro IWAMURA , Takehiko ITOH, Mitsuru SAKANO,
Satosi SAKAI and Shizuma KURIBAYASHI

Advanced Technology Research Center, Mitsubishi Heavy Industries, Ltd.
1-8-1, Sachiura, Kanazawa-ku, Yokohama, 236-8515, Japan

ABSTRACT

Recent progress on the low energy nuclear reactions induced by D_2 gas permeation through Pd complexes (Pd/CaO/Pd) is described. The experimental set-ups and the procedures are basically the same in the following references[1-4]. Quantitative analysis of Pr and measurement of deuterium flux through Pd complexes have became available. A lot of experimental results suggest that the quantity of Pr was proportional to the deuterium flux through Pd complex. The cross section of transmutation of Cs into Pr can be roughly estimated at 1 barn if we consider the deuterium flux as an ultra low energy deuteron beam.

Analysis of the depth profile of Pr suggests that a very thin surface region up to 100 angstroms is the active transmutation zone. The surface distribution of Pr basically seems to be uniform. There is no correlation between Pr and grain boundaries.

1. INTRODUCTION

We have established an experimental method characterized by "permeation of D through Pd complex". We reported that anomalous elemental changes, Cs transmutation into Pr and Sr transmutation into Mo, have been observed on the Pd complexes, which consist of a thin Pd layer, alternating CaO and Pd layers and bulk Pd, after subjecting the Pd complexes to D_2 gas permeation as we reported at ICCF-9[3] and in the paper[1] of JJAP.

In this paper, we describe our recent progress. The following points have been improved or changed.

1) Cs ion injection into Pd complexes (instead of the electrochemical method) was performed.
2) Depth profile and surface distribution of Cs and Pr was obtained by TOF-SIMS (Time of Flight Secondary Ion Mass Spectrometry).
3) Correlation between deuterium flux and Pr production.

2. EXPERIMENTAL

The experimental method and setup are basically the same as former reports[1-4]. Therefore we shall omit a detailed description, and describe only the changed and improved aspects of the experiment. Cs is now added to the surface by the ion injection method, in addition to the electrochemical method, for exact depth profile analysis.

Figure 1 shows experimental apparatus and calibration method for D_2 gas flow rate. The D_2 gas flow rate was estimated by measuring the pressure of the chamber B. (Chamber B is evacuated, but the vacuum is gradually filled with the gas that permeates through the Pd complex.) The calibration curve for pressure versus the D_2 gas flow rate was obtained in advance by letting D_2 gas into the vacuum chamber through a precision gas flow meter.

3. RESULTS

Figure 2 shows the cross sectional view of the Pd complex (Pd/CaO/Pd). This image was taken by TEM (Transmission Electron Microprobe). During the process of Pd complex preparation, Pd substrate is etched by aqua regia[1,2]. The wave-like shape of the Pd substrate is formed by the etching process. On the Pd substrate, Pd and CaO complex layer are formed by Ar ion beam sputtering. The white lines correspond to CaO and the black parts to Pd. The 400-angstrom Pd thin film is located on the Pd and CaO complex layer.

Depth profiles of Cs and Pr were plotted in Fig.3. Two Pd complex samples were prepared and Cs was injected into them by ion implantation method. Acceleration voltage and Cs fluence for the ion implantation were all the same for the two

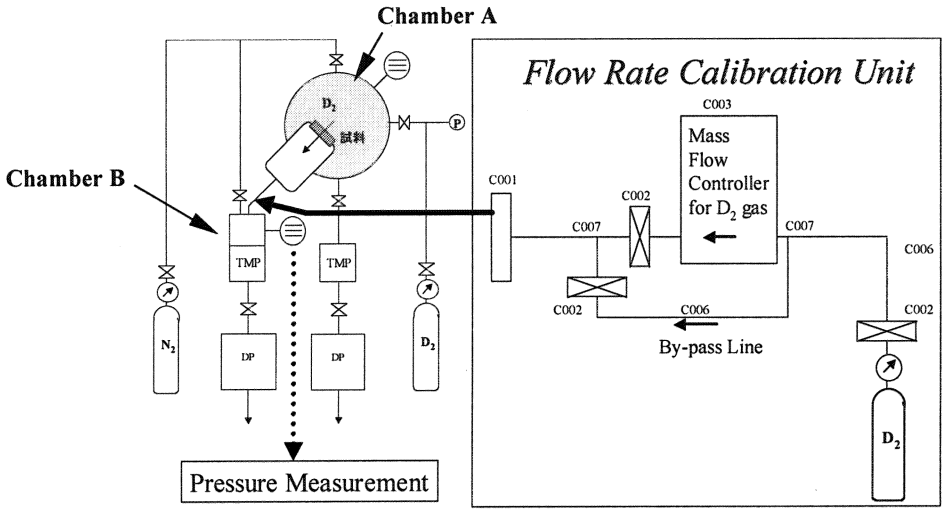

Fig. 1 Experimental apparatus and calibration method for D2 gas flow rate

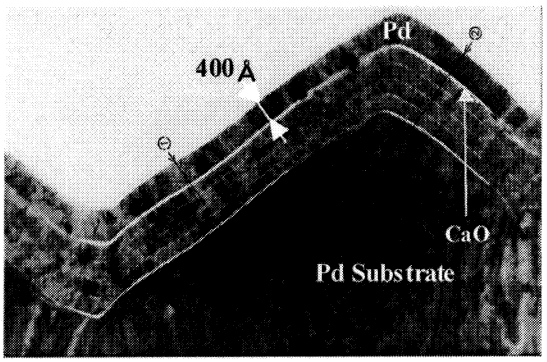

Figure 2. Cross sectional view of Pd complex (Pd/CaO/Pd) observed by TEM (Transmission Electron Microscopy)

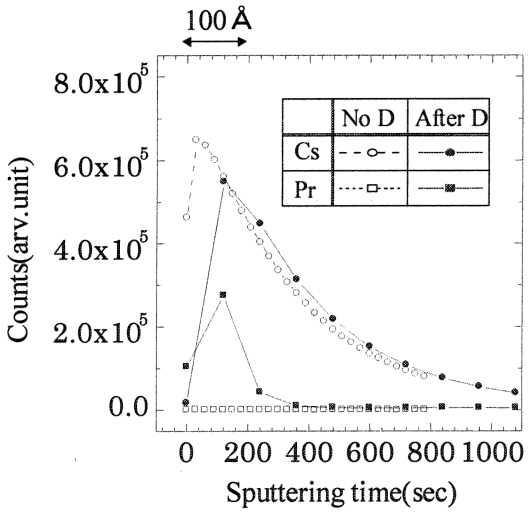

Figure 3. Depth Profiles of Cs and Pr for a Pd complex (Pd /CaO/Pd) sample after D2 gas permeation and a Pd complex (Pd /CaO/Pd) sample without D2 gas permeation

samples, 18keV and 10^{15} ions/cm^2, respectively. The depth profiles were estimated by TOF-SIMS analysis. Physical Electronics TRIFT II was applied for the analysis and the condition of Ga^+ ion was 15keV-600pA. Relation between the sputtering time and the real depth was estimated in advance using a Pd thin film on Si substrate; thickness of the Pd thin film is known. This measurement shows

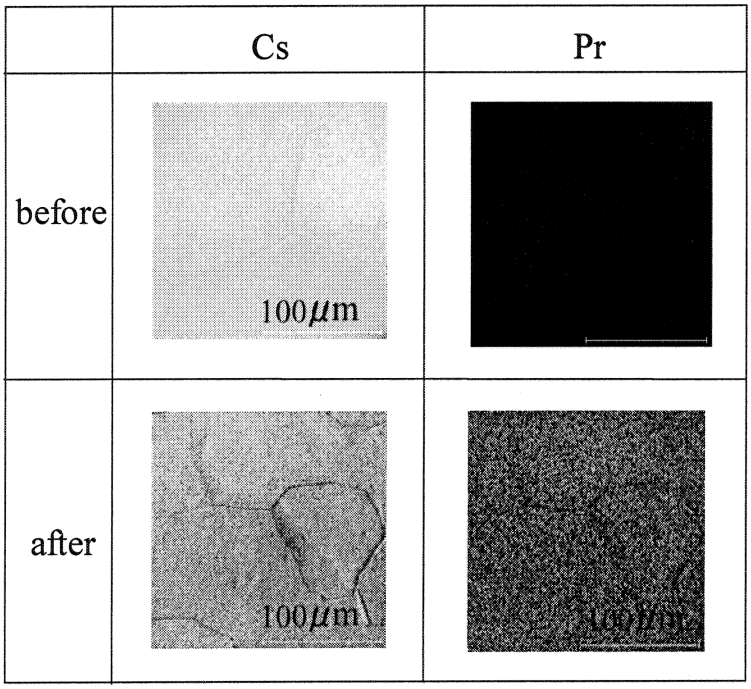

Figure 4. Surface Distributions of Cs and Pr for a Pd complex (Pd /CaO/Pd) sample after D_2 gas permeation and a Pd complex (Pd /CaO/Pd) sample without (before) D_2 gas permeation

that 200 sec sputtering time corresponds to 100 angstrom.

Cs and Pr depth profiles for the Pd complex without permeation show reasonable results in Fig.3. Cs decreases continuously from the surface and there is no Pr in the sample.

On the other hand, Cs and Pr depth profiles for the Pd complex after D_2 gas permeation exhibit interesting results. Cs depth profiles for the foreground and background samples agree in the deep area. However, Cs decreases near the surface after D_2 gas permeation. We can see that there is Pr, which is the same order as given Cs, in the near surface area. This experimental fact suggests that Cs transmutation reaction into Pr occurs in the near surface region up to 100 angstrom. This transmutation active zone might be correlated with D/Pd. Anyway, further investigation for the surface region is important. Figure 3 also shows that Cs atoms do not diffuse and migrate by D_2 gas permeation under our experimental condition. Therefore it is very difficult to assume that the detected Pr was not transmuted product but a gathered impurity. Figure 4 shows surface distributions of Cs and Pr for the two samples mentioned above. Space resolving power is 1 micron. Grain boundaries can be seen in each image. These images show that the surface distribution of Pr basically seems to be uniform and has no correlation with the grain boundaries.

Using ICP-MS analysis, a quantitative estimate of the mass of Pr has been performed. The correlation between D_2 gas permeation rate and conversion rate is shown in Fig. 5.

The conversion rate is defined as

$$\eta = \frac{N_{Pr}}{N_{Cs}} \times 100\% = \frac{N_{Pr}}{N'_{Cs} + N_{Pr}} \times 100\% \quad (1)$$

η : conversion rate(%),

N_{Pr} : detected Pr(ng),

N_{Cs} : given Cs(ng),

N'_{Cs} : det ected Cs after an experiment (ng).

Since ICP-MS analysis is a destructive analysis method, we cannot measure the starting mass of Cs directly. Assuming that a Cs atom is transmuted into a Pr atom, the sum of the detected Pr and the detected Cs after permeation should be equal to the starting Cs.

Figure 5 suggests that the conversion rate defined as above is proportional to the average D_2 gas permeation rate. Experimental results for both the electrochemical addition and the ion implantation of Cs are plotted in the figure. It seems that they have linear correlation for the both cases.

4. DISCUSSION

Let us consider on the situation that D beam irradiates the Pd complex with Cs. The reaction rate is expressed as the following equation.

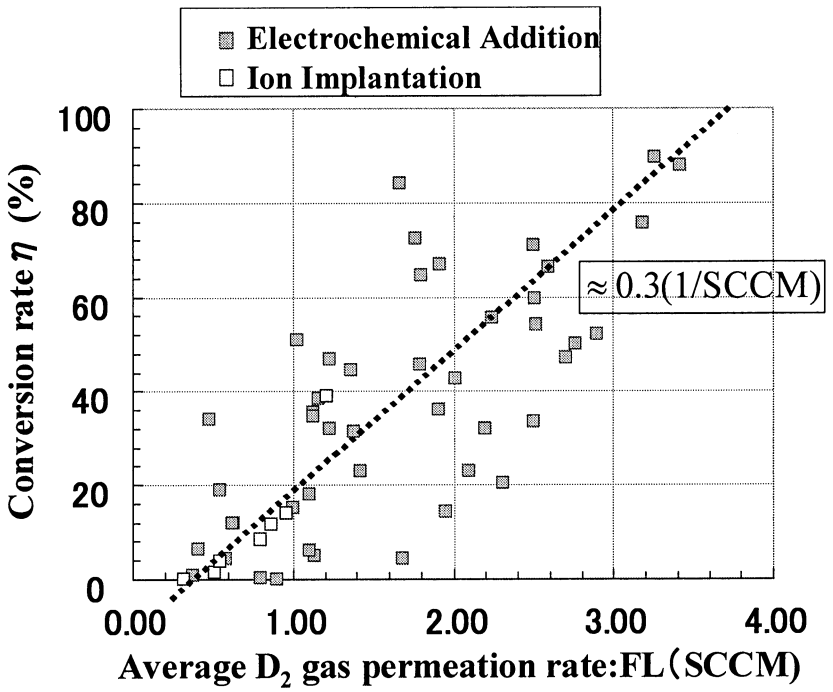

Figure 5. Correlation between D_2 permeation rate and conversion rate

$$R = \sigma \cdot N_{Cs} \cdot \phi \qquad (2)$$

R : reaction rate(event/cm^3/sec),

σ : cross section(cm^2),

N_{Cs} : number of Cs(1/cm^3),

ϕ : deuteron beam flux (1/cm^2/sec).

If we regard D_2 gas permeation as a kind of deuteron beam, the following relation is obtained by equation (2).

$$\eta = \int_t (R / N_{Cs})dt = \int_t (\sigma \cdot \phi)dt = \sigma \int_t \phi dt \approx \sigma \cdot f \cdot FL \cdot T_{exp} / S \qquad (3)$$

FL : flow rate(sccm),

T_{exp} : reactiontion time(sec),

S : permeation surface area(cm^2).

$$\therefore \eta \propto FL$$

This equation agrees with the experimental results shown in Figure 5. Therefore we can roughly estimate the cross section using the obtained experimental results. If we input experimental parameters into equation (3), we obtain

$$\eta = \sigma \cdot f \cdot FL \cdot T_{exp} / S$$

$$= \sigma[cm^2] \cdot FL[sccm] \cdot 3 \times 10^{23}[1/cm^2/sccm]$$

$$= \sigma \cdot \frac{2 \times 6 \times 10^{23}}{22.4 \times 10^3 \times 60} \cdot FL \cdot 100 \times 3600/1.0 \qquad (4)$$

The experimental results show the gradient between FL and conversion rate is about 0.3(1/sccm). (The term sccm means standard cubic centimeter per minute.) Therefore the following result is obtained.

$$0.3 \approx \sigma \cdot 3 \times 10^{23}$$

$$\therefore \sigma \approx 1 \times 10^{-24}[cm^2] = 1[barn]$$

This cross section seems to be extremely large if we take it into consideration that the transmutation reaction belongs to multi-body reactions. And we should notice that we regard the deuterium permeation velocity as deuteron velocity, and the deuteron flux is estimated relatively low, leading to very large cross section. If the deuteron behavior on the microscopic level in the Pd thin film could be clarified, a more precise physical model would be developed. In any case, on the macroscopic level deuterium permeation through Pd complex can be regarded similar to an ultra low deuteron beam, and the cross section of

transmutation of Cs into Pr is estimated at 1 barn according to our experimental results.

5. CONCLUDING REMARKS

We prepared the Pd complex samples that Cs was added using ion implantation instead of the electrochemical method and we detected Pr after D_2 gas permeation. Analysis of the depth profile of Pr indicated that a very thin surface region up to 100 angstroms might be the active transmutation zone. The surface distribution of Pr basically seems to be uniform. There is no correlation between Pr and grain boundaries.

Quantitative analysis of Pr and measurement deuterium flux through Pd complexes was performed. A lot of experimental results suggest that the quantity of Pr was proportional to the deuterium flux through Pd complex. The cross section of transmutation of Cs into Pr can be roughly estimated at 1 barn if we consider the deuterium flux as an ultra low energy deuteron beam.

REFERENCES

[1]Y.Iwamura, M.Sakano and T.Itoh, *Elemental Analysis of Pd Complexes: Effects of D_2 gas permeation.* Jpn. J. Appl. Phys. **41** (2002), pp. 4642-4648.

[2]Y.Iwamura, T.Itoh, M.Sakano, S.Sakai and S.Kuribayashi, *Low Energy Nuclear Reaction in Condensed Matter induced by D_2 Gas permeation through Pd Complexes: Correlation between Deuterium Flux and Nuclear Products.* Proc. of ICCF-10 24-29 August 2003 Cambridge (USA) to be published. (see http//www lenr-canr.org/)

[3]Y.Iwamura, T.Itoh, M.Sakano and S.Sakai, *Observation of Low Energy Nuclear Reactions induced by D_2 gas permeation through Pd Complexes.* Proc. of ICCF-9 19-24 May 2002, Beijing (China); pp.141-146.

[4]Y.Iwamura, T.Itoh and M.Sakano, *Nuclear Products and Their Time Dependence Induced by Continuous Diffusion of Deuterium through Multi-layer Palladium Containing Low Work Function.* Proc. of ICCF-8, 21-26 May 200 Lerici (Italy), SIF Conf. Proc.Vol.70, pp.141-146.

[5]M.Sakano, S.Sakai, T.Itoh , Y.Iwamura and S.Kuribayashi, Proc. of JCF-5

[6]A.Takahashi, *Tetrahedral and octahedral resonance fusion under transient condensation of deuterons at lattice focal points.* Proc. of ICCF9 19-24 May 2002, Beijing (China); pp.343-348.

[7]A.Takahashi, *Mechanism of Deuteron Cluster Fusion by EQPET model.* Proc. of ICCF-10 24-29 August 2003 Cambridge (USA) to be published. (see http//www lenr-canr.org/)

[8]Y.Iwamura, T.Itoh, M.Sakano and S.Kuribayashi; SOLID STATE PHYSICS, Agne, Vol.39 (2004), p.p.203-210.

The Phenomena of Nuclear Transmutation by D_2 Gas Permeation Through Pd Complex

Taichi HIGASHIYAMA*, Hiroyuki MIYAMARU, Akito TAKAHASHI (Osaka University)
Mitsuru SAKANO (Mitsubishi Heavy Industries)
* higashiyama@stu.nucl.eng.osaka-u.ac.jp

Abstract

As a replication of Mitsubishi Heavy Industries (MHI) experiment, we performed D_2 gas permeation through Pd complexes with additional Cs on the surface at 3 times. After permeating D_2 gas, the sample was analyzed by Inductively Coupled Plasma Mass Spectrometry (ICP-MS) and we confirmed production of Pr with each run. And also the results analyzed by fast Neutron Activation Analysis (NAA) show the existence of Pr.

Therefore, it was confirmed that the nuclear transmutation reaction, from ^{133}Cs to ^{141}Pr, was occurred. This transmutation suggests mass number and atomic number increase 8 and 4, respectively. It is considered that the 8D multibody fusion reactions proposed by A. Takahashi can explain this mass-8-and-charge-4 increased transmutation.

Keywords: Cs, Pr, Pd Complex, ICP-MS, NAA, Transmutation

1. Introduction

We received a report from Iwamura's group in Mitsubishi Heavy Industries (MHI) that unusual nuclear reactions were occurred by permeating D_2 gas through Pd complexes with added Cs or Sr on the surface[1]. The condition was as follows: D_2 gas flow rate through the sample (Pd complex) was over 1 sccm, the temperature was 343 K, D_2 gas pressure was 1 atm and the flow time was 1 week. (Note: the unit "sccm" is a flow rate of one cc per a minute in standard conditions.)

In contrast, they performed permeating H_2 gas instead of D_2 gas, but it showed no change (no decreasing of Cs and no generation of Pr). The elemental analysis was done by X-ray photoelectron spectroscopy (XPS).

Following the MHI procedure exactly, we performed D_2 gas permeation experiments through Pd complexes and analyzed whether Pr was generated. The following is the report of this replication experiment.

2. Experiments

2.1 Samples

The samples were composed of a Pd thin film, alternating CaO and Pd layers and bulk substratum Pd as shown in Fig. 1. At first, the alternative layers of CaO and Pd (thickness: 1000 Å) was covered the surface of the substratum Pd plate. Then the 400-Å-thick Pd layer was sputtered on the surface of the alternative CaO and Pd layers. These processes were performed by Ar ion beam sputtering. After forming the Pd complex, Cs was deposited on the surface of the thin Pd layer in 1 mM $CsNO_3$ solution by applying a weak electric field. A 1 V negative voltage was applied to the Pd complex for 10 seconds.

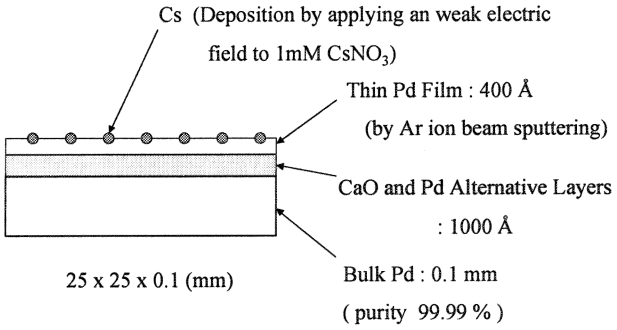

Figure 1: Sample fabricated by MHI.

In order to remove hydrocarbon contamination on the sample, we performed following pre-cleaning operation before depositing Cs. An electric field was applied between the sample and a Pt plate in 1 mM HNO_3. At first, the sample was anode and the Pt plate was cathode. Then the bubble was formed on the surface of the Cs deposit side. Next, in order to reduce the oxidized sample, we performed electrolysis turning over the electrodes (the Pt plate was anode and the sample was cathode). And Teflon (chemically stable) was used to set up the sample and the Pt plate.

2.2 Experimental Equipments

Chamber A was filled with 1 atm D_2 gas, and Chamber B was evacuated by a turbo-molecular pump (TMP) as shown in

Fig. 2, so that deuterium atoms permeate from the Cs-deposit side to the backside of the sample in Chamber B. The sample was normally heated to 70 degree Celsius and measured the data of the temperature during these experiments by the thermo-couple.

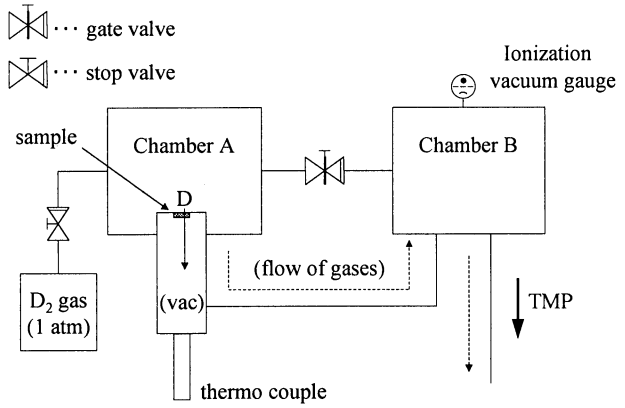

Figure 2: Experimental equipments.

2.3 D_2 Gas Permeation Experiments

2.3.1 The First Run

Using the experimental system as shown in Fig. 2, we have performed three runs of D_2 gas permeation through Pd complexes. In the first run, we changed the temperature stepwisely to 70, 60 and 80 degree Celsius and permeated D_2 gas for about 120 hours.

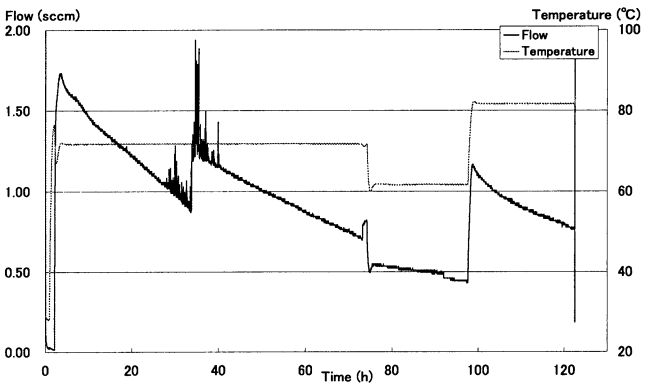

Figure 3: Relation between deuterium flow rate and temperature in the first run.

We show the result in Fig. 3. The flow rate exceeded 1.5 sccm initially, then decreased slowly, and finally fell below 1 sccm. (According to the MHI group, 1 sccm is considered to be the critical value for transmutation.) As the temperature was stepped up, the flow rate increased and exceeded 1 sccm again, but it soon declined again. We observed unnatural fluctuations in the flow rate between 20 and 40 hours. We think that electrical miscontact of the ionization vacuum gauge caused this.

2.3.2 The Second Run

In the second run, the flow rate was below 1 sccm wildly from the beginning, so we raised the temperature from 70 to 80 degrees Celsius and lengthened D_2 gas permeation time to about 200 hours as shown in Fig. 4, in order to raise the flow rate and amount. But the flow rate was still below 1 sccm. We consider the possible reason is that many impurities (almost are moisture) attached in the chambers from atmosphere because of being left long time (about 14 hours) from stopping the bake to fitting the sample in Chamber A. And these impurities formed on the sample surface, which prevented D_2 gas from permeating through the sample efficiently. The data gap near 30 hours occurred when we stopped the vacuum equipment because of a shortage of N_2 gas which operates the evacuating system.

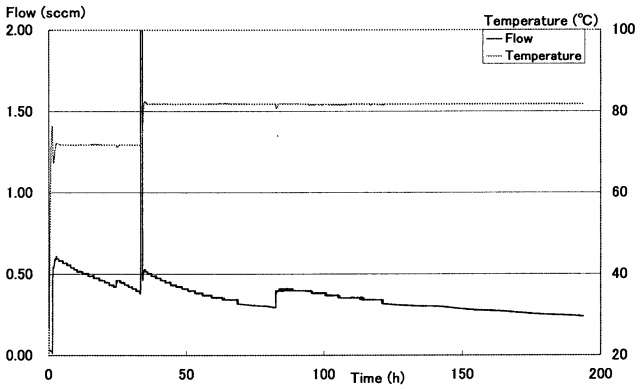

Figure 4: Relation between deuterium flow rate and temperature in the second run.

2.3.3 The Third Run

We kept the temperature constant at 70 degree Celsius and permeated D_2 gas for about 120 hours in the third run. To minimize the effect from these impurities, N_2 gas was fed and evacuated before setting up the sample and the sample was fixed quickly after stopping the bake and feeding N_2 gas. As the results, flow rate was improved to over 2 sccm at first. But because D_2 gas left in the bottle was little, we couldn't maintain the D_2 gas pressure in the Chamber A at 1 atm, and the flow rate decreased gradually. The detailed flow rate data before 40

hours was lost because of a problem in the data acquisition system, so the curve is approximated with data of 0 and 20 hours taken manually from the values of the ionization vacuum gauge, as shown in Fig. 5.

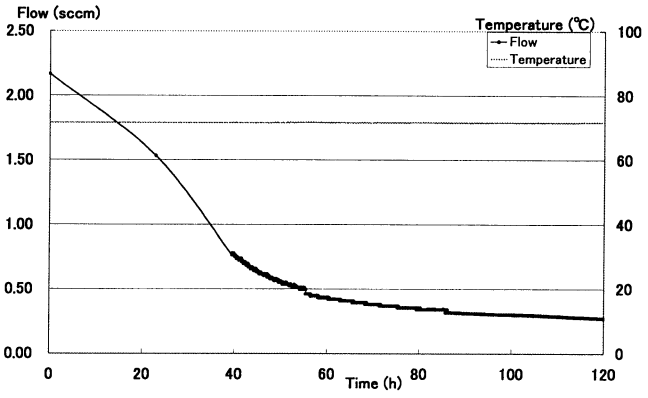

Figure 5: Relation between deuterium flow rate and temperature in the third run.

3. Results of Elemental Analysis

3.1 Analysis by ICP-MS

The elements on the sample were analyzed by ICP-MS in MHI. The result revealed the production of Pr atoms as shown in Table 1, although amounts were different with each run. And a correlation seems to exist between the amounts of the produced Pr and the maximum flow rates.

Table 1: Amounts of produced Pr analyzed by ICP-MS in the MHI.

	Pr (ng)	Cs (ng)	max flow (sccm)	average (sccm)	minimum (sccm)
1st run	18	180	1.73	0.93	0.43
2nd run	5.1	141	0.61	0.35	0.29
3rd run	36	330	2.17	0.76	0.27

3.2 Analysis by Neutron Activation Analysis

We also analyzed a Pd complex sample by Neutron Activation Analysis (NAA) using 14 MeV fast neutrons in Fusion Neutronics Source (FNS) of Japan Atomic Energy Research Institute (JAERI). The sample had been permeated D_2 gas and analyzed by XPS in MHI[1].

When ^{141}Pr is irradiated by 14 MeV fast neutron, ^{141}Pr(n,p)^{141}Ce reaction occurs, and then ^{141}Ce releases 145 keV gamma-ray to be stable to ^{141}Pr (with 32.5 days half-life). So the reason why we used 14 MeV fast neutrons is as follows: Because of the half-life of ^{141}Ce is longer than the other elements comprising almost of the sample (Pd, Ca and so on), we can determine that gamma-rays by proper cooling after irradiation even if the amount of ^{141}Pr is a little.

And there is another reason. When ^{88}Sr was used instead of ^{133}Cs, then ^{96}Mo will be formed. If ^{96}Mo is irradiated by 14 MeV neutron, ^{96}Mo(n,p)^{96}Nb reaction occurs and then ^{96}Nb decays, so we can know the existence of ^{96}Mo. But if ^{96}Mo is irradiated by thermal neutron, ^{96}Mo(n,g)^{97}Mo reaction occurs and ^{97}Mo don't decay (stable). So we can't measure when using thermal neutron.

Figure 6 shows the Ge gamma-ray spectra of the NAA sample after the irradiation by 14 MeV fast neutrons in FNS. In the first measurement, the sample was irradiated for 11 days, cooled for 25 days and measured for 7 days. And at the second measurement, the sample was cooled for 8 days after the first measurement and measured for more 9 days. We increased the efficiency of the HPGe detector by setting the sample very close to the detector window for the second measurement, to improve counting statistics.

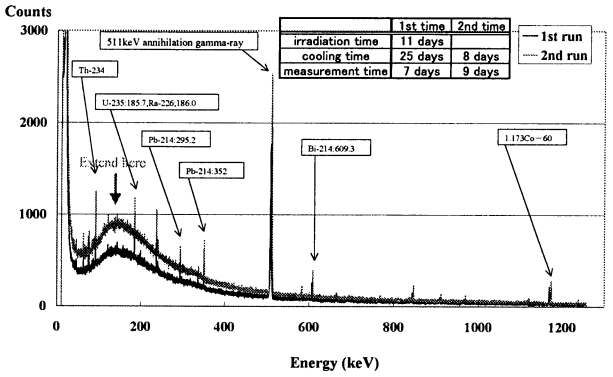

Figure 6: Ge gamma-ray spectra by NAA of 14 MeV neutron irradiation.

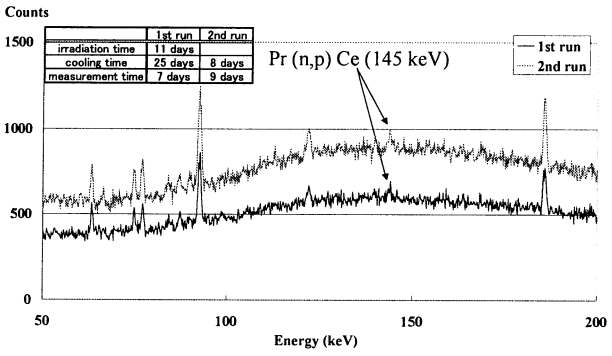

Figure 7: Expanded spectra for detail analysis

by NAA of 14 MeV neutron.

Figure 7 shows the energy region near 145 keV, which indicates the existence of Pr. For the second measurement, we increased Ge detector efficiency so that we normalized with 511 keV peaks of background gamma-rays before comparing with two (first and second measurement) spectra. We could see a decay of 145 keV peaks of ^{141}Ce from the first measurement to the second measurement, with half-life of about 40 days with large (more than 50 %) error bar obtained by only two data points (32.5 days is the exact half-life). This 145 keV peak with decay convinced us of the existence of ^{141}Pr in the sample. However the counting statistics for peaks of ^{141}Ce were not high enough to obtain the exact half-life. So, now we are performing another irradiation to improve the statistics.

4. Discussion and Conclusion

After the three runs of permeating D_2 gas through the samples in our laboratory and analysis by ICP-MS in MHI, we could confirm the existence of Pr from three runs, as shown in Table 1.

And we also confirmed the existence of Pr by 14 MeV NAA in FNS as shown in Fig. 7, for the sample which D_2 gas permeation was done by MHI.

In order to explain this phenomenon that Cs changes to Pr, a "theory of 8D multibody fusion reactions" is considered.[2] This model holds that two high energy ^{8}Be nuclei (Be*) are produced by octahedral resonance fusion of eight deuterons in the Pd lattice, and these Be particles may be absorbed by Cs (or Sr) to cause transmutation with mass number 8 and atomic number 4 increased reaction, as shown in Fig. 8. Also, since these ^{8}Be nuclei have very short lifetime 6.7×10^{17} sec, they decay to two stable ^{4}He atoms as soon as they are formed. But we have enough collisions with Cs (or Sr) nuclei within the range.

Reaction formula is as follows:

(Primary reaction):

$$8D \rightarrow {}^{16}O^{*} \rightarrow {}^{8}Be + {}^{8}Be + 95.2\ (MeV)$$

(Secondary reaction):

$$^{133}Cs + {}^{8}Be\ (47.6\ MeV) \rightarrow {}^{141}Pr^{*}\ (50.47\ MeV)$$

or

$$^{8}Be \rightarrow {}^{4}He + {}^{4}He$$

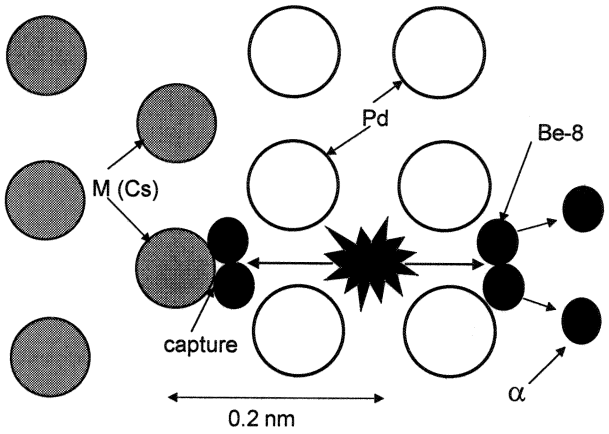

Figure 8: Model of 8D nuclear fusion.

If the nuclear transmutation is induced by the secondary reactions of the 8D fusion, ^{4}He gas also must be produced. So we are planning another experiment to confirm ^{4}He production by using Quadruple Mass Spectrometer (QMS) system.

References

1) Y. Iwamura et al., Proc. ICCF 9, May 19-23, 2002, Beijing, China, pp.141-146.

2) A. Takahashi, Proc. ICCF9, May 19-23, 2002, Beijing, China, pp.343-348.

ELEMENTAL ANALYSIS ON PD-FOIL AFTER HYDROGEN PERMEATION AT ROOM TEMPERATURE BY TOF-SIMS

H. YAMADA, S. NARITA, H. ONODERA, H. SUZUKI, N. TANAKA, T. NYUI
AND T. USHIROZAWA, Iwate University
yamada@dragon.elc.iwte-u.ac.

Abstract: Time-of-flight secondary ion mass spectroscopy was employed for elemental analysis of the palladium foil surface. Increase in count intensity of several elements including Ag was found after hydrogen permeation. Introducing of hydrogen gas at a pressure of 10 atm has sometimes yielded a large count intensity of Fe. The isotopic ratios of Ti and Cr have been observed to differ from the natural ones. These elements could have been produced by some nuclear transmutation.
Keywords: Pd-hydride, Hydrogen permeation, Transmutation, Time-of-flight secondary ion mass spectroscopy

1. Introduction

The possibility of inducing nuclear reactions at low temperature in solid-state has been widely investigated for about fifteen years. Among several experimental methods for the reaction, the gas permeation method is one of the promising methods. Iwamura et al.[1] has studied using this method with Pd film complexes, which consist of thin Pd layers, a CaO layer and a bulk Pd. They have reported observation of element production in deuterium permeation experiment and recently have found a certain rule of nuclear transmutation, that is, 8 mass number and 4 atomic number increase in the process. The phenomenon has been observed with good reproducibility. The result suggests that there is a key to understand the reaction in terms of the mobility of deuteron in Pd lattice.

In this present study, we have performed similar permeation experiment using hydrogen with Pd foil without any additional layer, and have searched for the products as a result of low energy nuclear reaction. The method has an advantage of involving less contamination in the palladium sample in contrast to other methods; the method is preferably used in investigating small amount of elements. This study would provide us information to understand transmutation process systematically. In addition, we would consider the possibility of nuclear transmutation not only in deuterium system but also in hydrogen system as some researchers have claimed in various experiments [2,3].

2. Experiment

The Pd foil (99.95% pure) sample ($0.1\times 12.5\times 12.5$mm and $0.3\times 12.5\times 12.5$mm) was rinsed with acetone and pure water, then washed by aqua regia to remove impurities on the sample surface. No hydrogen gas was loaded to the sample before hydrogen permeation experiment. The Pd plate was set into a stainless steel holder placed between two chambers.[4] The upper chamber was filled with hydrogen gas at a pressure up to 10 atm, and the lower was evacuated by a diaphragm pump to prevent the Pd sample from being contaminated from the atmosphere. The gas atoms were driven through the Pd sample to the evacuated chamber by the pressure gradient. The gas was kept flowing for about 2 weeks, then the sample ("After sample") was taken out from the holder. Before the element analysis, the sample was heated to 400℃ to purge the hydrogen atoms remaining in. The sample surface of gas-filled side was analyzed by time-of-flight secondary mass spectroscopy (TOF-SIMS) (ULVAC-PHI: TFS-2100).

TOF-SIMS has a good sensitivity for a small quantity of the elements on the sample with high resolution in mass number although it is difficult to deduce the absolute quantities from its output data alone. The primary ion in TOF-SIMS was Ga^+ and measured area was 40×40 micron square. In order to take into account the contamination from the environment, we prepared the control sample ("Control sample"), which was set into the holder for the same period of about 2 weeks as that for "After sample" without flowing the hydrogen gas. Comparing the composition of the elements on the surface between them, we specified newly produced elements during the hydrogen gas permeation. As TOF-SIMS is capable of analyzing most of all the elements with their isotopes, we also tried to analyze the isotopic compositions for some of the elements detected.

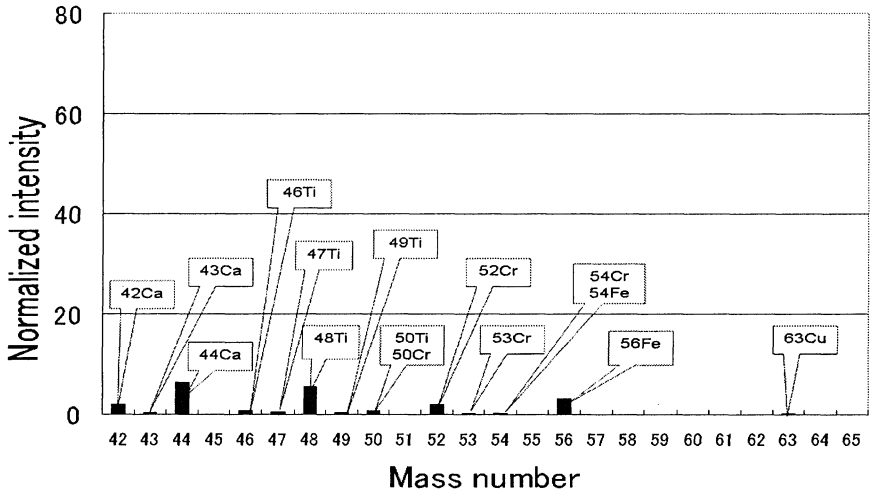

Fig. 1 Normalized count intensity for the control Pd sample with 10 sec sputtering.

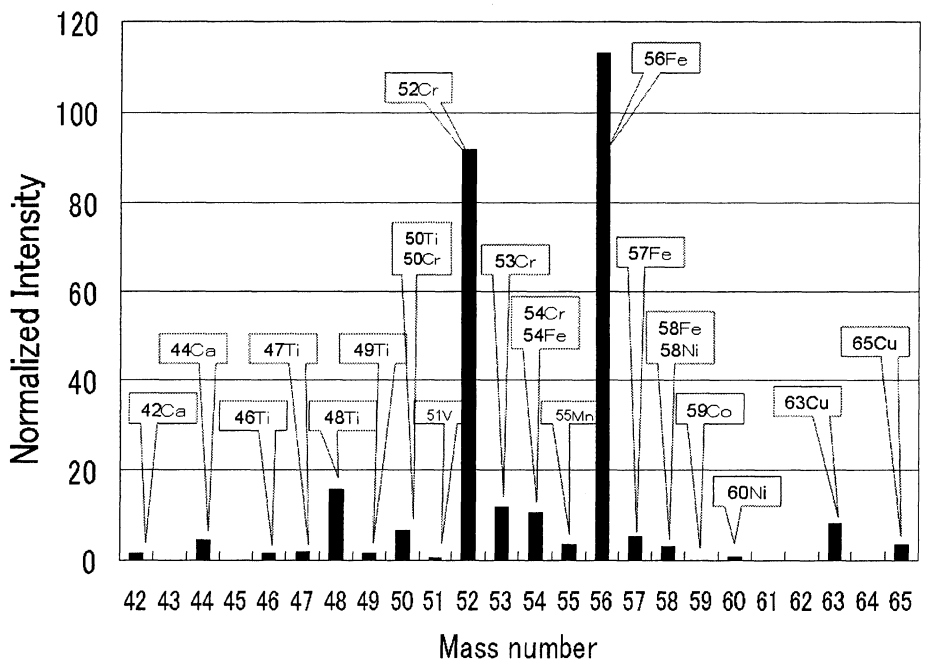

Fig. 2 Normalized count intensity after hydrogen permeation with 10 sec sputtering.

3. Results and Discussion

In TOF-SIMS analysis, we performed on three randomly selected areas (40 μ m $\times$ 40 μ m) of each sample. The TOF-SIMS system is capable of removing the uppermost surface layers of the sample by Ga sputtering for surface cleaning. The average values of total count for "Control samples" and "After samples" with 10sec sputter cleaning divided by ^{69}Ga count, were 3.9 and 3.4, respectively. The value for "Control samples" is fairly close to that for "After samples". Most of the total counts for both samples have been revealed to be those of molecules induced from environments. This means that "Control samples" include almost same amount of contaminants as "After samples" have, even though 10 sec sputter cleaning has been conducted. Further, it was found that the SIMS intensity of ^{69}Ga beyond 4×10^5 count was

Control		After permeation		
		0.1mm 1atm 0.1mm 3atm	0.1mm 10atm	0.3mm 10atm
0.5	1.7	0.2	0.3	1.1
0.5	2.5	0.3	0.4	2.9
0.7	3.5	0.3	0.5	4.1
0.8	4.8	0.3	1.3	13.1
0.9	6.6	0.4	2.4	
1.4	6.8	0.6	2.4	16.7
1.4	7.3	0.6	4.4	18.1
1.4	11.9	2.4	6.9	68.5
1.5	12.8		9.9	183.5
			12.5	
			18.4	
			34.7	

Table 1. The signal intensity of ^{56}Fe, defined as the count of the secondary ions of ^{56}Fe divided by that of ^{69}Ga and multiplied by 1000, in case of ^{69}Ga count more than 400,000.

	Natural	After permeation
$^{49}Ti/^{47}Ti$	0.727	0.867 0.906 0.943 (+30%)
$^{53}Cr/^{52}Cr$	0.113	0.125 0.131 0.145 (+28%)

Table 2. Change in isotopic ratio for Ti and Cr

required to present reliable result.

3.1 Possible elements production

In this study, we do not discuss absolute quantities of the elements, since we have difficulties in quantitative analysis using the TOF-SIMS. Instead, we use a normalized intensity that is defined here as the count of the secondary ions of each element divided by the total count of ions recorded and multiplied by 10000. We did not find any significant difference in the mass spectrum for every selected area of the Pd samples at a fixed test condition.

Figure 1 shows a typical mass spectrum in the range of mass numbers 42−65 for the surface of "Control sample" with 10 sec sputter cleaning by $^{69}Ga^+$ ion beam. Low count intensities of several mass numbers, corresponding to elements Ca, Ti, Cr, Fe and Cu, were detected. Of these, most parts of the elements are considered to be the impurities included in the Pd foil.

Figure 2 illustrates a typical mass spectrum for the Pd surface after the hydrogen permeation with 10 sec sputter cleaning. Appreciable increase in the count intensity for mass numbers 46, 47, 48, 49, 50, 52, 53, 54, 55, 56 and 63 is seen. These mass numbers correspond to elements Ti (^{46}Ti, ^{47}Ti, ^{48}Ti, ^{49}Ti, ^{50}Ti), Cr (^{50}Cr, ^{52}Cr, ^{53}Cr, ^{54}Cr), Mn (^{55}Mn), Fe (^{54}Fe, ^{56}Fe) and Cu (^{63}Cu), respectively. In particular, marked increase in the intensities of Cr, Fe and Cu is found for several Pd samples after the hydrogen gas permeation at a pressure of 10 atm. We also detected signals of mass numbers 51, 57, 58, 59 and 65 only for the Pd samples after the permeation, which correspond to elements ^{51}V, ^{57}Fe, ^{58}Fe, ^{58}Ni, ^{59}Co, and ^{65}Cu, respectively. Furthermore, considerable increase in the count intensities for mass numbers 107 and 108, corresponding

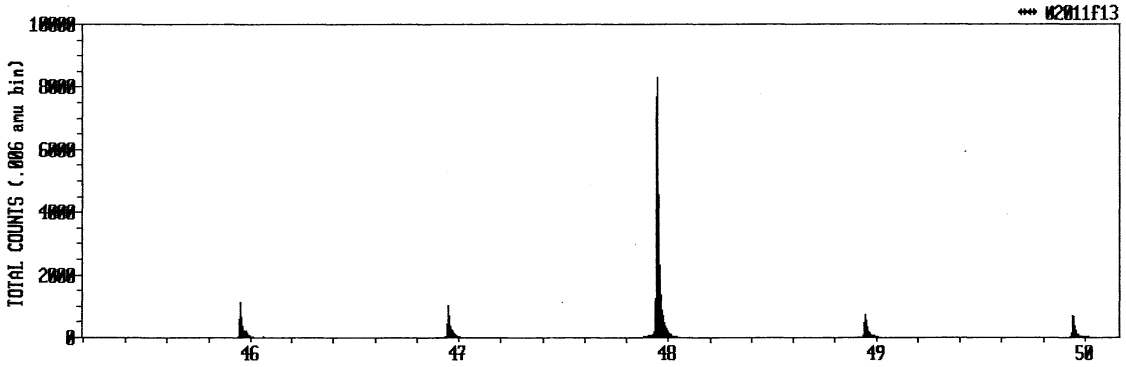

Fig. 3 Mass spectrum for mass number ranges 46-50 after hydrogen permeation with 10 sec sputtering.

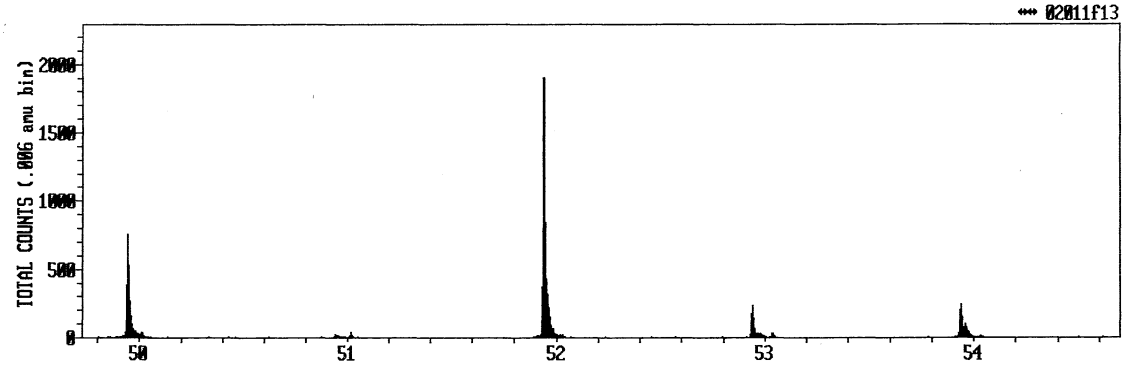

Fig. 4 Mass spectrum for mass number ranges 50-54 after hydrogen permeation with 10 sec sputtering.

to element Ag (^{107}Ag, ^{109}Ag), was observed. These results suggest that these eight kinds of elements could have been produced in the hydrogen gas permeation process.

3.2 Pressure effect on cont intensity of Fe

The count intensity of Fe on Pd samples after the permeation was most marked among those of several metal elements observed. Table 1 shows count intensities of ^{56}Fe at hydrogen gas pressures of 1, 3 and 10 atm. The intensity is defined as the count of secondary ions of ^{56}Fe divided by that of ^{69}Ga and multiplied 1000, being obtained from each selected measured area of 40×40 micron square.

In view of the count intensities presented in Table 1, the intensity for "After sample" with 0.1 mm thickness at pressures of 1 and 3 atm does not give big difference from that for "Control sample". On the contrary, considerable large count intensities were observed for the samples after the permeation at 10 atm. In case of 0.1 mm thickness and 10 atm, two out of twelve selected areas provided large count intensities. Such large values were obtained at four out of eight selected areas for samples with thickness 0.3 mm at 10 atm. This suggests a possibility of a thickness effect on Fe production, although the detail is not clear. The pressure effect could well be explained in terms of proton density near the surface of Pd foil during permeation; the higher density could be expected by applying higher pressure of the hydrogen gas. This idea might be in line with the report by McKubre et al. [5] that the average loading ratio D/Pd should exceed a critical one to observe excess power production.

3.3 Change in isotopic ratio

We could not distinguish the count intensity of ^{48}Ti from that of ^{48}Ca using the TOF-SIMS, because the mass number ^{48}Ti is close to that of ^{48}Ca. Similarly, the count intensity of ^{50}Ti could not be distinguished from that of ^{50}Cr. While, there is no element with mass number close to those of ^{47}Ti, ^{49}Ti, ^{52}Cr and ^{53}Cr.

Table 2 gives the isotopic ratios of count intensity of ^{49}Ti to ^{47} Ti, ^{53}Cr to ^{52}Cr for a Pd sample after the hydrogen gas permeation and these natural ratios. The natural isotopic ratio of ^{49}Ti to ^{47}Ti is 0.73. On the other hand, counts

of ^{49}Ti and ^{47}Ti detected from a selected area of "After sample" were 2147 and 2276, respectively. The latter yields a large ratio of 0.94. Next, it is necessary to know count intensities of molecules having mass numbers close to 47, 49 and 53. Because each of these intensities might overlap with those of elements ^{47}Ti, ^{49}Ti and ^{53}Cr, there is a possibility that the apparent deviation of the isotopic ratios of these elements from their national isotopic ratios was observed. The approximate order of the intensities of molecules ^{46}TiH, ^{48}TiH and ^{52}CrH can be estimated as follows

The mass number of ^{49}Ti determined by TOF-SIMS was 48.9506. The mass number of H is 1.0078. Therefore, if molecule ^{49}TiH was formed in the permeation process, a count intensity of mass number 49.9584 should be observed. As is seen in Fig. 3, the mass number corresponding to the peak presented in the vicinity of mass number 50 is 49.9835. TOF-SIMS is capable of distinguishing between these two values. This is well illustrated in the figure, where no peak corresponding to the mass number 49.9584 was detected, the result of which indicated little formation of molecule ^{49}TiH by the hydrogen gas permeation. Accordingly, little formation of molecules ^{46}TiH and ^{48}TiH is expected. Thus, the count intensities due to the formation of these molecules are considered to have no effect on the count intensities for mass numbers at around 47 and 49.

The natural isotopic ratio of ^{53}Cr to ^{52}Cr is 0.113. The obtained ratios for three selected areas of an "After sample" were 0.125, 0.131 and 0.145. The value 0.145 is 28% larger than the natural ratio. The mass number of ^{53}Cr determined by TOF-SIMS was 52.9417. Therefore, if molecule ^{53}CrH was formed in the hydrogen permeation process, a signal corresponding to mass number 53.9495 should be observed. The peak mass numbers of the two signals detected at around 54 in Fig. 4 are 53.9399 and 53.9655, being clearly different from 53.9495 of ^{53}CrH. Namely,, no peak corresponding to mass number 53.9495 was detected. This means that the formation of molecule ^{53}CrH is improbable. Consequently, the formation of molecule ^{52}CrH is expected to be negligible, having no appreciable effect on the total count of signal at around mass number 53. Further, most of the count of other molecules having mass number about 47, 49, 52 and 53 can be distinguished from these of ^{47}Ti, ^{49}Ti, ^{52}Cr and ^{53}Cr by the TOF-SIMS.

On the contrary, no anomaly of the isotopic ratio was seen for Fe, Cu, Ag and Pd; the ratio of "After sample" for these elements was consistent with natural one. The deviation of the isotopic ratio from natural one observed for Ti and Cr is one of a positive evidence of the nuclear transmutation occurring in/on Pd foil.

4. Conclusion

Elements analysis on the Pd foil were performed for a sample after hydrogen permeation experiment and a control sample using TOF-SIMS. Increase in count intensity of elements Ti, Cr, Mn, Fe, Ni, Cu and Ag was observed for the Pd sample after the hydrogen gas permeation. These elements might be produced during the permeation by some nuclear transmutation. Pressure effect on count intensity of Fe has been investigated by changing hydrogen gas pressure of the gas-filled side of Pd, resulted in the observation of a large count intensity of Fe for the Pd sample after the permeation at a hydrogen pressure of 10 atm. In the isotopic ratio of Ti and Cr, considerable deviation from the natural one was found in all of the three selected areas of the sample. While, no change in isotopic ratio was seen for other elements. The results suggest strongly that the reaction occurs in hydrogen system as well as in deuterium system.

References:

1) Y. Iwamura, T. Itoh and, M. Sakano, Jpn. J. Appl. Phys., 41, 4642 (2002).
2) J. Deform, D. Murat. X. Dufour and J. Foos, Proceedings of 8-th International Conference on Cold Fusion, p. 153 (2000).
3) T. Ohmori, H. Yamada, S. Narita and T. Mizuno, Proceedings of 9-th International Conference on Cold Fusion, p. 284 (2002).
4) H. Onodera, S. Narita, H. Yamada, H. Suzuki, N. Tanaka and T. Nyui, Proceedings of the 4-th Meeting of Japan CF research Society, p. 42 (2003)
5) M. C. H. McKubre, S. Crouch-baker, A. M. Riley, S. I. Smedley and F. L. Tanzella, Proceedings of 3-rd International Conference on Cold Fusion, p. 5 (1993)

Clean Fusion by Tetrahedral and Octahedral Symmetric Condensations

Akito Takahashi
Osaka University
akito@nucl.eng.osaka-u.ac.jp

Abstract: Super screening of Coulomb barrier on deuteron cluster fusion is modeled by formation of quasi-molecular states with electronic quasi-particles under tetrahedral and octahedral symmetric condensations of deuterons in the transient motion of metal-deuteride lattices. Cluster fusion resonates for 4D and 8D fusion processes, of which products are clean (radiation-less) to be major products of ^{4}He with secondary transmutation reactions. Possible reaction branches and products are discussed.
Keywords: 4D fusion, 8D fusion, symmetric condensation, electronic quasi-particle, clean products

1. Introduction

Major claims of experiments for condensed matter nuclear reactions (so called "cold fusion"), such as ^{4}He generation in correlation with excess heat[1,2], selective two-alpha-added transmutations[3,4], and fission-like products[5], can not be attributed to "cold fusion" of known d-d fusion reactions in condensed matter, but can be solely explained by "new reaction theory in condensed matter". Key issues in problems of theorization are; how to construct a consistent theory to explain in linkage of the above major claimed results, and to keep compatibility to already established physics.

We have developed a cluster fusion theory based on the EQPET (Electronic Quasi-Particle Expansion Theory) model[6-8], to explain consistently the above major experimental claims. First, we had to look for the possibility of super-screening of Coulomb barrier between deuterons in lattice. We considered transient or dynamic conditions of deuterons and electrons motion in PdDx lattice.

Time-dependent motion of deuterons at O-sites of PdDx was treated as plasma oscillation in lattice harmonic potentials, and focal point in periodical time domain was assumed[11]. We still use this approximate treatment in the present work. We treat a transient condensate of deuteron cluster at focal point by a steady multi-body cluster with certain life time (more than several fs), and considering the period of lattice plasma oscillation (about 10 to 100 ps) plasma we estimate a relative weight for effective existing time of transient condensate to multiply with fusion rate of steady EQPET molecule.

We looked for the condition that overcame the Thomas-Fermi gas limitation of Coulomb screening by electrons. We assumed in transient motion of deuterons at tetrahedral and octahedral condensations that transient molecular state dde* with electronic quasi-particle e* could be formed under symmetric condensation conditions that are some kind of dynamic Bose-type condensation. Focal points of deuteron cluster were imagined in T-sites of PdD full loaded lattice (TSC: tetrahedral symmetric condensation) and O-sites of PdD_2 overloaded lattice (OSC: octahedral symmetric condensation), as shown in **Fig.1 (a) and (b)** respectively, and in some defects or deformed lattice points at grain boundaries. Speculated mechanisms are: D-cluster fusion in lattice dynamics produces 23.8MeV two ^{4}He-particles in 180 degree opposite directions and/or 47.6MeV two ^{8}Be-particles in 180 degree opposite directions, per 4D and/or 8D fusion respectively. Transmutation reactions including fission may take place as secondary reaction of these high-energy particles with lattice metal nuclei.

This paper treats first to briefly summarize the EQPET model for TSC and OSC conditions. Then discussions are extended to estimate power levels of deuteron cluster fusion reactions, possible branches of outgoing channels with characteristic products (particles) and quality of

clean fusion process. Discussions are also given comparing results of the present model and experimental results by Krabut[9] and Iwamura[4].

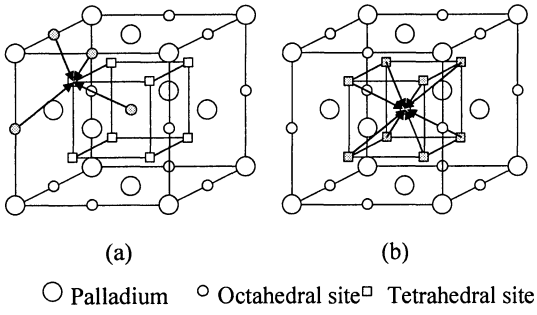

Fig.1: Tetrahedral (a) and octahedral (b) condensation of deuterons in PdDx

2. Deuteron Cluster Fusion

Model example of deuteron cluster fusion was proposed as the Tetrahedral Symmetric Condensation (TSC) and the Octahedral Symmetric Condensation (OSC) in PdDx lattice dynamics. As illustrated in Fig.1, TSC may take place at locally full loaded PdD regions (x=1.0), while OSC may happen much more difficultly at locally overloaded PdD_2 regions (x=2.0). As discussed later on power level, we only need to require local density of 1E-6 times (ppm order) of Pd density for the OSC condition, while much higher local density, e.g., 10 % of Pd atomic density is required for the TSC condition. To generate electronic quasi-particle states, basic mechanism is thought to be the dynamic formation of quadruplet deuteron molecule, which is an **orthogonal coupling of two D_2 molecules**, as illustrated in **Fig.2**.

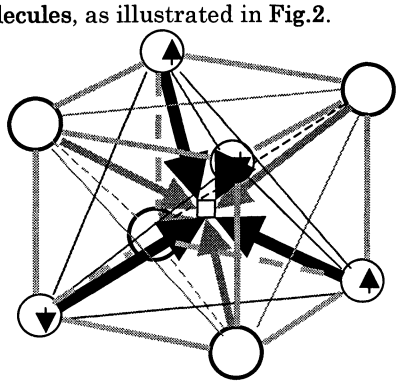

Fig.2: TSC, bigger circles for deuterons and smaller circles with arrow (spin) for electrons

Three-dimensional motion of TSC can be converted to two-dimensional motion using momentum vector conversion[10]. A two dimensional view of TSC is shown in **Fig.3**. To minimize total energy of the system, charge neutral condensation in average of 4D cluster (4 deuterons with alternately coupled 4 electrons with anti-parallel spins for counter-part electrons with reversed momentums) may cause the central point (T-site in this case) condensation from 4 O-sites of deuterons and 4-sites of electrons. Hence, transient condensate of electrons, namely quadruplet e*(4,4) may be formed at around the central T-site.

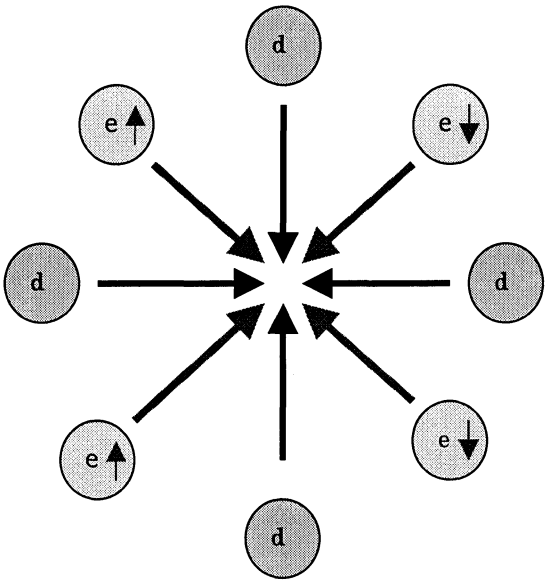

Fig.3: Two-dimensional view of TSC, plus charge for d, minus charge for e

We assume a similar condition for the OSC motion, as illustrated in **Fig.4**. When 4 electrons down-spins are happening to be arranged on upper half together with 4 electrons up-spins on lower half, averaged charge neutral condensation from 8 T-sites to the central O-site may become possible, to form 8D cluster with an octal-coupling state e*(8,8) of electrons at around the central O-site. This condition may realize super-screening for virtual d-d pairs in the 8D cluster, and 8D fusion rate can be calculated by the rapid cascade reaction model, i.e., D+(D+(D+(D+(D+(D+(D+D))))))[8,10].

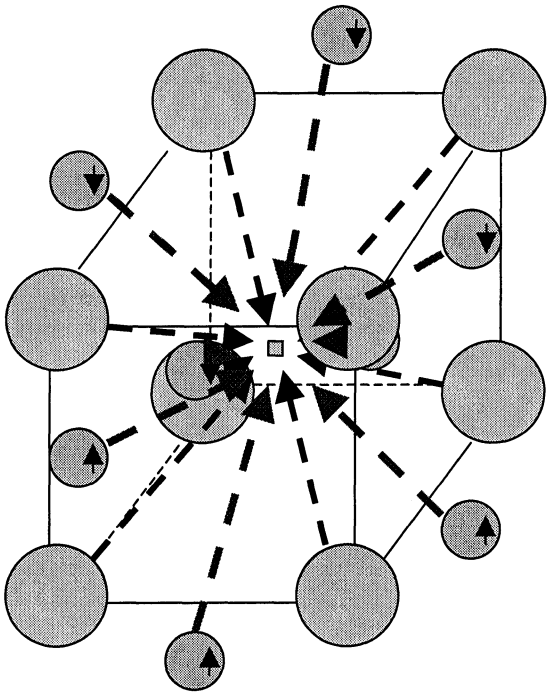

Fig.4: OSC (octahedral symmetric condensation), larger circles for deuterons, smaller circles with arrow (spin) for electrons

3. EQPET Model

A 4D cluster under TSC condition will cause 2D, 3D, and 4D nuclear fusion in competition, because the TSC state reflects the atomic level motion of deuterons in condensed matter and does not necessarily relate to 4D nuclear fusion reaction as strong interaction. In the same way, an 8D cluster causes the competition process of nuclear fusion reactions between 2D, 3D, 4D and 8D nuclear fusion reactions. We need therefore to define and estimate modal fusion rates to TSC and OSC processes[8]. Modal fusion rates are defined as:

$$\lambda_{2d} = a_1^2 \lambda_{2d(1,1)} + a_2^2 \lambda_{2d(2,2)} \quad (3.1)$$

$$\lambda_{4d} = a_1^2 \lambda_{4d(1,1)} + a_2^2 \lambda_{4d(2,2)} + a_4^2 \lambda_{4d(4,4)} \quad (3.2)$$

$$\lambda_{8d} = a_1^2 \lambda_{8d(1,1)} + a_2^2 \lambda_{8d(2,2)} + a_4^2 \lambda_{8d(4,4)} + a_8^2 \lambda_{8d(8,8)} \quad (3.3)$$

Here values for $\lambda_{nd(m,m)}$ as intrinsic microscopic fusion rates are defined and calculated for dde*(m,m) transient molecular sates[7],and extended to multi-body fusion rates assuming rapid cascade barrier penetration and multi-body strong interactions[6-8,10]. These values are given in Table-1 of reference-8.

Screened Coulomb potentials for dde* EQPET molecules were calculated by the variation method of quantum mechanics[7], to be given as the following equation:

$$V_s(R) = e^2/R + V_h + (J + K)/(1 + \Delta) \quad (3.4)$$

On the right hand side of equation (3.4), the first term is the bare Coulomb potential and the second and third terms reflect in the screening effect by e*, which are the measure of "simply defined screening energy", as many experimentalists often use. In **Table-1**, effective screening energies for dde* EQPET molecules are listed up. We see that screening effects by e*(4,4) · and e*(8,8) are very strong, in comparison with that a muon (mass is 208 times of electron mass) works between effects of e*(4,4) and e*(8,8). Thus, EQPET molecules may realize super screening of Coulomb potential.

Table-1: Effective screening energy of dde* molecule

e*	dde*	dde*e*
(1,1)	-14.87 eV	-30.98 eV
(2,2)	-260 eV	-446 eV
(4,4)	-2,460 eV	-2,950 eV
(8,8)	-21 keV	-10.2 keV

In equations (3.1) through (3.3), coefficients a_1 through a_8 are estimated by evaluating total wave function Ψ for deuteron cluster with electrons which is expanded by wave functions $\Psi(m,m)$ of quasi-molecular states to dde*(m,m) as,

$$\Psi = a_1\Psi(1,1) + a_2\Psi(2,2) + a_4\Psi(4,4) + a_8\Psi(8,8) \quad (3.5)$$

In reference-8, approximate values of a_1 through

a_8 were given by taking simple quantum mechanical statistics for electron spin arrangement in TSC and OSC conditions. Calculated modal fusion rates are shown again in **Table-2.**

Table-2: Modal fusion rates for TSC and OSC

TSC(tetrahedral)	OSC(octahedral)
λ_{2d} = 1.8E-21 f/s/cl	λ_{2d} = 7.9E-22 f/s/cl
λ_{3d} = 1.5E-13 f/s/cl	λ_{3d} = 3.5E-13 f/s/cl
λ_{4d} = 3.1E-11 f/s/cl.	λ_{4d} = 7.0E-11 f/s/cl
	λ_{8d} = 7.8E-4 f/s/cl

Table-3: Power level of 4D and 8D fusion rates

Item	TSC(tetrahedral)	OSC(octahedral)
density	1E22 cl/cc	1E16 cl/cc
power	3 W/cc	78 W/cc
neutron	10 n/s/cc	<1 n/s/cc

4. Products and Power Level of Cluster Fusion

Using modal fusion rates in Table-2, we estimated power levels of multi-body fusion rates for assumed deuteron cluster densities, as shown in **Table-3.** Height of periodical harmonic potential for deuteron in PdDx lattice is known to be 0.22 eV, so that 0.22 eV of deuteron (plasmon phonon) energy corresponds well to excited states of trapped deuterons for dynamic motion in PdDx lattice potentials. Under this excitation condition, all deuterons trapped at O-sites move to the central T-site, and we estimate roughly the average TSC cluster density to be on the order of 1E22 clusters per cc. In this condition, we get power level by 4D fusion rate to be 3 W/cc (3E11 f/s/cc) and 10 n/s/cc neutron production rate by 2D fusion. Therefore, neutron production rate is very small as on the 1E-10 order of ^{4}He production rate by 4D fusion.

The OSC condition requires local PdD_2 lattice of overloaded condition, so that we assume here the OSC cluster density is very low as 1E16 clusters/cc (namely 1 ppm level of Pd atom density). Under this condition, we have still surprisingly high power level as 78 W/cc (8E12 f/s/cc) by 8D fusion rates, which produce two high-energy ^{8}Be particles per fusion.

We have speculated that 4D TSC fusion generates two 23.8 MeV ^{4}He-particles in 180 degree opposite directions as:

$$4D \rightarrow {}^8Be^*(47.6\ MeV) \rightarrow {}^4He + {}^4He + 47.7\ MeV \quad (4.1)$$

However, we have at least once to consider the following possible branches of outgoing channels of threshold reactions for ^{8}Be(ground state) break-ups.

$$^8Be(g.s.) \rightarrow {}^4He + {}^4He + 91.86\ keV \quad (4.2)$$

$$\rightarrow {}^3He + {}^5He(n + {}^4He) - 11.13\ MeV \quad (4.3)$$

$$\rightarrow t + {}^5Li(p + {}^4He) - 21.68\ MeV \quad (4.4)$$

$$\rightarrow d + {}^6Li - 22.28\ MeV \quad (4.5)$$

$$\rightarrow p + {}^7Li - 17.26\ MeV \quad (4.6)$$

$$\rightarrow n + {}^7Be - 18.90\ MeV \quad (4.7)$$

Other channels than (4.2) are threshold reactions with high threshold energies. Therefore, we have regarded these threshold reactions as minor channels with very small branching ratios, even with high-excited energy state of (4.1). Another possibility of minor channels in relation of (4.1) is break ups from excited states of ^{4}He which may break up to n + ^{3}He or t + p channels as those for 2D fusion. We regard branching ratios to these minor channels are also small, due to very steady core of alpha-clusters of ^{8}Be nucleus.

For 8D fusion, we can make a similar discussion that alpha-clustered channels dominate.

$$8D \rightarrow {}^{16}O^*(109.84\ MeV) \rightarrow {}^8Be + {}^8Be + 95.2\ MeV \quad (4.8)$$

$$\rightarrow {}^{12}C + {}^4He + 50.12\ MeV \quad (4.9)$$

The lifetime of ^{8}Be(g.s.) is very short as 6.7E-17 s to break up to two alpha particles. Consequently, major products of 4D and 8D

fusion are primarily high-energy (23.8 MeV in kinetic energy) alpha particles. The slowing down and ionization process by 23.8 MeV alpha-particles in PdDx condensed matter has very small cross section to emit K-alpha X-rays (22 keV) from Pd K-shell electron ionization. Major source of X-ray emission is speculated to the bremsstrahlung continuous X-rays in the region less than 3 keV by convey electrons, which are hard to observe, due to attenuation in experimental cells. Thus energy deposit by 23.8 MeV alpha particles becomes apparently radiation-less, namely "clean".

5. Secondary Reactions

High-energy (23.8 MeV) alpha particles by 4D fusion can induce secondary nuclear reactions with host metal nuclei as the following capture reactions,

$$^{105}Pd + {}^{4}He \rightarrow {}^{109}Cd^{*}(1.27\ y) \quad (5.1)$$
$$^{106}Pd + {}^{4}He \rightarrow {}^{110}Cd \quad (5.2)$$
$$^{108}Pd + {}^{4}He \rightarrow {}^{112}Cd \quad (5.3)$$
$$^{110}Pd + {}^{4}He \rightarrow {}^{114}Cd \quad (5.4)$$
$$^{107}Pd(6.5E6\ y) + {}^{4}He \rightarrow {}^{111}Cd \quad (5.5)$$

Impurity Cd production rates in Pd cathode in the deuterium gas glow-discharge experiments by Karabut[9] may be explained by the above secondary reactions. Fission-like products also reported by Karabut[9] and Mizuno[5] can be explained by alpha-particle-induced fission process as reported by Ohta[12] in this meeting.
Even within short life of high energy ^{8}Be-particles by 8D fusion, more than 10 metal nuclei exist within the range and we expect capture reactions as,

$$M(A,Z) + {}^{8}Be \rightarrow M(A+8, Z+4) + Q \quad (5.6)$$

The kinetic energy 47.6 MeV of ^{8}Be by 8D fusion is well over the Coulomb barrier height 30.1 MeV for $^{133}Cs + {}^{8}Be$ to ^{141}Pr reaction. Due to the liquid-drop collision-like capture process of this reaction, kinetic energy of ^{8}Be will be transferred to kinetic energy of compound nucleus M(A+8, Z+4).
Selective nuclear transmutations reported by Iwamura[3,4] can be explained by this process, although we have few problems of possible radiation (gamma rays) emission in the process, which we will discuss elsewhere .

6. Conclusions

The EQPET model was proposed to explain super-screening for d-d pairs in condensed matter. Deuteron cluster fusion dominated will however take place by TSC and OSC conditions to make resonance multi-body fusion reactions for 3D, 4D and 8D strong interactions. Helium-4 is the major product, and neutron production rate is very small on the order of less than 1E-10 of helium production rate. High-energy alpha particles by 4D and 8D fusion reactions will induce secondary transmutation reactions with host or mounted heavy nuclei. Slowing down of high-energy alpha particles as products of 4D and 8D fusion reactions may emit low energy continuous X-rays which are difficult to observe from outside of experimental cells. We can say that deuteron cluster fusion in condensed matter is clean or almost radiation-less.

References:

1) M. McKubre: Power point slide for ICCF10 Short Course, see http://www.lenr-canr.org
2) Y. Arata, et al: Proc. ICCF10, see http://www.lenr-canr.org
3) Y. Iwamura, et al.: Jpn. J. Appl. Phys., 41(2002)4642-4648
4) Y. Iwamura, et al.: Proc. ICCF10, see http://www.lenr-canr.org
5) T. Mizuno, et al.: Denkikagaku, 64(1996)1160
6) A. Takahashi, et al.: Proc. ICCF9, 19-24 May 2002, China, pp.343-348
7) A. Takahashi, et al.: Proc. JCF4, 17-18 October 2002, Iwate U, Japan, pp.74-78
8) A. Takahashi: Mechanism of deuteron cluster fusion by EQPET model, Proc. ICCF10, see http://www.lenr-canr.org
9) A. Karabut, et al.: Proc. ICCF10, see http://www.lenr-canr.org
10) A. Takahashi: Theoretical background for transmutation reactions, Power-point slide for ICCF10 Short Course, see http://www.lenr-canr.org
11) A. Takahashi, et al.: Fusion Technology, 27(1995)71-85
12) M. Ohta, et al.: Proc. ICCF10, see http://www.lenr-canr.org

ANALYSIS OF NUCLEAR TRANSMUTATION AS SECONDARY REACTIONS OF MULTIBODY-FUSION

MASAYUKI OHTA AND AKITO TAKAHASHI

Osaka University
Yamadaoka 2-1, Suita, Osaka, 565-0871, Japan
E-mail: mohta@newjapan.nucl.eng.osaka-u.ac.jp

Abstract

Nuclear transmutation phenomenon is analyzed by the selective channel scission model from the viewpoint of secondary reactions of the multi-body fusion. The fission product yields are calculated for the reactions of Pd plus ^{4}He and ^{8}Be, which are products of multi-body fusions. The analytical results show good qualitative consistencies with experimental results. And anomalous isotopic ratios and γ-ray emissions are also analyzed.

Keywords: PdDx, nuclear transmutation, fission, γ-ray, anomalous isotopic ratio

1 Introduction

The selective channel scission (SCS) model has been proposed and improved to analyze the nuclear transmutation phenomenon [1]. In general, the nuclear transmutations have two features, roughly speaking. One of the features of the nuclear transmutation phenomenon is the production of the elements, which shows the fission-like distribution with their anomalous isotopic ratios. Another is the production of a little heavier element than the sample elements, for example the production of Cd and Sn for Pd-type experiment [2]. This type contains the mass-8 and Z-4 increased transmutation, for example from Cs to Pr, reported by Y. Iwamura [3].

The SCS model can predict the fission product yields of any elements' fission deterministically. Assuming the multi-photon excitation and the photo-fission of the cathode material, such as Pd, we have analyzed the former type of nuclear transmutations. This time, the latter one is analyzed from the view of the secondary reactions of multi-body fusions [4] and the fission product yields and γ-ray emissions accompanied with these processes are analyzed.

2 Models

Figure 1 shows the fission process and the potential.

The fission product yields are calculated on SCS model as follows. The value of channel-dependent fission barrier E_f is estimated by the Q-value and the bare Coulomb potential E_c' at the effective scission distance R_{eff} for all fission channels, which are possible combinations of atomic (Z) and mass numbers. The R_{eff} is obtained by setting the jointing factor η which reflects the jointing force of the strong interaction: $R_{eff} = \eta (R_1 + R_2)$, where R_1 and R_2 are the radiuses of the fission fragments (FP1 and FP2 in Fig. 1). The channel-opening probability for each channel, that is the tunnel fission probability, is calculated. If the nuclear excitation energy E_x is less than E_f, the tunnel fission needs to be considered. On the other hand, this value is 1 if the E_x is more than E_f.

Then, the fission product yield is obtained by summing up these probabilities all over fission channels. And the decay processes are considered for the fission products in this analysis.

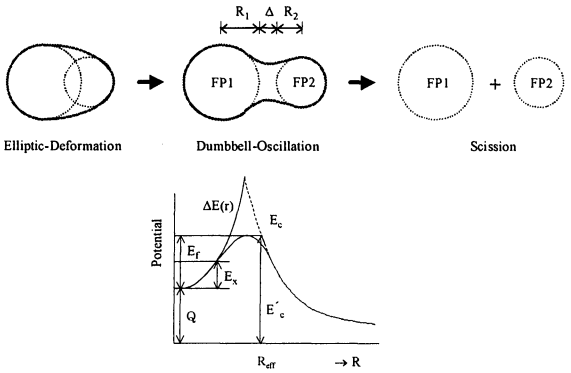

Figure 1. Fission process and potential.

We have developed the multi-photon induced fission (MPIF) model to analyze the former type of nuclear transmutations, assuming the photo-fissions of the cathode elements. Multi-photon excitation is assumed in the MPIF model. The X-ray productions or the production of photons from multi-body fusion reactions can be the photon source. If these are burst-like productions, the flux is very high and the nuclei can be excited by these photons through interferences such as Rayleigh scattering and Compton scattering. These photons induce MPIF, which is the collective excitation by these many low energy photons to E1 giant resonance region to make fissions.

We have calculated the fission product yields by MPIF

and the results showed qualitative agreements with the experimental results [1].

On the contrary, the latter type of nuclear transmutations, which cannot be explained by fission, must be the results by fusions with ^{4}He and/or ^{8}Be particles, judging from the specific changes of Z and mass number. These fusions may be occurred as secondary reactions of multi-body fusion. Also, the fissions may be induced for the excited nuclei.

The multi-body fusion model [4] assumes that the fusion reaction rate is enhanced in the transient process by the coherent motions of hydrogen isotopes located in octahedral or tetrahedral sites of Pd lattice. The symmetric properties of hydrogen isotopes and Copper pair-like couplings in Pd lattice may realize the situation and the strong electron-screening effect inducing the multi-body fusion reactions. It is known that the electron-phonon interaction becomes strong because of the contribution of the optical mode [5] and the superconductivity arises for high loading ratios of PdH_x or PdD_x [6]. The strong electron-phonon interaction induces the Cooper pair-like coupling and may enhance 4D and 8D fusion reaction rates [7, 8].

$$4\,D \rightarrow {}^8Be^* \rightarrow 2\,{}^4He + 47.6\ MeV, \quad (1)$$
$$8\,D \rightarrow {}^{16}O^* \rightarrow 2\,{}^8Be + 95.2\ MeV. \quad (2)$$

The ^{4}He and ^{8}Be produced by these reactions induce the productions of Cd and Sn for Pd and the mass-8 and Z-4 increased transmutation, respectively. The excited nucleus may make fission in these reaction processes.

$$M(Z, A) + {}^4He \rightarrow M(Z+2, A+4), \quad (3)$$
$$M(Z, A) + {}^8Be \rightarrow M(Z+4, A+8), \quad (4)$$
$$M(Z, A) + {}^4He\ (\text{or } {}^8Be) \rightarrow \text{Fission product 1} + \text{Fission product 2}, \quad (5)$$

where M (Z, A) shows the element in the sample with atomic number Z and mass number A.

Two types of the nuclear transmutations and also the ^{4}He production are explained by these processes consistently.

3 Analytical results

3.1 General

If the multi-body fusion reactions occur, fissions can occur as secondary reactions that the sample metal Pd plus the major products, which are ^{4}He and ^{8}Be, because these excitation energies of the excited nucleus are enough high to induce fission reactions.

These excitation energies are listed in Table 1 for the compound nuclei that the natural Pd, which has six isotopes, plus ^{4}He and ^{8}Be reactions, respectively. And the natural abundances for Pd isotopes are listed altogether in the table.

Fission product yields for these reactions and the isotopic abundance for Fe are analyzed.

3.2 Pd + ^{4}He reaction

The compound nuclei of Cd are produced for Pd isotopes plus ^{4}He reactions. In this SCS analysis of fission product yields, the jointing factor η was taken as 1.84 for all Cd's isotopes in Table 1. The fission barriers and the channel opening probabilities for their excitation energies were calculated for each Cd's isotopes. The yield data of fission products are obtained with considerations of the isotopic abundances.

The Z-distribution of the fission product yields for Pd + ^{4}He reactions is shown in Fig. 2-(a) with the experimental data by T. Mizuno, which is the same in the analysis by Pd photo-fission [1]. And the mass-distribution of fission products is obtained as shown in Fig. 2-(b).

The dominant products are Fe, Ti and Cr. The fission product yields at right and left wings are slightly larger than the Mizuno's experimental data. This may depend on the effect of the fission-modes [9], which should be considered in future analysis. But the center part keeps good qualitative agreements with the Mizuno's data in rough approximation. The effect of nuclear shell structure may appear in this analysis.

3.3 Pd + ^{8}Be reaction

The compound nuclei of Sn produced for Pd isotopes plus ^{8}Be reactions are also listed in Table 1.

The fission product yields from the compound nuclei of Pd + ^{8}Be reactions were obtained. The jointing factor η was taken as 1.20 for all Sn's isotopes. The Z- and mass-distributions of fission product yields were shown in Fig. 3-(a) and -(b), respectively. The fission products in the center part are also Fe, Ti, Cr and so on. The fission product yields at right and left wings increase, corresponding to the distributions of their fission barriers. Fission-modes should be considered also in this process.

3.4 Isotopic abundance

The feature of the nuclear transmutation products is its anomalous isotopic ratio, which is different from the natural abundance. This is the strong evidence to suggest that some nuclear reactions occur in the experiment.

Figure 4 shows the comparison of the isotopic ratios of Fe with some experimental results: the natural abundance, the experimental results by Mizuno [1], Iwamura [3], Karabut [2] and the analytical results by MPIF (photo-fission) [1], Pd + ^{4}He and Pd + ^{8}Be reactions.

The high ratio of ^{58}Fe is the notable feature of the analytical results calculated by the SCS model. This result suggests that the anomalous isotopic ratio of the nuclear transmutations can be explained by fission reactions.

Table 1. Natural abundance of Pd isotopes and the excitation energies of the compound nucleus by + ^{4}He and + ^{8}Be reactions.

Nuclides	Natural abundance (%)	+ ^{4}He (23.8 MeV)	Excitation energy (MeV)	+ ^{8}Be (47.6 MeV)	Excitation energy (MeV)
^{102}Pd	1.02	^{106}Cd*	25.4	^{110}Sn*	50.4
^{104}Pd	11.14	^{108}Cd*	26.1	^{112}Sn*	51.8
^{105}Pd	22.33	^{109}Cd*	26.3	^{113}Sn*	52.5
^{106}Pd	27.33	^{110}Cd*	26.7	^{114}Sn*	53.2
^{108}Pd	26.46	^{112}Cd*	27.3	^{116}Sn*	54.5
^{110}Pd	11.72	^{114}Cd*	27.9	^{118}Sn*	55.8

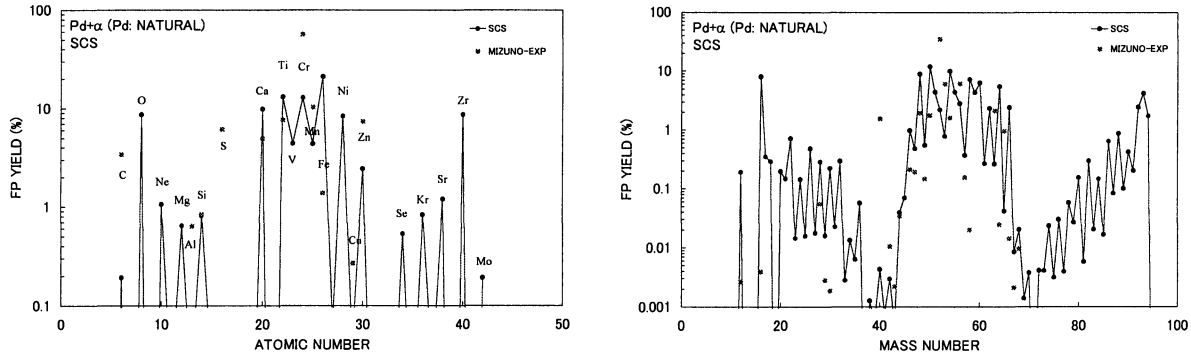

Figure 2. Fission product yield for Pd + ^{4}He reaction: (a) Z-number and (b) mass-number.

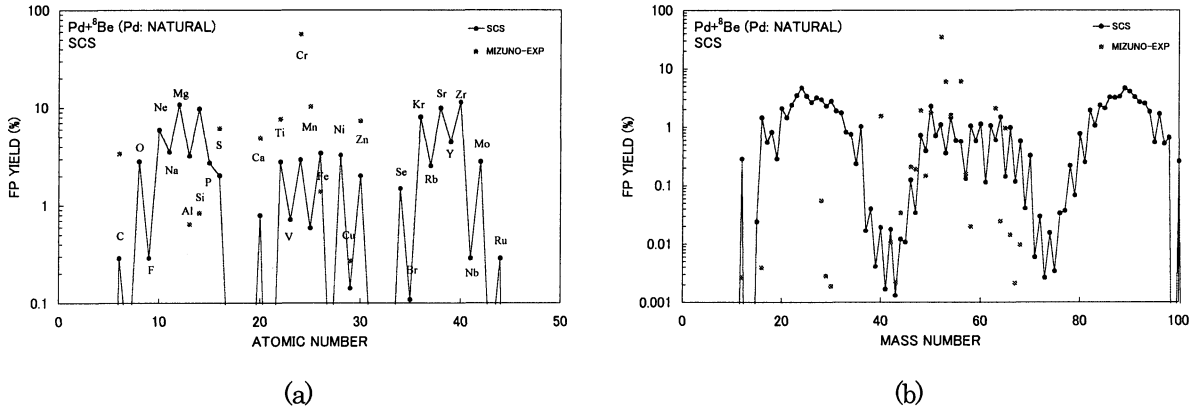

Figure 3. Fission product yield for Pd + ^{8}Be reaction: (a) Z-number and (b) mass-number.

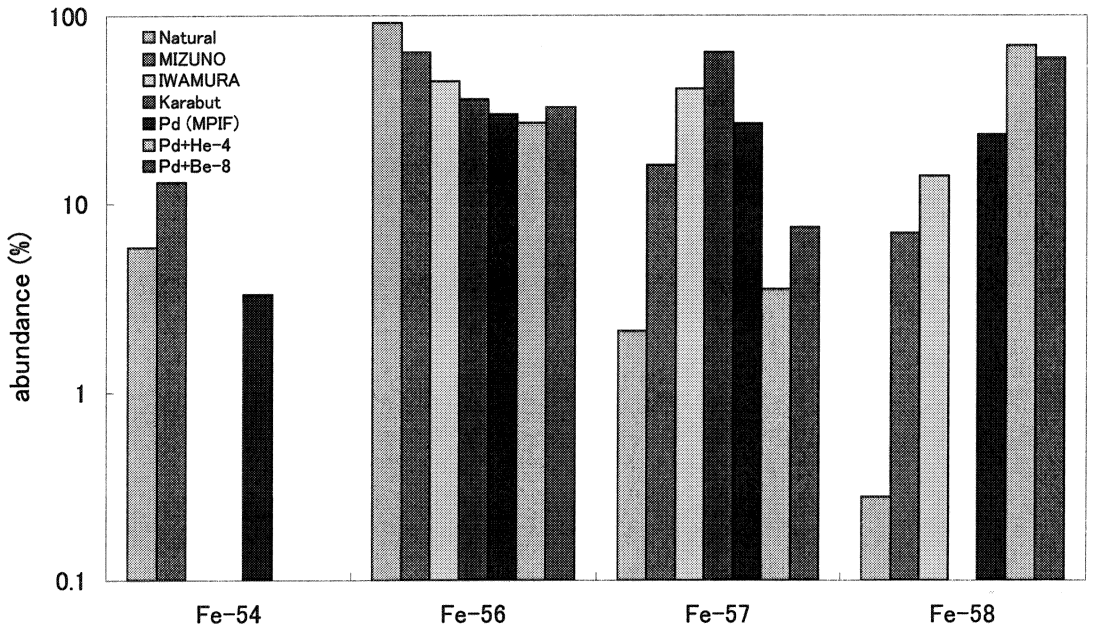

Figure 4. Comparison of the isotopic ratios of Fe between the natural abundance, the SCS analysis and the experimental results.

3.4 γ-ray emission

The energies of γ-ray and the isotopes, which emit the □-ray predicted by the SCS model, are listed in Table 2. These isotopes are the major products of Pd photo-fission, Pd + ^{4}He and Pd + ^{8}Be reactions which have the yields of the each reaction more than 0.1 %. And only energies, which have the emitting ratios of the element more than 10 %, are shown in the table.

The isotopes, which have short lifetimes, are included in the table. Some energies of γ-ray will not be observed in some experiments, for example, which have a long cooling time.

4 Discussion and Conclusion

The fission product yields were calculated for processes of Pd + ^{4}He and Pd + ^{8}Be reactions in addition to the Pd photo-fission [1] in by the SCS model.

The productions of Cd and Sn were detected simultaneously in the experiments using Pd sample in addition to the productions of lighter elements than Pd [2]. The Z-numbers of Cd and Sn are two and four larger than Pd, respectively. The transmutations from Cs to Pr and from Sr to Mo, which are mass-8 and Z-4 increased type transmutations, were reported in Mitsubishi-type experiments [3]. It stands to reason that ^{4}He and/or ^{8}Be induce this type of nuclear transmutations as secondary reactions. These ^{4}He and ^{8}Be may be produced from multi-body fusion reactions.

The another-type of nuclear transmutations, which produces lighter elements than elements in the sample, will probably be explained by fission. We have assumed three processes of photo-fission [1], Pd + ^{4}He and Pd + ^{8}Be reactions for this type of nuclear transmutations. These processes are analyzed by the SCS model in this analysis independently. These processes will occur simultaneously, because both Cd and Sn, which are compound nuclei of Pd + ^{4}He and Pd + ^{8}Be reactions, respectively, were detected simultaneously [2]. We cannot decide which process of fissions is dominant only in this analysis. It should be estimated by the composition of these processes.

The fission-mode should be considered for the fine adjustment of the calculations of the fission product yields. We have already analyzed the neutron-induced fission for U-235 [9]. The effect of the fission-modes is indispensable for more detailed analyses of fission product yields.

The γ-ray emissions are analyzed for the fission products of the photo-fission of Pd, Pd + ^{4}He and Pd + ^{8}Be reactions calculated by the SCS model. The comparison with the experimental results is the future task.

Table 2. γ-ray emissions from the fission products of Pd photo-fission, Pd + ^{4}He and Pd + ^{8}Be reactions estimated by the SCS model.

γ (keV)	and isotope	γ (keV)	and isotope	γ (keV)	and isotope	γ (keV)	and isotope	γ (keV)	and isotope
14.4	^{57}Mn	400.6	^{28}Mg	863.9	^{58}Mn	1273.4	^{29}Al	1779.0	^{28}Al
17.0	^{52}Ti	402.6	^{87}Kr	880.7	^{55}V	1289.6	^{53}V	1808.6	^{26}Na
26.6	^{56}Cr	429.1	^{34}Si	898.0	^{88}Rb	1291.6	^{59}Fe	1810.8	^{56}Mn
30.6	^{28}Mg	440.0	^{23}Ne	898.0	^{88}Y	1293.6	^{41}Ar	1836.1	^{88}Rb
67.4	^{61}Co	443.6	^{30}Mg	909.0	^{89}Zr	1297.1	^{47}Ca	1836.1	^{88}Y
71.6	^{50}Ca	459.2	^{58}Mn	934.5	^{92}Y	1312.1	^{48}Sc	1847.5	^{33}Si
83.9	^{56}Cr	472.2	^{24}Ne	941.7	^{28}Mg	1323.1	^{58}Mn	1886.0	^{44}Ar
87.1	^{63}Co	472.7	^{59}Mn	960.3	^{29}Mg	1332.5	^{60}Co	1904.0	^{53}Ti
93.3	^{67}Cu	506.1	^{62}Fe	974.7	^{25}Na	1346.0	^{46}K	1941.9	^{38}S
100.8	^{53}Ti	511.6	^{71}Zn	975.0	^{43}Ar	1368.6	^{24}Na	1944.3	^{46}Ar
108.2	^{84}Se	514.0	^{85}Sr	983.5	^{48}Sc	1383.9	^{92}Sr	1961.5	^{54}V
122.1	^{57}Mn	517.7	^{55}V	989.01	^{54}V	1397.9	^{29}Mg	2013.5	^{47}K
124.5	^{52}Ti	520.4	^{58}Cr	994.8	^{63}Fe	1421.7	^{53}Ti	2113.1	^{56}Mn
126.0	^{58}Cr	523.8	^{50}Sc	1006.1	^{53}V	1431.6	^{33}Si	2127.5	^{34}P
127.6	^{53}Ti	564.8	^{47}K	1007.5	^{69}Cu	1434.1	^{52}V	2144.1	^{51}Sc
145.0	^{72}Zn	570.8	^{59}Mn	1014.4	^{27}Mg	1437.3	^{51}Sc	2150.8	^{44}K
159.4	^{47}Sc	585.0	^{25}Na	1024.3	^{91}Sr	1439.5	^{43}Ar	2167.4	^{38}Cl
182.6	^{44}Ar	586.0	^{47}K	1027.4	^{61}Fe	1481.8	^{65}Ni	2195.8	^{88}Kr
184.6	^{67}Cu	593.4	^{43}K	1031.9	^{89}Rb	1517.5	^{39}Cl	2196.0	^{89}Rb
196.3	^{88}Kr	617.5	^{43}K	1037.6	^{48}Sc	1519.3	^{50}Ca	2201.7	^{72}Ga
228.4	^{53}Ti	630.0	^{72}Ga	1077.4	^{68}Cu	1529.8	^{88}Kr	2223.9	^{29}Mg
243.9	^{30}Mg	657.8	^{89}Rb	1099.3	^{59}Fe	1553.8	^{50}Sc	2235.2	^{30}Al
250.3	^{39}Cl	682.9	^{58}Cr	1115.5	^{65}Ni	1553.8	^{50}V	2259.4	^{54}V
256.9	^{50}Ca	726.7	^{59}Mn	1121.1	^{50}Sc	1567.5	^{51}Sc	2301.8	^{62}Co
264.7	^{75}Ge	738.1	^{43}Ar	1128.9	^{62}Co	1572.3	^{35}P	2316.7	^{31}Al
277.3	^{78}Ge	749.8	^{91}Sr	1157.0	^{44}K	1590.9	^{50}Ca	2353.6	^{45}K
289.5	^{58}Cr	810.8	^{58}Mn	1172.9	^{62}Co	1607.6	^{34}Si	2392.1	^{88}Kr
297.3	^{73}Ga	834.0	^{72}Ga	1173.2	^{60}Co	1642.7	^{38}Cl	2507.82	^{72}Ga
297.9	^{61}Fe	834.4	^{69}Cu	1178.5	^{34}Si	1674.7	^{58}Mn	2754.0	^{24}Na
320.1	^{51}Ti	834.8	^{88}Kr	1205.1	^{61}Fe	1675.5	^{53}Ti	3084.4	^{49}Ca
325.7	^{73}Ga	834.8	^{54}V	1248.2	^{89}Rb	1694.9	^{31}Al	3498.4	^{30}Al
372.8	^{43}K	834.8	^{54}Mn	1261.0	^{68}Cu	1703.4	^{44}Ar		
389.7	^{25}Na	843.7	^{27}Mg	1263.2	^{30}Al	1705.6	^{45}K		
396.9	^{43}K	846.8	^{56}Mn	1267.2	^{39}Cl	1754.1	^{29}Mg		

References

1. A. Takahashi et al., *Proc. ICCF8*, 397 (2000); and A. Takahashi et al., *Jpn. J. Appl. Phys.*, **40**, 7031 (2001).
2. A.B. Karabut, *Proc. ICCF9*, 151 (2002).
3. Y. Iwamura et al., *Jpn. J. Appl. Phys.*, **41**, 4642 (2002).
4. A. Takahashi et al., *Fusion Technol.*, **27**, 71 (1995).
5. J.P. Burger, Metal Hydrides, G. Bambakidis ed. (Plenum, 1981), p. 243.
6. R.W. Standley et al., *Solid State Commun.*, **31**, 801 (1979).
7. M. Ohta et al., *Proc. ICCF8*, 403 (2000).
8. A. Takahashi, *Proc. JCF4*, 74 (2002); and *Proc. ICCF10* (to be published).
9. M. Ohta et al., *Jpn. J. Appl. Phys.*, **42**, 645 (2003).

QUANTUM STATES OF CHARGED BOSE PARTICLES IN SOLIDS

Ken-ichi TSUCHIYA

Department of Chemical Science and Engineering, Tokyo National College of Technology,
1220-2 Kunugida, Hachioji, Tokyo 193-0997,
e-mail: tsuchiya@tokyo-ct.ac.jp

ABSTRACT: Local deuteron density at defects in Pd may become higher than mean density, because many deuterons can be accumulated in Pd. When it becomes high enough, Bose-Einstein condensation (BEC) may happen and induce nuclear reactions. In this work, nuclear reactions in Pd induced by BEC are estimated. The equivalent linear two-body (ELTB) method, which is based on an approximate reduction of many-body problems by variational principle, is used for the calculation. Thomas-Fermi and non-linear screening d-d interactions are used for the calculations. The nuclear reaction rates and critical temperatures of BEC are obtained from the ELTB solutions. For the case of non-linear screening, Tc's of BEC are higher than room temperature. But Tc's are lower than room temperature for the case of Thomas-Fermi screening. Nuclear fusion rates are order of $10^7 sec^{-1}$. They are extremely high. However, if a nuclear reaction happens, local temperature will immediately reach Tc and higher. This means that cold and calm fusions induced by BEC and screening effects may happen in solid.
Keywords: Bose-Einstein condensation, non-linear screening, cold fusion

1. INTRODUCTION

The tendency of identical bosons to clump in ordinary space has an important role for the problems of deuterons in metals. This tendency was applied to the explanation of cold fusion phenomenon by R.T.Bush and R.D.Eagleton [1]. In their theory, the symmetry force is hypothesized to produce clusters of deuterons in the lattice for a high enough stoichiometric ratio to Pd atoms and to catalyze tunneling to achieve cold fusion. We also applied this tendency of identical charged bosons to the cold fusion problem [2]. This paper shows another approach to this problem by considering the property of bose particles.

When charged bosons are confined in an ion trap device [3], the Hamiltonian for the system is given by the summation of three terms. They are total kinetic energy, isotropic harmonic potential due to ion trap device and repulsive Coulomb interaction between charged bosons. By applying the equivalent linear two-body (ELTB) method to the trapped deuterons in an ion trap device, Y.E.Kim and A.L.Zubarev [4] derived the ground-state wave function and the nucleus-nucleus fusion rate. In this work, Kim-Zubarev theory is modified in the following two points. Firstly, lattice defects in solid are regarded as ion traps and the potentials including anharmonic terms are estimated. The ELTB ground state wave function can be calculated numerically and also the rate of nuclear fusion in some kinds of lattice defects including N charged bosons can be obtained. As an interaction between two deuterons Thomas-Fermi and non-linear screening potentials are adopted. Secondly, the dependence of this phenomenon on the temperature is introduced by using the well-known formula for the critical temperature of BEC, which depends on the number density of the particle. This is done by calculating the number density from ELTB solutions.

In section 2, Kim-Zubarev method is briefly shown and new approaches in solid state physics are described. In section 3, non-linear screening effect is introduced for this study. In section 4, the methods how to calculate the nuclear reaction rate and the critical temperature of BEC are explained. In section 5, calculated results are discussed. In the last section, conclusions are described.

2. ION TRAPS IN SOLID

We start to show an outline of Kim-Zubarev method. They assumed the potential for the ion trap device as an isotropic harmonic potential. Then the Hamiltonian of the system including N charged particle in the ion trap is

$$\mathcal{H} = -\frac{\hbar^2}{2m}\sum_{i=1}^{N}\nabla_i^2 + \frac{m\omega^2}{2}\sum_{i=1}^{N}\mathbf{r}_i^2 + \sum_{i<j}\frac{e^2}{|\mathbf{r}_i - \mathbf{r}_j|}, \quad (1)$$

where m is the rest mass of the particle and $\mathbf{r}_i$ is the position of an ion. They used ELTB method, which is based on the variational principle. The ground state of this many-body problem is written

as

$$\Psi(\mathbf{r}_1, \mathbf{r}_2, ..., \mathbf{r}_N) \approx \frac{\phi(\rho)}{\rho^{(3N-1)/2}}, \quad (2)$$

where new quantity ρ is defined as

$$\rho = \left(\sum_{i=1}^{N} \mathbf{r}_i^2\right)^{1/2}. \quad (3)$$

The wave function ϕ in eq.(2) satisfies

$$h = -\frac{\hbar^2}{2m}\frac{d^2}{d\rho^2} + \frac{\hbar^2}{2m}\frac{p}{\rho^2} + \frac{m\omega^2\rho^2}{2} + \frac{qe^2}{\rho}$$

$$h\phi(\rho) = E\phi(\rho), \quad (4)$$

where p and q are defined as

$$p = \frac{(3N-1)(3N-3)}{4}$$

$$q = \frac{2N\Gamma\left(\frac{3N}{2}\right)}{3\sqrt{2\pi}\Gamma\left(\frac{3(N-1)}{2}\right)}. \quad (5)$$

It is easy to see that the third term in eq.(4) corresponds to the second term in eq.(1). The first and second terms correspond to the first term in eq.(1). The fourth term in eq.(4) corresponds to the third term in eq.(1). The exact proofs of them are given in Kim-Zubarev paper [4]. For example the fourth term in eq.(4) is derived by transforming the summation of two body potentials $\sum_{i<j} v_{ij}$ into ρ space. This is done by using

$$V(\rho) = \frac{\sum_{i<j} \int d\mathbf{R} \int d\Omega v_{ij}}{\int d\mathbf{R} \int d\Omega}, \quad (6)$$

where integrals for $\mathbf{R}$ and Ω mean integral over all space for gravity center of N-body and integrals for $3(N-1)$-angle, respectively. The fourth term in eq.(4) is derived by substituting $v_{ij} = e^2/|\mathbf{r}_i - \mathbf{r}_j|$ into eq.(6). Generally, these differential equations for harmonic oscillators are rewritten by using nondimensional quantities $x = \sqrt{\frac{m\omega}{\hbar}}\rho$ and $\varepsilon = 2E/\hbar\omega$. As a result, eq.(4) is rewritten as

$$\left(-\frac{d^2}{dx^2} + x^2 + \frac{p}{x^2} + \frac{q'}{x}\right)\phi(x) = \varepsilon\phi(x). \quad (7)$$

In this equation q' are given by $q' = 2\alpha q\sqrt{mc^2/\hbar\omega}$, where $\alpha = e^2/\hbar c$ is the fine structure constant.

Now we show the application of Kim-Zubarev method to the phenomenon in solid. The Hamiltonian of a system including N deuterons in solid consists of kinetic energy of deuterons, deuteron-deuteron interactions and deuteron-host ion interactions. Therefore, Hamiltonian of the N-deuteron systems in solid is written as

$$\mathcal{H} = -\frac{\hbar^2}{2m}\sum_{i=1}^{N}\nabla_i^2 + \sum_{ij}\frac{Ze^2\exp(-K|\mathbf{R}_j - \mathbf{r}_i|)}{|\mathbf{R}_j - \mathbf{r}_i|} + \sum_{i<j}\frac{e^2\exp(-k|\mathbf{r}_i - \mathbf{r}_j|)}{|\mathbf{r}_i - \mathbf{r}_j|}, \quad (8)$$

where $\mathbf{R}_j$ is the Bravais lattice vector of the host lattice and Z is the effective charge of a host ion. In eqs.(4) and (7) of Kim-Zubarev theory, harmonic term is the electro magnetically induced attractive potential in the ion trap device [3]. For the case of the problems in crystalline solids, this term corresponds to the repulsive interaction between positively charged host ions and positively charged impurity deuterons. The second term of eq.(8) has a same role with the harmonic term in eqs.(4) and (7). The second and third terms of eq.(8) should be transformed into ρ space. If we define new function u as

$$u(\mathbf{r}) = \sum_j \frac{Ze^2\exp(-K|\mathbf{R}_j - \mathbf{r}|)}{|\mathbf{R}_j - \mathbf{r}|}, \quad (9)$$

the transformation of the second term in eq.(8) into ρ space is written as

$$U(\rho) = \frac{\sum_i \int d\mathbf{R} \int d\Omega u(\mathbf{r}_i)}{\int d\mathbf{R} \int d\Omega}, \quad (10)$$

where $\mathbf{r}_i$ means the position of a deuteron. Almost all the part of the multiple integrations are cancelled between the numerator and the denominator in eq.(10) and it is reduced to

$$U(\rho) = \frac{1}{2}m\omega^2\sum_{m=2}^{\infty} A_{N,m}\rho^{2m-2} + U_0, \quad (11)$$

where the constant term U_0 can be omitted by selecting the origin of the energy at U_0. In this equation, the frequency ω is defined as

$$\frac{1}{2}m\omega^2 = \frac{Ze^2K^2}{3!}\sum_j \frac{e^{-KR_j}}{R_j}, \quad (12)$$

where R_j is the norm of the Bravais lattice vector $\mathbf{R}_j$. The structure of the host lattice is introduced thorough this equation. For example, the value of ω for perfect lattice is larger than that for the lattice including vacancies because vacant points are omitted from the lattice summation in eq.(12).

The coefficients $A_{N,m}$ for $m \geq 2$ are defined as

$$A_{N,m} = \frac{K^{2m-4}(3N)!!}{2^{m-2}(m-1)!(3N+2m-4)!!}. \quad (13)$$

If we cut the summation in eq.(11) at $m = 2$, then $U(\rho) = \frac{1}{2}m\omega^2\rho^2$ is obtained. This means that $U(\rho)$ in rough approximation is consistent with the third term in eq.(1) of Kim-Zubarev theory. However higher order terms exist in this problem. The transformation of the third term in eq.(4) into ρ space is done by substituting $v_{ij} = e^2 \exp(-k|\mathbf{r}_i - \mathbf{r}_j|)/|\mathbf{r}_i - \mathbf{r}_j|$ into eq.(6). The result is not similar to the fourth term in eq.(4) because of the existence of the screening factor. In ρ space, effects of screening are described by the screening function for Thomas-Fermi potential, which is written as

$$f_{TF}(\rho) = 3(N-1)\int_0^{\frac{\pi}{2}} d\theta \sin\theta \cos^{3N-4}\theta \times \exp\left(-k\sqrt{2}\rho\sin\theta\right) \quad (14)$$

For the case of Coulomb potential with $k = 0$, we obtain $f_{TF}(\rho) = 1$ which is consistent with fourth term in eq.(4) of Kim-Zubarev theory. For the case of screened Coulomb potential with $k \neq 0$, we obtain $V_k(\rho) = V_0(\rho) f_{TF}(\rho)$. Therefore, if we transform eq.(8) into x space, it is written as

$$h = -\frac{d^2}{dx^2} + \sum_{m=2}^{M} A'_{N,m} x^{2m-2} + \frac{p}{x^2} + \frac{q'}{x} f_{TF}$$
$$h\phi(x) = \varepsilon\phi(x), \quad (15)$$

where M is the cut-off of the summation for m. For the case of $M = 2$ and $k = 0$, it is completely consistent with eq.(7) of Kim-Zubarev theory. In practice, M should be selected to keep required accuracy. Hence anharmonic terms are included in eq.(15). The coefficient $A'_{N,m}$ in eq.(15) is defined as $A'_{N,m} = (\frac{\hbar}{m\omega})^{m-2} A_{N,m}$.

3. NON-LINEAR SCREENING d-d INTERACTIONS

It is well known that deuterons provide very strong potentials to the electron gas. This effect is introduced by using the density functional formalism of Hohenberg-Kohn-Sham [5,6]. The density of the non-linear screening cloud around a deuteron is obtained by using their theory. The non-linear screening interactions between two deuterons are obtained by considering the change in energy due to the embedding of two deuterons in electron gas. It is written as

$$V_{dd}(r) = \frac{2}{r} - 2v_s(r)$$

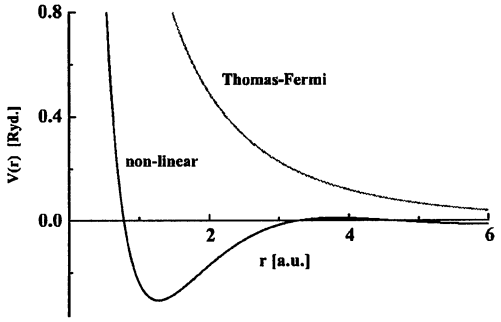

Fig. 1. Screening interaction between two deuterons

$$+ \int d\mathbf{r}' \Delta n(\mathbf{r}')\{v_s(|\mathbf{r}-\mathbf{r}'|) + \phi_{xc}(|\mathbf{r}-\mathbf{r}'|)\} \quad (16)$$

where Δn, v_s and ϕ_{xc} are deviation of electron density from mean density n_0, induced static potential and exchange-correlation potential, respectively. Induced static potential is written as

$$v_s(r) = \int d\mathbf{r} \frac{2\Delta n(|\mathbf{r}-\mathbf{r}_1|)}{|\mathbf{r}-\mathbf{r}_2|}, \quad (17)$$

where $\mathbf{r}_i$ means the position of the deuteron. Induced exchange-correlation potential is written as

$$\phi_{xc}(r) = v_{xc}(n_0 + \Delta n(r)) - v_{xc}(n_0)$$
$$v_{xc} = \frac{d\varepsilon_{xc} n}{dn}, \quad (18)$$

where ε_{xc} is the exchange-correlation energy per one electron. Calculated results for V_{dd} are plotted in Fig.1. The screening function for non-linear screening interaction V_{dd} is written as

$$f_{NL}(\rho) = 3(N-1)\int_0^{\frac{\pi}{2}} d\theta \sin\theta \cos^{3N-4}\theta \times v_{dd}\left(\sqrt{2}\rho\sin\theta\right), \quad (19)$$

where $v_{dd}(r) = V_{dd}(r)r/2e^2$.

4. NUCLEAR REACTION RATE AND PROBABILITY OF GROUND STATE OCCUPATION

The ground state wave function Ψ for N identical charged Bose nuclei gives the nuclear reaction rate as

$$R = -\frac{2\sum_{i<j}\langle\Psi|ImV_{ij}^F|\Psi\rangle}{\hbar\langle\Psi|\Psi\rangle}, \quad (20)$$

where imaginary part of Fermi pseudopotential V_{ij}^F [4] is written as $ImV_{ij}^F = -\frac{A\hbar}{2}\delta(\mathbf{r}_i - \mathbf{r}_j)$. The short-range interactions of nuclear forces between two Bose nuclei are introduced by using δ function [4]. This rate can be calculated by using numerical solution of eq.(15), because ϕ gives Ψ. The constant A is given by Bohr radius $r_B = \hbar^2/me^2$ and the S factor of the nuclear reaction between two nuclei as $A = 2Sr_B/\pi\hbar$.

If the ELTB solution is obtained, the critical temperature T_c of BEC is estimated by well known formula which is written as

$$T_c = \frac{h^2}{2\pi m k_B}\left(\frac{n}{\zeta(\frac{3}{2})}\right)^{2/3}, \qquad (21)$$

where n is the number density of Bose particles and $\zeta(z)$ is the Riemann's zeta function. This temperature gives probability of the ground-state occupation. It is written as

$$\Omega = 1 - \left(\frac{T}{T_c}\right)^{2/3} \quad for\ T < T_c\ . \qquad (22)$$

If we account the ground state occupation for $T < T_c$, the fusion rate is given by $R\Omega$. When $T \geq T_c$, no nuclear reactions have happened because $\Omega = 0$.

5. RESULTS AND DISCUSSIONS

In this work, ELTB solutions for the system including N deuterons trapped in VacT in fcc Pd lattice have been obtained, and d-d nuclear reaction rate has been estimated. VacT means tetrahedral void, which is constructed by four vacancies. The ELTB solutions are known to be accurate for a large N [7]. The accuracy of the ELTB solutions are for small N is not known. The calculations were performed within the following conditions.

(i) Thomas-Fermi screening potential is adopted as d-Pd interactions. The screening constant K in eq.(8) is $2/R_{1NN}$, where R_{1NN} is the first nearest neighbor (NN) distance. This means that in the vicinity of the defect center deuterons are nearly free from host ions.

(ii) Thomas-Fermi and non-linear screening potentials are adopted as d-d interactions. The constant k in eq.(8) is $2/R_{dd}$, where R_{dd}=0.74Å is the d-d separation of D_2 molecule.

(iii) The effective charge Z of a host Pd ion is one.

(iv) In eq.(12), the convergences of the lattice summations are kept to be smaller than 10^{-4}. In order to clear this condition, more than 20th NN lattice points should be needed.

(v) In eq.(15), the convergences of the summation for m are kept to be smaller than 10^{-10}. They have rapid convergences. For example, the cut-off M is about ten at $x \approx 10$.

(vi) The value of the S factor is 110kevb. This is consistent with Kim and Zubarev [4].

The examples of the trapped solutions are plotted in Figs.2 and 3. Seeing them, sharp peak exists at the potential well. Comparing these two figures, the position of the peak for non-linear screening shifts to the left. This means that the electronic screening cloud around a deuteron produce small and condensed deuteron cluster. The main reason for the shift of the peak to the left depends on the shape of f_{NL}. The non-linear screening potential in Fig.1 has a well, while Thomas-Fermi screening potential does not have it. This makes the difference between screening function f_{TF} in eq.(14) and f_{NL} in eq.(19). Calculated results of nuclear reaction rates are given in Table 1. In eq.(3), if all the particles exist at the same radial component r, ρ would become $\sqrt{N}r$. Therefore, if a position of the right foot of the sharp peak of ELTB solution is smaller than $\sqrt{N}R_v$, where R_v is the radius of the defect, we can say that the condensed deuterons are completely included in the defect. Within the same approximation, we can say that deuterons are condensed between the left foot $\rho_1 = \sqrt{N}r_1$ and the right foot $\rho_2 = \sqrt{N}r_2$ of the peak. Therefore, the number density can be regarded as $n = N/\frac{4}{3}\pi(r_2^3 - r_1^3) = 3N^{5/2}/4\pi(\rho_2^3 - \rho_1^3)$. The critical temperature T_c in eq.(21) can be calculated from them. These values are also given in Table 1. They indicate following things.

(a) Positions of the sharp peak are completely included in VacT, because $\sqrt{N}R_v > \rho_2$.

(b) For the case of Thomas-Fermi d-d interaction, T_c's are lower than the room temperature. For the case of non-linear screening d-d interactions, they are higher than room temperature.

(c) Nuclear reaction rates appear extremely high. However, if a nuclear fusion happens in VacT, local temperature becomes higher than T_c immediately. Then Ω becomes zero. And the reaction will be stopped. Therefore, they are not always high rate.

6. CONCLUSIONS

These results lead us to the conclusion that BEC of condensed deuterons trapped in VacT in Pd can induce cold and calm fusion. The screening effects of electrons around deuterons also contribute to the reactions.

Calculations for other types of voids in Pd should give similar results. For example, calculation for octahedral void (VacO) which is constructed by six vacancies should give similar results.

Table 1
Nuclear reaction rate R $[10^7 sec^{-1}]$ and critical temperature T_c $[K]$ for the case of N deuterons in VacT in Pd.

		Thomas-Fermi screening				non-linear screening			
N	$\sqrt{N}R_v$	ρ_{max}	ρ_2	T_c	R	ρ_{max}	ρ_2	T_c	R
3	5.59	2.73	2.86	61	2.4	1.12	1.20	262	34.6
4	6.45	3.52	3.64	71	3.9	1.36	1.44	334	67.7
5	7.21	4.23	4.35	82	5.7	1.57	1.65	409	110.3
6	7.90	4.90	5.02	92	7.6	1.76	1.84	486	162.5
7	8.53	5.53	5.64	102	9.6	1.94	2.01	564	224.2

ρ_{max}: position of the peak in ELTB solution [Å]
ρ_2: position of the right foot of the peak [Å]
R_v: Radius of the spherical defect is 3.23[Å].

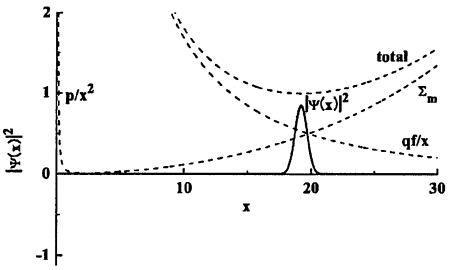

Fig. 2. The ELTB solution for the system including 4 deuterons in VaT in fcc Pd. Thomas-Fermi screening potential is used as the d-d interaction. The nondimensional quantity x is defined as $x = \sqrt{m\omega/\hbar}\ \rho$, where $\omega = 0.94 \times 10^{14} sec^{-1}$. The screening constant is defined as $k = 1/(2R_{dd})$, where R_{dd}(=0.74Å) is the d-d separation of D_2 molecule. The solid line means the ELTB solution. The dashed lines mean each potential in eq.(15) normalized by ε.

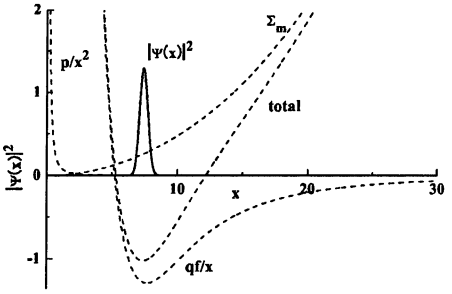

Fig. 3. The ELTB solution for the system including 4 deuterons in VacT in fcc Pd. Non-linear screening potential is used as the d-d interaction. The nondimensional quantity x is defined as $x = \sqrt{m\omega/\hbar}\ \rho$, where $\omega = 0.94 \times 10^{14} sec^{-1}$. The solid line means the ELTB solution. The dashed lines mean each potential in eq.(15) normalized by ε.

ACNOWLEDGEMENTS

The author wishes to thank Professor Y.E.Kim of Purdue University and Professor H.Yamada of Iwate University for helpful discussions and encouragements.

REFERENCES

[1] R.T.Bush and R.D.Eagleton, ""Cold Nuclear Fusion": A Hypothetical model to Probe an Elusive Phenomenon", J. Fusion Energy, **9**(1990)397

[2] K.Tsuchiya, K.Ohashi and M.Fukuchi, "A Possible Mechanism for Nuclear Reactions in Solids", Fusion Technology, **27**(1995)452

[3] P.K.Ghosh, "Ion Traps", Oxford Clarendon Press, 1995.

[4] Y.E.Kim and A.L.Zubarev, "Nuclear Fusion for Bose Nuclei Confined in Ion Trap", Fusion Technology **37**(2000)151

[5] H.Hohenberg and W.Kohn, "Inhomogeneous Electron Gas", Phys.Rev.**136**(1964)B864

[6] W.Kohn and L.J.Sham, "Self-Consistent Equations Including Exchange and Correlation Effects", Phys.Rev. **140**(1965)A1133

[7] Y.E.Kim and A.L.Zubalev, "Equivalent Linear Two-Body Method for Many-Body Problems", J.Phys B **33**(2000)3905

Revisiting Anomalous Explosion of Hydrogen and Oxygen Mixture from a View Point of Cold Fusion

Hiroshi Yamamoto, Free Journalist
3110-17, Tsuzuki, Mikkabi-Cho, Inasa-Gun, Shizuoka-Pref. Zip:431-1402, Japan
e-Mail: hughy@aqua.ocn.ne.jp

ABSTRACT: It has been reported that extraordinary powerful explosions occurred during experiments of cold fusion(1) and in nuclear power plants(2). The magnitude of explosion is far beyond the one which the current combustion theory predicts. As there was no clue to explain these anomalous explosions, it has been neglected to study the real cause of these explosions but just has been categorized as hydrogen explosion. In order to establish safer hydrogen economy in which hydrogen is the main energy carrier for fuel cells, and to avoid unnecessary hydrogen explosion during experiments of cold fusion, it is imperative to clarify the mechanism of the anomalous explosion of hydrogen. It has been demonstrated that hydrogen atoms can achieve lower states than ground state by a resonant collision with a near by atom or combination of atoms having the capability to absorb the energy to effect the transition, namely, an integer multiple of the potential energy of atomic hydrogen, $m \times 27.2eV$ (m=integer) (3) . This reaction was named as the Black-Light Process. The Black-Light Process can generate energy somewhat between nuclear and chemical reaction. This paper revisits the anomalous hydrogen explosions at nuclear power plants from a view point of the Black-Light Process and proposes its explosion mechanism.

Key words: hydrogen explosion, high concentration of hydrogen and oxygen, Hydrino

1. INTRODUCTION

The explosion of a cold fusion cell at SRI International in Menlo Park, California in 1992 is the most memorable one in the history of cold fusion research. The detonating cell (only 2 inches in diameter and 8 inches long), not only killed one researcher but peppered three other researchers in the lab with debris.

It was so powerful that people wondered it might be the first cold fusion bomb. Even though intensive investigation on this accident had been carried out but no radio active substances had been detected and the final conclusion was that it was just a hydrogen explosion. In Aug 2003, Tokyo Electric Power Company disclosed that it experienced 8 unusual pressure rises believed to be hydrogen explosion in its nuclear power plants during the time period of 1993-1997.

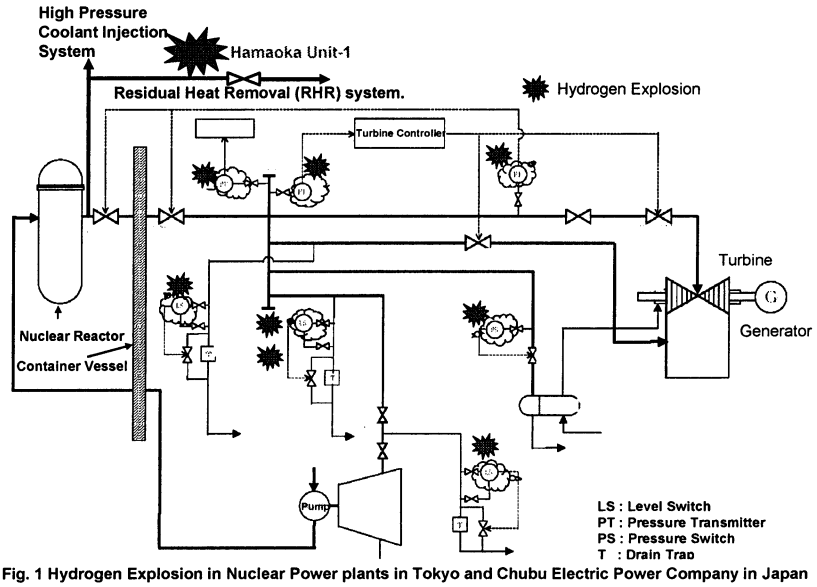

Fig. 1 Hydrogen Explosion in Nuclear Power plants in Tokyo and Chubu Electric Power Company in Japan
Source:http://www.tepco.co.jp/cc/press/03082103-j.html

The mechanism of these explosions was not identified and it was rather natural to have more severe one which took place in 2001 at the Hamaoka nuclear power plant of Chubu Electric Power Company in Japan. Fig 1 shows the places of hydrogen explosion in nuclear power plants in Tokyo and Chubu Electric Power Company.

After the Hamaoka's incident, an intensive investigation on the mechanism of ignition and explosion of hydrogen was done. Fig 2 shows the result of such an investigation. This paper revisits the hydrogen explosions at nuclear plants in Japan.

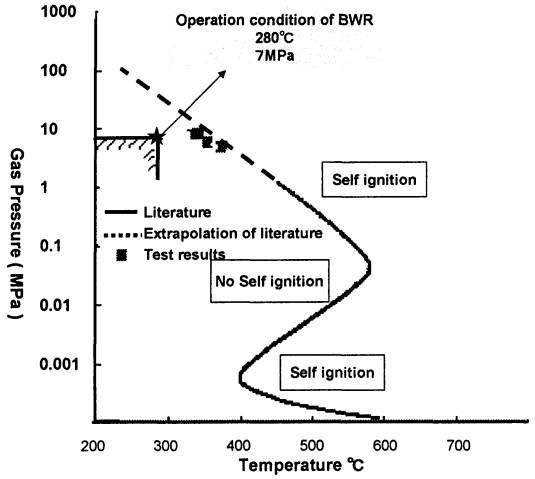

Fig. 2 Self Ignition Area of Stoichiometric Mixture of Hydrogen and Oxygen

Source:Chubu Electric Power Company:
Reactor Manual Shutdown Caused by Pipe Rupture in Residual Heat Removal System at the Hamaoka Nuclear Power Station Unit-1 (Final Report), April 2002 (in Japanese).

2. CHARACTERISTICS OF HYDROGEN EXPLOSION AT NUCLEAR POWER PLANTS

1) Not only stoichiometric mixture of hydrogen and oxygen

Most of explosions took place with stoichiometric mixture of hydrogen and oxygen produced due to radiolysis of water by nuclear reaction in power plants, but in the case of the Hamaoka unit-1, the story is totally different because of the injection of hydrogen and noble metal catalysts into cooling water for prevention of stress corrosion of internal parts made of stainless steel alloy. The purpose of these injections is to enhance the recombination of oxygen that causes corrosion with hydrogen.

Chubu Electric power Company had been operating 4 nuclear power plants at Hamaoka. The unit-1 (in which the incident took place) and unit-2 are boiled water reactor and have a very similar operating history including injection of hydrogen and noble metal catalysts into cooling water. After the incident of unit-1, non-condensable gasses of the unit-2 that were accumulated at the upward dead end of the pipe were taken and its contents were measured as is shown in Fig 3.

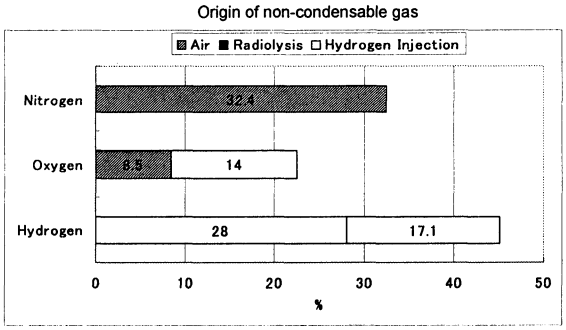

Fig. 3 Concentration of non-condensable gases and its origin in RHR of Hamaoka Unit-2

Source:
Chubu Electric Power Company:
Reactor Manual Shutdown Caused by Pipe Rupture in Residual Heat Removal System at the Hamaoka Nuclear Power Station Unit-1 (Final Report), April 2002 (in Japanese).

Nitrogen came in because the valves had been opened at the previous periodic inspection. This means that the origin of 8.5 % oxygen in Fig 3 is from air, not generated in the nuclear reactor. So, it is obvious that the mixture ratio of hydrogen and oxygen generated in the unit-2 is not 2:1 but over 3.2:1 as is shown in Fig. 3. In the case of unit-1 (in which the incident took place), the valves had not been opened at the previous inspection and most of non-condensable gasses were replaced with hydrogen and oxygen generated in the power plant. That is to say, there were very little air (nitrogen and oxygen) in the pipe at the beginning of the restart of operation. Chubu Electric Power Company claims that the mixture ratio of hydrogen and oxygen in the non-condensable gas in the unit-1 was 2:1, based on the above mentioned measurement and also computer simulation but a rather simple and crude calculation which can be done by deducting the portion of oxygen (8.5%) reveals that the mixture ratio of hydrogen and oxygen in the unit-1 was more than 3.2. Another problem to accept the Chubu's assertion is that hydrogen which was injected into the cooling water must disappear but this is totally out of the principle of physics. In order to explain the anomalous explosion of the Unit-1, it is needed to have another way different than stoichiometric mixture of hydrogen and oxygen.

2) Extraordinary powerful explosion

According to the Tokyo Electric Power's report[4], the pressure rise was estimated to be around 50MPa, resulting in a disengagement of the connector to the pressure gage for measuring the pressure of the main steam line, but it seems no damage to the pressure gage near by. In this configuration, one end is closed but the other is open or in other words, it is like an engine without a piston. In order to have this kind of

rapid pressure rise, one must establish a new combustion or energy release mechanism.

3) Ignition starts at lower temperature

The temperature and pressure in the pipe line of boiled water reactor is around 280 centigrade and 7 MPa which is far lower temperature than the self ignition line shown in Fig 2 which was obtained for the stoichiometric mixture of molecular hydrogen and oxygen. This discrepancy is another point to be studied for identification of the cause of hydrogen explosion.

3.A CANDIDATE HYPOTHESIS: BLACK-LIGHT PROCESS BY DR. R. MILLS

Dr. Randlle Mills demonstrated that hydrogen atoms can achieve lower states than ground state by a resonant collision with a near by atom or combination of atoms having the capability to absorb the energy to effect the transition, namely, an integer multiple of the potential energy of atomic hydrogen, m×27.2eV (m=integer) (3) . He named this shrunken hydrogen atom "Hydrino" and claims that this Hydrino can be a catalyst to shrink other hydrinos to further lower states. He named this reaction the Black-Light Process. Fig 4 illustrates the Black-Light Process.

Based on his hypothesis, he succeeded in generating energy somewhat between chemical and nuclear reaction using water vapor plasma. It is conceived that hydrogen and oxygen in the steam in nuclear power plants are molecular, not atomic, but since these hydrogen and oxygen are generated due to dissociation of water by nuclear radiation, it is quite conceivable that atomic hydrogen and oxygen can co-exist with molecular ones in the nuclear power plants.

4. PROPOSED MECHANISM OF ANOMALOUS HYDROGEN EXPLOSION

The author postulated that 3 body reaction of atomic hydrogen and oxygen can make the Black-Light Process because ionization energy of hydrogen and oxygen is very close as is shown below(5,6).

Hydrogen =13.598 eV, Oxygen =13.618 eV

It can be expected that the following reactions can take place:

$O + O + H \rightarrow H[n=1/2] + 2\,O^{+} + 2\,e^{-}$ ----(a)

$H + H + O \rightarrow H\,[n=1/2] + H^{+} + O^{+} + 2e^{-}$ ----(b)

$H + H + H \rightarrow H[n=1/2] + 2\,H^{+} + 2\,e^{-}$ ----(c)

H[n=1/2] designates a hydrogen whose electron orbit is shrunken to 1/2 the radius of a normal one and these will be shrunken further to lower orbits as reaction continues.

Ions and electrons thus produced will recombine, resulting in generation of energy.

Hydrogen itself is a good candidate for catalyst, but oxygen atom is about 2 times bigger than hydrogen atom. This will give the equation (a) more chances of simultaneous multi-body collision of 3 atoms than equation (c).

It is reported that the Black-Light Process can produce up to 200W/cm3 at 700mTorr(7), but in the case of nuclear power plant, the pressure is almost 5 order bigger than the case of the Black-Light Process and it can be expect that a hydrogen explosion can produce energy about 70MW/cm3 which is powerful enough to destroy the pipeline instantaneously.

Hydrogen and oxygen are atomic only in such cases as very low pressure, very high temperature, or on the noble metal catalysts. But once atomic hydrogen and oxygen are produced and if there is not heat sink at the collision point, collision of atomic hydrogen for a instance, H + H → H2 wouldn't take place but just repulse each other. This suggests that atomic hydrogen and oxygen produced in nuclear plants can exist much longer than normally expected.

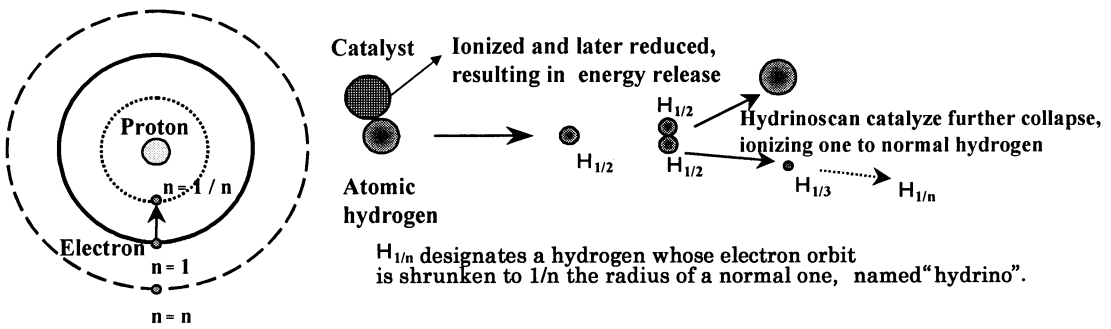

Fig. 4 Mechanism of "hydrino " generation and energy release

SUMMARY

1) Considering the magnitude and nature of damage caused by nuclear power plant's accidents, it is imperative to determine the real cause of hydrogen explosion.
2) In the case of hydrogen explosion in nuclear power plants, it is presumed that hydrogen and oxygen accumulated in the pipe are molecular and the mixture ratio is stoichiometric. But this assumption can't explain the reason why ignition starts at much lower temperature than the reconstruction test result and why the explosion is so powerful.
3) Even though there have been anomalous explosion of hydrogen and oxygen mixture in the past, the lack of plausible hypothesis hindered the research on the real cause of the explosion. But the advent of the new hypothesis namely the Black-Light Process gave us a clue to find out the real cause of hydrogen explosion.
4) It is conceived that hydrogen and oxygen in nuclear power plants are molecular, not atomic, but considering the nature of radiolysis of water, it can be assumed that atomic hydrogen and oxygen can also co-exist with molecular one and this would trigger the Black-Light Process that can produce energy somewhat between chemical and nuclear reaction.
5) It is recommended to pay much attention to the closed electrolysis of water in which noble catalysts are added for recombination of hydrogen and oxygen. In this case, pressure relief valves would not work because of a rapid pressure rise as was seen in the hydrogen explosion in Tokyo Electric Power's nuclear power plants.

REFERENCE

(1) Mallove ,E, Mysterious melt-down event, http://www.escribe.com/science/vortex/Date: 18 Jun 2002
(2) Nuclear and Industrial Safety Agency (NISA), Ministry of Economy, Trade and Industry (METI), JAPAN, Investigation Report on Pipe Rupture Incident at Hamaoka Nuclear Power Station Unit-1, July 2002
(3) Mills, R.L.; Ray, P.C.; Nansteel, M.; Chen, X.; Mayo, R.M.; He, J.; Dhandapani, B., Comparison of Excessive Balmer/Spl Alpha/Line Broadening of Inductively and Capacitively Coupled RF, Microwave and Glow-Discharge Hydrogen Plasmas with Certain Catalysts, IEEE Transactions on Plasma Science, Vol. 31, Issue 3, June 2003, pp. 338-355
(4) http://www.tepco.co.jp/cc/press/03082103-j.html (in Japanese)
(5) Yamamoto, H., Explanation of Anomalous Combustion of Brown's Gas using Dr. Mills' Hydrino Theory , SAE1999-01-3325
(6) Yamamoto, H, Catalytic Role of Atomic Oxygen on Anomalous Heat Generation, The Proceedings of ICCF-9, pp. 424-426.
(7)http://www.blacklightpower.com/pdf/ItalyTech%20Paper%203.27.03.pdf

Nuclear-fusion chemistry through nucleonic liquid crystals

Norio YABUUCHI
High Scientific Research Laboratory
204 Marusen Building, 28-16 Marunouchi, Tsu City, Mie 514-0033, JAPAN
E-mail yabu333@lilac.ocn.ne.jp

Abstract
Nucleons exchanging mesons, causing attraction between the nucleon, is explained on analogy with the Yukawa theory of nuclear forces in which electrons exchange photons, causing attraction between the electrons. Newton postulated seven types of sounds and seven types of optical colors through analogy between sound and light. The pursuit of the existence of the unknown through such analogy is known in many other examples, and can be extremely useful. This derives from the principle of analogy of existence in Aristotelian philosophy. The author has previously proposed a Platonic Yabuuchi structure of the atomic nucleus on analogy with Platonic crystals in molecules, thereby explaining the nuclear-fission ratios for uranium. Accordingly, through analogy with the liquid-crystal structure of molecules composed of atoms, the authors proposes a liquid-crystal structure for the atomic nucleus composed of nucleons. It is explained that just as molecular liquid crystals are susceptible to chemical reaction, nuclear liquid crystals are similarly susceptible to chemical reaction. As is seen in halo nuclei, the nuclear force of the nucleus becomes weak, and the distances between nucleons can increase. Consequently, on analogy with the transformation of solid to liquid in light water, the author develops a theory of nuclear reaction in which an atomic nucleus on the surface of a metal in a sea of deuterium undergoes liquid crystallization and the distances between nucleons increase, and even if the arrangement of the nucleons does not change, their degree of freedom increases, resulting in greater susceptibility of reaction with other nuclei or nucleons, thereby facilitating nuclear reaction. The nucleus has a liquid-crystal bar arrangement.

Key words: liquid crystal, nano-space, Platonic structure of atomic nucleus, block arrangement of atomic nucleus, subsidence of Coulomb barrier

1. Introduction

Nuclear fusion in solids appears to be approaching the final phase at long last. The surface of a solid is at the boundary with the surrounding gas, and because the solid and gas act mutually upon each other, what has heretofore be considered unthinkable is becoming possible. Wolfgang Pauli's musings on the "devilish" properties residing in the surface of a solid are completely on target. In the nanometer-order world of a solid surface, lattices and locations exert effects, giving rise to a "devil." However, because God abhors chaos, order must prevail, and it is the conviction of the author that natural laws apply.

The author has been a proponent of nucleonic crystals composed of Platonic structures, but it appears that in nuclear fusion this nucleonic crystal first becomes a liquid crystal, and this nucleonic liquid crystal fuses with another nucleonic liquid crystal. On the molecular level as well, reactions between two solids are difficult. However, this can also be inferred by analogy from the fact that when in a liquid or liquid-crystal state, the reaction between the molecules are larger and easier than with solids. Using these reasons, the author conducted chemical investigation

into fusion by liquid-crystal atomic nuclei in a state intermediate between liquid and crystal.

2. Characteristics of nucleonic liquid-crystal reactions

In a nucleonic liquid-crystal reaction, heavy-hydrogen decomposition causes the mutual distances between nucleons to expand, weakening proton reaction and lowering the Coulomb barrier, and entry by the neutron and proton nucleons in the atomic-nuclei blocks is facilitated. In short, the tunnel effect increases and nuclear fusion can easily take place even at low temperatures.

At JCF4, the author explained the results of Iwamura et al. at Mitsubishi Heavy Industries as nuclear fusion from iron to aluminum in terms of the theory of the Platonic Yabuuchi structure of the atomic nucleus. In the present case, similarly, the conversions by deuteron gas of $^{133}Cs \Rightarrow {}^{141}Pr$ and $^{88}Sr \Rightarrow {}^{96}Mo$ in the experiments by Iwamura et al. are explained by Platonic Yabuuchi structure with the addition of the theory of nucleonic liquid crystals.

3. Fusion of nuclei in a liquid-crystal state

The author obtained the chemical formula shown by equation (1) below for the nuclear fusion of liquid-crystal $^{133}Cs_{55}$ with 2(2D) – that is, two 2D liquid-crystal compound nuclei – rather than with helium, which presents strong proton reaction. Atomic nuclei that have become liquid crystals in nanometer-order space are respectively arranged and bonded in blocks that have crystallized into Platonic structures. Because these bonds are between liquid crystals, the attraction between the respective blocks is weakened by the large distance between the blocks. Here, blocks are indicated by square brackets ("[ ]"), and the bond between two blocks by a dash ("-"). Because the distance between two bonded blocks is large, the proton reaction can be termed small.

At JCF4, the author described how the spherical surface of the shell is externally and internally tangent with the Platonic Yabuuchi structure, yielding the nuclear chemical formula for $^{133}Cs_{55}$ shown in Figure 1. The items have been labeled to aid understanding.

$^{133}Cs_{55}$ [T, C, O, I D]-[T]-[T, C, O, I -7]-[O]-[T, C, O, I, D]
= (25n + 25p) (2n + 2p) (23n) (3n + 3p) (25n + 25p) (1)

The third term from the left in equation (1) represents the outermost shell, which in terms of Platonic structures is an icosahedron, indicated here as an I polyhedron. As shown here, its configuration has been stripped of seven crystalline nucleons (here neutrons). The state in which the two 2D units in equation (1) react is indicated by equation (2).

$\Rightarrow$ 2(n + p) + 2(n + p) + $^{133}Cs_{55}$ (2)
= (25n + 25p) (2n + 2n + 2p + 2p) (23n) (2n + 2p + 3n + 3p) (25n + 25p) (3)

Equation (3) depicts the state in which the 2D units in the second (b) and fourth (d) blocks of the nucleons of the $^{133}Cs_{55}$ nucleus have undergone liquid-crystal fusion.

Because items (b) and (d) have fewer protons than the other items, proton reaction is small. Item (c) is a crystal composed solely of neutrons and lacking protons, and so because it has no power to attract the neutrons of the liquid-crystal compound nucleus 2(n + p), the 2(n + p) block is the result of reaction between (b) and (d). Its shell structure cannot be explained in terms of Victor

Weisskopf's Platonic structures. Further, under the solar-system model of the atomic nucleus, the reaction between (b) and (d) seen here cannot be produced by proton reaction.

$$= (25n + 25p)\ (4n + 4p)\ (23n)\ (2n + 2p + 3n + 3p)\ (25n + 25p) \quad (4)$$

$$= {}^{141}Pr_{59}\ [T, C, O, I, D]\text{-}[C]\text{-}[T, C, O, I - 7]\text{-}[T, O]\text{-}[T, C, O, I, D] \quad (5)$$

Equation (4) indicates the change in the numbers of protons and neutrons that occur due to nuclear reaction in the blocks within the atomic nucleus.

In the atomic nucleus that has undergone nuclear change to become $^{141}Pr_{59}$, indicated by equation (5), in the second block, (2n + 2p) has become (4n + 4p), indicating that the T polyhedron (tetrahedron) has reacted to the C polyhedron (cube) and changed.

Similarly, in the fourth block, (2n + 2n) has become (2n + 2p + 3n + 3p), indicating that the O polyhedron (octahedron) has changed to a T-polyhedral structure in the inner shell and an O-polyhedral structure in the outer shell. This is as shown in Figure 2.

The result is as follows:

$$^{133}Cs_{55} + 2\cdot 2D \Rightarrow {}^{141}Pr_{59} + \Delta E \quad (6)$$

The reason why a change in the crystal is produced because of the change in the numbers of neutrons and protons is related to Kepler's theory of space-filling polyhedra and to quantum change in spaces, and like the mystery of crystallization of snowflakes, remains a topic for future study.

Nuclear reaction can be explained similarly for $^{88}Sr_{38}$ as well. This is represented first by Figure 3, followed by the chemical formula.

$$^{88}Sr_{38}\ [T, C, O, I, D - 12]\text{-}[I]\text{-}[T, C, O, I, D - 12]$$

$$= (19n + 19p)\ (12n)\ (19n + 19p) \quad (7)$$

$$\Rightarrow {}^{88}Sr_{38} + 2(n + p) + 2(n + p) \quad (8)$$

$$= 2(n + p) + (19n + 19p)\ (12n)\ 2(n + p) + (19n + 19p) \quad (9)$$

$$= (21n + 21p)\ (12n)\ (21n + 21p) \quad (10)$$

$$= {}^{96}Mo_{42}\ [T, C, O, I, D - 8]\text{-}[I]\text{-}[T, C, O, I, D - 8] \quad (11)$$

The result is as follows:

$$^{88}Sr_{38} + 2\cdot 2D \Rightarrow {}^{96}Mo_{42} + \Delta E \quad (12)$$

Figure 4 illustrates equation (11).

Because item (b) in equation (7) is composed entirely of neutrons and does not attract protons, the 2D does not react. Accordingly, items (a) and (c) are each lacking six neutrons and protons, for a total of 12, and the 2D reacts ate locations.

The riddle of nuclear fusion is thus explained. The bonds described are not formed in a chaotic integral atomic nucleus. Fusion can take place in an atomic nucleus having crystalline blocks with weak bonds.

References

Norio YABUUCHI. Proc. JCF4, 82 (2002)
Yasuhiro IWAMURA, Mitsuru SAKANO, Takehiro ITOH. Jpn. J. Appl. Phys. Vol. 41 (2002) pp. 4642-4650

Figure 1 – Liquid-crystal nucleus structure of $^{133}Cs_{55}$

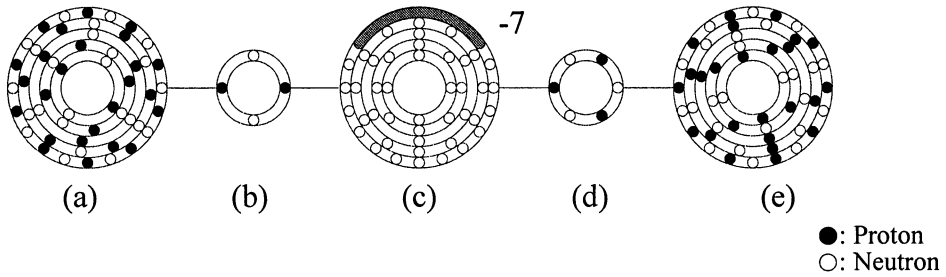

Figure 2 – Liquid-crystal nucleus structure of $^{141}Pr_{59}$

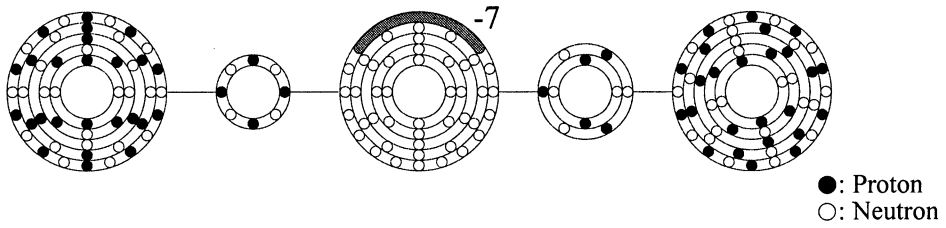

Figure 3 – Liquid-crystal nucleus structure of $^{88}Sr_{38}$

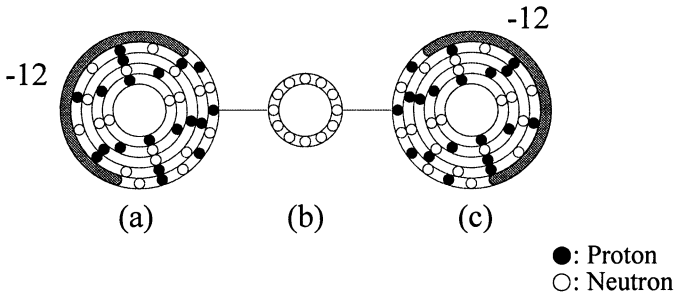

Figure 4 – Liquid-crystal nucleus structure of $^{96}Mo_{42}$